

Pattern formation of cortical microtubules and cellulose microfibrils

Jelmer Lindeboom

Thesis committee

Promotor

Prof. dr. A.M.C. Emons
Emeritus Professor of Plant Cell Biology
Wageningen University

Co-promotors

Dr. Ir. M.J. Ketelaar
Assistant Professor, Plant Cell Biology
Wageningen University

Prof. dr. B.M. Mulder
Professor of Theoretical Cell Physics
Wageningen University

Other members

Dr. S. Shaw, Indiana University, Bloomington, United States of America
Prof. dr. M. Dogterom, FOM Institute AMOLF, Amsterdam
Prof. dr. A. Akhmanova, Utrecht University
Prof. dr. T. Bisseling, Wageningen University

This research was conducted under the auspices of the Graduate School
Experimental Plant Sciences.

Pattern formation of cortical microtubules and cellulose microfibrils

Jelmer J. Lindeboom

Thesis

submitted in fulfillment of the requirements for the degree of doctor
at Wageningen University

by the authority of the Rector Magnificus,

Prof. dr. M.J. Kropff,

in the presence of the

Thesis Committee appointed by the Academic Board

to be defended in public

on Wednesday 14 November 2012

at 4 p.m. in the Aula.

Jelmer J. Lindeboom

Pattern formation of cortical microtubules and cellulose microfibrils

142 pages.

Thesis Wageningen University, Wageningen, NL (2012)

With references, with summary in Dutch

ISBN 978-94-6173-389-4

Outline

The research presented in this thesis focuses on organization of cortical microtubules and cellulose microfibrils. Chapter 1 is a review of literature on the organization and function of cortical microtubules and cellulose microfibrils. We discuss the relation between cortical microtubules and cellulose microfibrils and how their organization influences the cell shape.

In chapter 2 we investigate how cortical microtubules reappear and become ordered after absence from the cell cortex during cell division or depolymerization by microtubule depolymerizing drugs. We combine quantitative analysis of microtubule order and microtubule nucleations. We use probabilistic simulations to characterize how the ordered cortical microtubule array is created.

Chapter 3 investigates the journey cellulose synthase complexes take after their assembly in Golgi bodies until their insertion into the plasma membrane. We study how the actin cytoskeleton influences the global distribution of Golgi bodies and we study interactions between compartments containing cellulose synthase complexes and cortical microtubules. We also study the role of cortical microtubules in guiding the location at which cellulose synthase complexes are inserted in the plasma membrane.

In plant cells, there are two major classes of cytoskeleton, the microtubules and the actin cytoskeleton. Microtubules are important for the localization of certain cellular processes and the actin cytoskeleton is important for movement of proteins, organelles and metabolites. In chapter 4 we study physical interactions between the actin and microtubule cytoskeleton.

Plants can change the direction of growth in response to light perception. We know that for changes in growth, changes in cortical microtubule organization are often needed. In chapter 5 we study how, and by what mechanism, blue light signaling causes reorientation of the cortical microtubule cytoskeleton.

Cortical microtubules are essential for anisotropic expansion in plant cells, but the processes downstream of cortical microtubule organization that facilitate regulated cell growth is not known. In chapter 6 we discuss what kind of processes the cortical microtubules may be regulating that actually result in anisotropic cell expansion.

Contents

1	Introduction	1
1.1	Abstract	1
1.2	Introduction	1
1.3	Membrane turnover	3
1.4	Cellulose synthase complex	6
1.5	Physical aspects of cellulose production	7
1.6	Cell wall texture	8
1.7	Cortical microtubules	10
1.8	Activity at the plasma membrane	11
1.9	Acknowledgements	12
2	Cortical microtubule array initiation	13
2.1	Abstract	13
2.2	Introduction	13
2.3	Results	15
2.4	Discussion	22
2.5	Materials and methods	26
2.6	Acknowledgements	30
2.7	Supplementary information	31
3	Cellulose synthase complex trafficking	37
3.1	Abstract	37
3.2	Introduction	37
3.3	Results	39
3.4	Discussion	49
3.5	Materials and methods	55
3.6	Acknowledgements	59
3.7	Supplementary information	61
4	Associations between the actin and microtubule cytoskeleton	71
4.1	Abstract	71
4.2	Introduction	71
4.3	Results	73
4.4	Discussion	82
4.5	Materials and methods	85
4.6	Acknowledgments	86

4.7	Supplementary information	87
5	Mechanism of blue light induced microtubule reorientation	91
5.1	Abstract	91
5.2	Introduction	92
5.3	Results	94
5.4	Discussion	106
5.5	Materials and methods	111
5.6	Acknowledgements	114
5.7	Supplementary information	114
6	General discussion	115
6.1	Cell expansion and turgor pressure	115
6.2	The plant cell wall as a gel	116
6.3	Cortical microtubules are required for anisotropy of growth	116
6.4	Regulation of cell wall properties by cortical microtubules	117
6.5	A model for microtubule localized regulation of cell wall extensibility	117
6.6	A possible role of MAP65 family proteins in anisotropic cell expansion	118
6.7	Cellulose deposition to counterbalance cell wall extension	119
	Bibliography	121
	Summary	135
	Samenvatting (<i>Dutch summary</i>)	137
	Acknowledgements	139
	List of publications	143



Introduction

1.1 Abstract

Plant cell wall production is a membrane-bound process. Cell walls are composed of cellulose microfibrils, embedded inside a matrix of other polysaccharides and glycoproteins. The cell wall matrix is extruded into the existing cell wall by exocytosis. This same process also inserts the cellulose synthase complexes into the plasma membrane. These complexes, the nanomachines that produce the cellulose microfibrils, move inside the plasma membrane leaving the cellulose microfibrils in their wake. Cellulose microfibril angle is an important determinant of cell development and of tissue properties and as such relevant for the industrial use of plant material. Here, we provide an integrated view of the events taking place in the not more than 100 nm deep area in and around the plasma membrane, correlating recent results provided by the distinct field of plant cell biology. We discuss the coordinated activities of exocytosis, endocytosis, and movement of cellulose synthase complexes while producing cellulose microfibrils and the link of these processes to the cortical microtubules.

1.2 Introduction

Plant cell walls are sophisticated, complex and dynamic structures composed of networks of various polysaccharides, glycoproteins and phenolic compounds (Carpita and Gibeau, 1993; McCann et al., 2001). In many plant cell types, cellulose, the most abundant biopolymer on earth, is the main cell wall component. Cellulose is present in cell walls as long cellulose microfibrils (CMFs) that wrap around the cells providing them with a load-bearing framework and necessary rigidity to restrain the cell's turgor pressure that results from hydrostatic pressure exerted on the cell walls (Diotallevi and Mulder, 2007). The orientation of CMFs, which have a tensile

strength comparable to that of steel, is central to regulation of cell elongation, and CMF deposition orientation after cell elongation is essential to ensure proper wall strength.

Cell walls are biphasic structures; they are composed of CMFs, embedded inside a matrix of other polysaccharides and glycoproteins. This biphasic structure is produced by two separate, but connected deposition mechanisms. The matrix materials are extruded by exocytosis into the cell wall. This same process also inserts the cellulose synthase complexes (CSCs) into the plasma membrane. These complexes are the nanomachines that produce the CMFs from UDP-glucose recruited from the cytoplasm, depositing them into the wall in a membrane-bound process.

The CMFs are crystalline arrays of β -1,4-linked chains of glucose residues (Delmer, 1999). Measurements with wide angle (WAXS) and small angle (SAXS) X-ray scattering and NMR have revealed that the diameter of cellulose microfibrils of celery collenchyma is between 2.4 and 3.6 nm (Kennedy et al., 2007), which is consistent with previously published data, including measurements from TEM images (Emons, 1988). Kennedy et al. (2007) argue that this diameter range corresponds to between 15 and 25 cellulose polymers per microfibril, rather than the commonly quoted number of 36, which is strongly based on the implications of the observed 6-fold symmetry of the membrane-embedded part of the CSC, the so-called particle rosette.

The angle with respect to the long axis of the cell at which the CMFs are deposited is an important determinant of cell growth behaviour and cell wall properties. The totality of all individual CMFs is organized into a variety of patterns, cell wall textures, which are species- and cell developmental stage-specific and thus regulated by the cells they surround. Therefore, the regulation of CMF angle is an important issue. In elongating cells, CMFs at the outside and cortical microtubules at the inside of the plasma membrane are often in the same net orientation, transverse to the cell's elongation direction (Lloyd and Chan, 2004), and cortical microtubules border the area in tracheary elements where wall thickening of almost 100% cellulose occurs (Oda et al., 2005). Topical work, in which both cortical microtubules and CSCs were visualized in living cells, epidermis cells of elongating etiolated hypocotyls, shows that cortical microtubule orientation and the oriented movement of CSCs are correlated (Paredes et al., 2006). This seems to reduce the question of CMF ordering to the question of the ordering of cortical microtubules, at least in these cells. However, in the absence of the cortical microtubules the CSCs move in a definite pattern as well, pointing to the existence of an underlying non-cortical microtubule based ordering mechanism for CMFs.

All this CMF production activity and alignment occurs in and at the plasma membrane while exocytosis and endocytosis are going on. Figure 1.1 (A) shows the cytoplasmic side of the plasma membrane of the sub-apex of a growing radish root with microtubules longitudinal to the long axis of the root hair and an abundance of coated pits. In this review, we discuss the current knowledge of these processes. First, we discuss membrane turn over: the exo- and endocytosis mechanisms. Then we present the CSCs, physical considerations of CMF production, the organization of the CMFs, and confer attention to the organization of the polymers at the other

side of the plasma membrane, the cortical microtubules. Lastly, we discuss the coordination of all this activity, taking into account the physical aspects pertaining to the processes occurring in that limited area of approximately 100 nm bordering the plasma membrane.

1.3 Membrane turnover

Exocytosis is the process in which the membrane of cargo containing vesicles fuses with the plasma membrane, while delivering their cargo to the outside of the cell. Figure 1.1 (B) shows exocytotic structures at the plasma membrane of embryogenic carrot suspension cells. Exocytosis is an important part of the generally coupled processes of plant cell elongation and cell wall deposition. Material contained inside (Golgi) vesicles is extruded out of the cytoplasm into the existing cell wall, and this is combined with insertion of integral membrane proteins, such as for instance the CSCs, into the plasma membrane. The vesicle membrane encloses a three-dimensional sphere, whereas the plasma membrane by comparison is effectively a flat plane. This purely geometrical mismatch in surface-to-volume ratio between these two structures results in an excess of membrane that is inserted into the plasma membrane when compared with the deposition of the vesicle contents into the extra-cellular lumen. To ensure that the membrane lies straight against the cell wall, and does not ruffle, excess membrane retrieval is required. Indeed, the cytoplasmic side of the plasma membrane is covered with many coated pits, demonstrating that clathrin-mediated endocytosis occurs abundantly (Emons and Traas, 1986). Besides regulating the amount of plasma membrane, endocytosis has been hypothesized to be involved in rapidly generating membrane supply during cell plate formation (Dhonukshe et al., 2006). However, recently it has been shown that this hypothesis is not true and that also vesicles that form the cell plate are Golgi-derived (Reichardt et al., 2007).

Figure 1.1 (C) is a detail of a coated pit in the sub-apex of a growing *Equisetum hyemale* root hair. Calculations have been made to estimate the number of exocytosis and/or endocytosis vesicles required for cell elongation to occur. Miller et al. (1997) calculated that in *E. hyemale* root hairs, in which the growth velocity is approximately $0.67 \mu\text{m min}^{-1}$ (Emons and Wolters-Arts, 1983), the extension of the plasma membrane requires 148 exocytotic vesicles with a measured diameter of 300 nm (Emons, 1987) per minute. In combination with an estimated membrane turnover time of 20-40 min, calculated from the amount of coated pits (Emons and Traas, 1986), this leads to a requirement of 445 vesicles per minute to sustain membrane recycling and cell expansion. In this calculation, 67% of the inserted membrane needs to be recycled. In *Lilium* pollen tubes, Morre and Van der Woude (1974) estimated the amount of exocytotic vesicles by assuming that the volume of the exocytotic vesicles contributed to the cell wall expansion stoichiometrically. They obtained a value of approximately 1000 vesicles per minute. Ketelaar et al. (2008) assumed that the plasma membrane surface area and cell wall volume increase stoichiometrically by

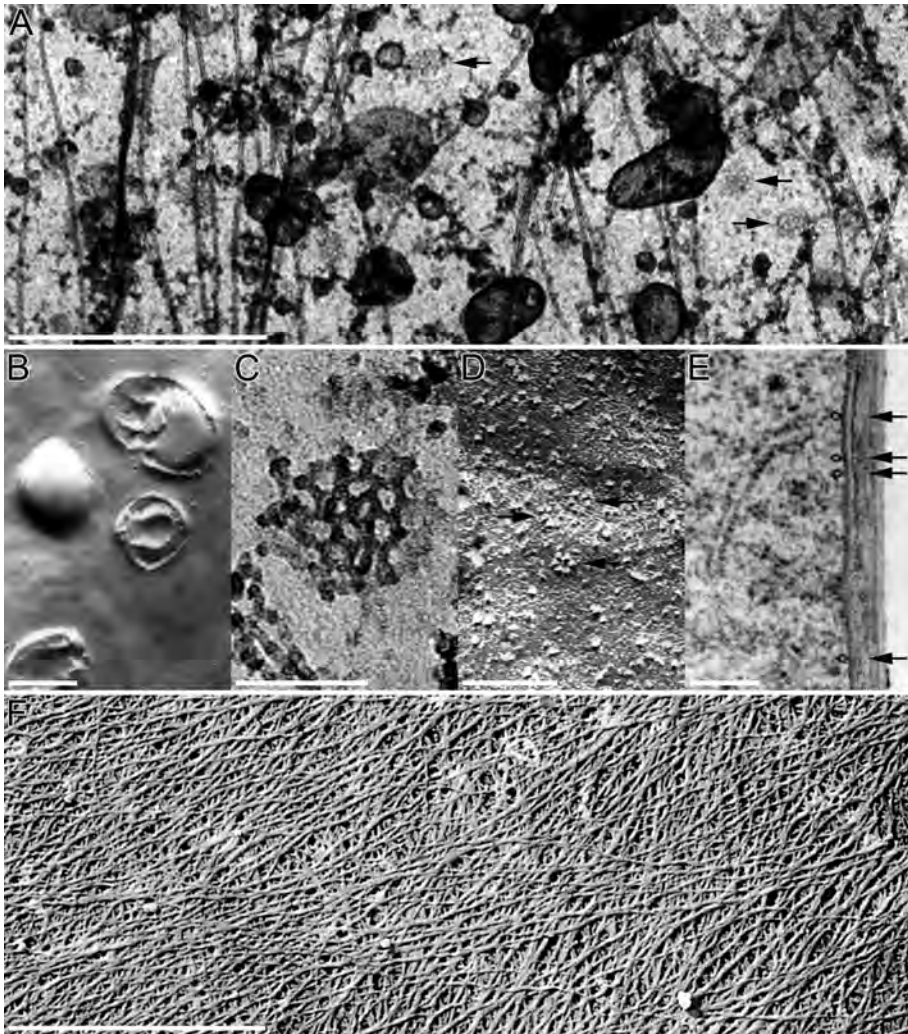


Figure 1.1: (A) Micrograph of the sub-apical part of the cortex of a growing root hair of *Raphanus sativus* prepared with the dry-cleaving technique (Emons and Traas, 1986) showing coated pits on the plasma membrane and microtubules on top of the membrane. The dark structures in this micrograph are unidentified vesicles and small organelles. Bar is 1 μm . (B) Micrograph of a freeze-fracture image of a carrot suspension cell showing exocytosis figures in the plasmatic fracture face of the plasma membrane of a young cell. These complex horseshoe-shaped structures are fractures through plasma membrane and vesicle membrane and arise because, after insertion of a piece of vesicle membrane into the plasma membrane, the vesicle flattens, and the flattened vesicle flips over parallel to the plasma membrane (Emons et al., 2006). Bar is 200 nm.

Figure 1.1: (C) Detail of coated pit from a growing *Equisetum hyemale* root hair prepared as described in (A). Bar is 100 nm. (D) Micrograph showing three particle rosettes (arrows) in the plasma membrane of a freeze fractured root hair of *Equisetum hyemale* (Emons, 1985). Bar is 100 nm. (E) Micrograph of a transverse section through a root hair of *Vicia sativa* prepared with the freeze-substitution method (Miller et al., 2000) showing cortical microtubules (arrows) close to the plasma membrane. This method, in which sections are stained with uranyl acetate and lead citrate, has been shown not to reveal the cellulose microfibrils in the cell wall (Emons, 1988), although stripes seen in such preparations have often been called cellulose microfibrils. Bar is 200 nm. (F) Micrograph of a dry-cleaved platinum-carbon shadowed preparation showing cellulose microfibrils in a cell wall of the tube of a growing root hair of *Equisetum hyemale* from which cell wall matrix was extracted with hydrogen peroxide glacial acetic acid (Emons, 1989). Cellulose microfibril orientations of three successive lamellae on top of each other can be observed. Bar is 1 μm .

the membrane surface area and cell wall matrix contents of exocytotic vesicles. They estimated that 86.7% of the inserted plasma membrane in *Arabidopsis* root hairs and 79% in *Arabidopsis* pollen tubes are recycled by endocytosis. These values are higher than the value found by Morre and Van der Woude (1974), but of the same order of magnitude.

Picton and Steer (1983) used a different approach to estimate the amount of Golgi-derived vesicles that are required for pollen tube growth. Using $0.3 \mu\text{g mL}^{-1}$ (approximately $0.6 \mu\text{M}$) of the actin depolymerizing drug cytochalasin D, they inhibited growth of *Tradescantia* pollen tubes. As the actin cytoskeleton serves as a transport system to deliver exocytotic vesicles to the apex of the pollen tube, the delivery of newly synthesized exocytotic vesicles from the Golgi apparatus to the growing tip should be inhibited. Assuming that the production of exocytotic vesicles continues at the normal rate when actin is depolymerized, the accumulation of vesicles around the Golgi stacks in the cytoplasm was counted. After 5 min, they calculated the increase in the density of Golgi-derived vesicles and used this value to calculate the number of exocytic vesicles that would be consumed for pollen tube growth during that time. They estimate a production of 3000-5000 exocytic vesicles per minute. The reliability of this approach depends on the assumption that exocytic vesicle production is not inhibited by actin depolymerization, which these authors have shown not to occur in these cells (Picton and Steer, 1981).

Besides sustaining cell expansion, maintaining the ratio between cell wall volume and plasma membrane surface area, the large numbers of exocytotic vesicles that fuse with the plasma membrane and the large percentage of membrane recycling

that occurs could serve as a mechanism to tightly control the amount and type of trans-membrane proteins at the plasma membrane. One trans-membrane protein complex of which the amount (and/or activity) in the plasma membrane requires tight regulation for cell wall deposition is the CSC. In the next paragraph, we will discuss the current knowledge about this complex.

1.4 Cellulose synthase complex

The supramolecular complexity of CMFs is reflected in their synthetic machinery, the CSCs (Somerville et al., 2004). CSCs are large transmembrane protein complexes, which move through the plasma membrane while producing CMFs (Paredes et al., 2006). They have been visualized by transmission electron microscopy of freeze-fractured membranes. These electron micrographs of plasmatic fracture faces of higher plant plasma membranes show six particles in a hexagonal arrangement, often at the end of a CMF. These arrangements of six particles have been called 'particle rosettes', or briefly, 'rosettes'. In higher plant cells, only single rosettes have been reported. The composing six particles are each approximately 8 nm wide, and the total rosette diameter is approximately 24 nm (Mueller and Brown Jr., 1980; Emons, 1985) both sizes including the 2- to 5-nm-thick platinum/carbon shadow of the freeze fracture/replication technique.

The catalytic enzyme cellulose synthase was the first component of the CSC that has been cloned (Pear et al., 1996). Direct genetic evidence that the CESA gene was the cellulose synthase came from the work of Arioli et al., who complemented the root swelling (*rsw1*) *Arabidopsis* mutant (Arioli et al., 1998). The availability of the CESA sequence enabled the manufacture of antibodies that were used by Kimura et al. (1999) to show that the particle rosettes indeed contain cellulose synthase proteins.

In *Arabidopsis thaliana*, the cellulose synthase family contains at least ten different isoforms, AtCESA1 to AtCESA10, reviewed by Sommerville (2006), of which the encoded proteins have eight membrane-spanning regions, thought to form a pore. The catalytic centre contains the D,D,D,QxxRW motif, in which the D,D,D part could bind UDP-glucose (Richmond and Somerville, 2000). The N-terminus contains a double zinc finger motive called LIM domain. LIM domains in human cells are involved in protein-protein interactions. The zinc fingers of cellulose synthase could well be involved in protein interactions, for instance between CESA sub-units within the complex, or between a CESA and another protein.

During xylogenesis in *Arabidopsis*, three functionally different genes CESA4, -7 and -8 are required to make functional CSCs (Taylor et al., 2003). These findings were supported by microarray co-expression which showed very high co-expression of CESA4, -7 and -8 during secondary cell wall production (Birnbaum et al., 2003; Persson et al., 2005). Persson et al. (2005) also showed that genes involved in primary cell wall synthesis CESA1, -3 and -6 were highly co-expressed. The *cesa1* and *cesa3* mutants are gametophytic lethal but *cesa2*, -5, -6 and -9 have relatively mild pheno-

types (Persson et al., 2007). Recent studies by Desprez et al. (2007) and Persson et al. (2007) show that the CESA6-like genes, CESA2, -5, -6 and -9, are at least partially redundant and *cesa2*, -6 and -9 triple mutants are gametophytic lethal. Very little is known about the function of the CESA10 gene.

It appears that there are two different classes of CSCs. One class of complexes, containing the CESA4, -7 and -8 proteins, is likely to be involved in secondary wall formation and the other class of complexes, containing CESA1, -3 complemented by either CESA2, -5, -6 or -9, is responsible for cellulose deposition during cell growth. The transcriptional regulation of the sub-units and subsequent assembly into functional CSCs is still poorly understood.

1.5 Physical aspects of cellulose production

Knowing from which components the CSC is built is not enough to understand its mode of operation. It is by now widely assumed that the force for CSC propulsion derives from the cellulose synthesis itself (Herth, 1980; Roberts et al., 1982). If that is indeed the case, we need to answer the question of how the energy released upon the synthesis of individual cellulose polymers by the CESAs and their subsequent aggregation into the CMFs is converted into motion. To that end, we must take into account the full set of physical constraints under which the CMF deposition process takes place.

Although many, if not most, of the details of this process are as yet experimentally inaccessible, we are still able to form a minimal model of CSC propulsion based on these constraints. The first is that the CSC itself is embedded in the plasma membrane. Both its 'top view' as seen in the inner plasma membrane leaflets (PF-face) of freeze fracture EM images (Herth, 1980; Mueller and Brown Jr., 1980; Emons, 1985) and its 'bottom view' provided by the recent work of the laboratory of R.M. Brown Jr. (Bowling and Brown, unpublished work) show a laterally extended and roughly circular aspect and to a first approximation one can assume that this disk-like structure lies parallel to the membrane surface. From symmetry considerations, one also expects that the cellulose polymer chains emerge perpendicularly to the plane of the complex.

As the CMF formed in the wake of the CSC is trapped in the space between the plasma membrane and the already extant cell wall, and the first is pressed against the second by the turgor pressure, the CMF itself must also lie in the plane of the membrane. This implies that, independently of the exact sequence of events in the crystallization process, the individual cellulose microfibrils must be bent in their path from the CSC to the CMF. As this bending of the polymers, be it individually or, as has been suggested, already partially crystallized into sheets (Brown Jr and Saxena, 2000), costs energy, forces are exerted at the location at which the chains are connected to the CSC and the CMF. At the connection point to the CSC, these forces can be decomposed into a downward component pointing into the plane of the CSC and to a lateral component parallel to this plane. The perpendicular forces

counteract the extrusion process and hence decrease the polymerization rate, and effect which is readily modelled by the classical Brownian ratchet mechanism (Peskin et al., 1993). As a by-product of these perpendicular forces, the CSC as a whole and part of the membrane connected to it will be pressed downward, an effect probably responsible for the membrane depressions seen in some of the freeze fracture images. As the bending of the chains can be alleviated by moving the attachment point to the CSC farther away from the other constraint point formed by the attachment to the CME, the in-plane components are responsible for moving the CSC, again by symmetry, in the direction into which the nascent CMF points. At the attachment point to the CME, any force loading will tend to hinder the crystallization process. These forces are decreased whenever the CSC moves farther away, allowing the CMF to grow, tracking the motion of the CSC. The interplay between the physical forces generated and the polymerization and crystallization process allows a stationary state to be reached in which a constant force is exerted on the CSC that in turn is balanced by the viscous stresses in the fluid media (membrane and cytoplasm) in which it is immersed, leading to a constant speed of propagation.

Based on the heuristic mechanism described earlier, Diotallevi and Mulder (2007) were able to formulate an analytical model of CSC propulsion that correctly estimates the order of magnitude of the speed (10^2 - 10^3 nm min⁻¹) of motion as observed in the recent experiments (Paredes et al., 2006). Furthermore, they provided a proof of principle of this mechanism by implementing a stochastic simulation, including all of the relevant ingredients explicitly, that shows how a CSC producing six cellulose strands progresses in the membrane.

Knowing how a single CSC is propelled, however, is still a long way from understanding how the often strikingly ordered textures of plant cell walls come about. To that end we must come to the grips with the question of which elements of the environment of a CSC determine its direction of motion within the plasma membrane.

1.6 Cell wall texture

In cell walls, CMFs are arranged in lamellae that together form the cell wall texture, the architecture of the totality of all the CMFs. The orientation of CMFs with respect to the long axis of the cell within a lamella is approximately constant, but may vary from lamella to lamella, depending on the type of texture. The distance between CMFs within a lamella varies from a few nanometres in cell wall thickenings of *Lepidium* xylem cells, up to 160 nm in helicoidal cell walls of root hairs, but exact numbers have hardly been reported (Emons, 1991). The most striking texture is the helicoidal cell wall texture, which consists of subsequent lamellae in which the orientation of the CMFs is shifted by a constant angle. Figure 1.1 (F) shows cellulose microfibrils with different orientations in three subsequent lamellae of the helicoidal cell wall of an *E. hyemale* root hair. Other wall textures are the axial, helical, crossed-polylamellate, transverse and the random wall textures and combinations of these. These names refer either to the relative orientation of the CMFs with respect to each other or to

their absolute orientation with respect to the long axis of the cell.

How is the biogenesis of wall textures regulated from within the cell? As mentioned earlier, CMFs are produced by CSCs, and it is by now widely assumed that these CSCs are propelled through the membrane by the force of the cellulose production itself, combined with the force that is generated by attachment of the nascent CMF to other cell wall components as soon as they are produced. CMFs are stiff, but have been seen to bend around pit fields (Mueller and Brown Jr., 1980), showing that their intrinsic orientation of deposition can be over-ruled by mechanical obstacles. The CSCs indeed move in straight lines inside the plasma membrane in etiolated *Arabidopsis* hypocotyl epidermis cells, and the direction of movement of the CSCs appears to be forced upon them by cortical microtubules (Paredez et al., 2006), which are potential obstacles they encounter in their plane of movement (Emons et al., 2007). Cortical microtubules could be over-ruling the self-orientation mechanism of CSCs in all elongating cells. They ensure that CMFs are aligned consistently across the growing *Arabidopsis* root (Baskin, 2001).

When the microtubules are completely depolymerized, the complexes move inside the plasma membrane in ordered patterns as well (Paredez et al., 2006). In addition, examples are known of non-parallel cortical microtubules and CMFs in secondary wall deposition, that is wall thickening after cell elongation (Emons et al., 1992). The ordering of cellulose microfibrils during their deposition in such cells has been explained with a geometrical model (Emons, 2006; Emons and Mulder, 1998; Mulder and Emons, 2001). This model provides a conceptual framework for the alignment mechanism of CMFs, which departs from the situation where cortical microtubules are not parallel to nascent CMFs. The basic assumption is that by default, CMFs go straight unless obstructed and that their alignment depends mainly on the number of CSCs simultaneously active at any position in the plasma membrane. Of course, this model does not rule out that cortical microtubules bind to the plasma membrane so tightly that synthase movement is obstructed (Emons et al., 2007). In addition, other work in which cellulose synthase and drugs against microtubules, and relevant mutants of *Arabidopsis*, were used does not point to a simple one-on-one relationship between the orientations of the two sets of polymers at both sides of the plasma membrane (Himmelspach et al., 2003; Sugimoto et al., 2003).

Despite these exceptions, and the, as yet, unexplained occurrences of incongruent CMFs and cortical microtubules, the work of Paredez et al. (2006) with CSCs and microtubules fluorescently labelled in the same cells, has made it clear that cortical microtubule orientation is an important regulator of CMF orientation, at least in epidermis cells of elongating etiolated *Arabidopsis* hypocotyls, and maybe in all elongating plant cells. This begs the question of how the cortical microtubules themselves are being organized.

1.7 Cortical microtubules

In inter-phase plant cells, microtubules are localized in the cortex, just underneath the plasma membrane (Ledbetter and Porter, 1963; Hepler and Newcomb, 1964). Figure 1.1(E) shows the typical close connection of microtubules to the plasma membrane in a root hair of *Vicia sativa*. Although they are indirectly linked to the plasma membrane, they are at the same time dynamic (Hardham and Gunning, 1978; Wasteneys, 2002; Shaw et al., 2003; Vos et al., 2004; Hirase et al., 2006; Debolt et al., 2007a). They behave according to a hybrid treadmilling mechanism; their minus ends mostly pausing or shrinking and their plus ends alternating between growing and shrinking phases (Shaw et al., 2003). For this behaviour, the properties of dynamic instability must be carefully regulated through the interaction with microtubule-associated proteins (MAPs). For example, during G2/prophase, the microtubules become more dynamic and possibly longer by means of a hypothetical search and capture mechanism that helps the formation of the pre-prophase band (Vos et al., 2004). Overexpression or knock out of a MAP can have severe effects. Typically, in such mutants, for example *emphmor1-1*, *katanin* and *wvd*, inter-phase cortical microtubules no longer organize perpendicularly to the growth axis of the cell, and the cells expand isotropically (Whittington et al., 2001; Burk and Ye, 2002; Yuen et al., 2003). The details of the mechanisms by which these MAPs determine the microtubule organization are largely unknown, but it could be that they control the stability and length of the microtubule and that these parameters in turn are essential for a self-organization mechanism that is based on microtubule-microtubule interactions.

So far, two distinct behaviours of cortical microtubules have been observed: zippering and catastrophic collisions (Dixit and Cyr, 2004). A microtubule that runs into another microtubule at a small angle ($<40^\circ$) will alter its direction of polymerization and become bundled with it in a parallel or antiparallel fashion. When the polymerizing microtubule collides with a pre-existing one at a larger angle ($>40^\circ$), the microtubule has a heightened chance of having a catastrophe: a switch from growing to shrinking. From this result, we can deduce that the unusually few, short or stable microtubules in several MAP mutants have fewer interactions with each other and therefore cannot align with each other. Nevertheless, although these two mechanisms together can align microtubules, they cannot dictate the direction of alignment.

We have shown, based on theoretical considerations and in vitro work, that microtubules can also change their direction by being bent and by polymerizing along the inner walls of (artificial) cells (Lagomarsino et al., 2007). However, confinement within the cell alone cannot organize the microtubules perpendicularly to the growth axis of the cell; rather the bending rigidity dictates the microtubules to become longitudinally arranged. This indicates that other, so far unknown, microtubule-microtubule interacting mechanisms must be at work to organize the microtubule array, or that the alignment perpendicular to the elongation axis of the cell is dependent on other, for example microtubule-plasma membrane mechanisms.

Chan et al. (2007) showed that domains of aligned microtubules move through the cortex of growing hypocotyl cells. The domains move and pivot a full 360° , on their way running into each other, splitting themselves or absorbing neighbouring domains. Whether or not these movements also occur in other cell types has not been shown yet, nor is it known if there is a relation between the moving domains and the formation of the helicoidal cell wall texture of CMFs. It is clear though that cortical microtubules do not exert a direct orienting influence on CMFs, but rather that they influence the path of the CSCs (Paredes et al., 2006). These complexes stick out below the plasma membrane into the cytoplasm where the cortical microtubules are located and which may act as tracks or as guard rail (Emons et al., 2007). The hypothesis that microtubules are ordered through a regulated cortical microtubule self-organization mechanism is still valid and the focus of research in several groups.

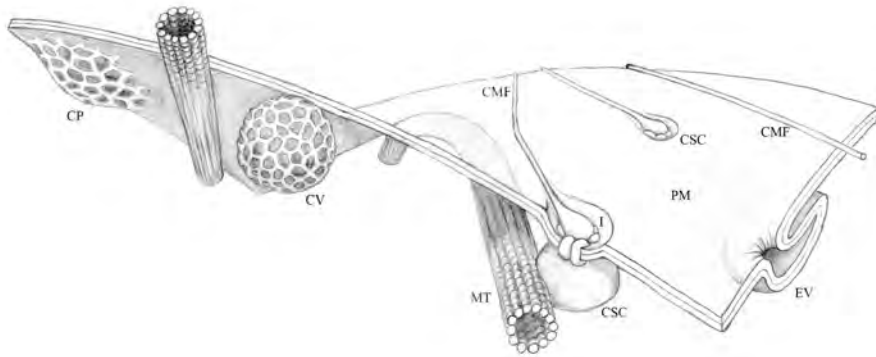


Figure 1.2: Schematic drawing of structures at the plant plasma membrane of plant cells involved in cell wall synthesis. In the drawing, the plasma membrane has been curled up in order to show both of its sides. CMF, cellulose microfibril; CP, coated pit; CSC, cellulose synthase complex; CV, coated vesicle; EV, exocytosis vesicle; I, indentation in the membrane at the site of cellulose microfibril production; MT, microtubule; PM, plasma membrane. (Drawing made by Giel van der Linden, Wageningen)

1.8 Activity at the plasma membrane

From the above, it is clear that cellulose deposition into the plant cell wall is a space-time process that involves a number of concurrent activities, all localized to a small area bordering the plasma membrane. In a drawing (Figure 1.2), we show the relevant structures occurring at the plasma membrane involved in the process of cellulose

production. Exocytosis delivers new CSCs to the plasma membrane, at the same time depositing other wall polymers, whereas concomitant endocytosis recycles the excess membrane area created by the exocytosis. The CSCs, once inserted into the plasma membrane, move in the plane of the membrane, driven forward by the energy released in the cellulose polymerization process, leaving a CMF in their wake. The cortical microtubule network, which itself is dynamically self-assembled from its component parts, seems to play a role in regulating the motion of the CSCs, possibly by guiding their direction of motion. Understanding how these local activities are coordinated to produce textured cell walls that show spatially coherent patterns over many micrometer (Emons et al., 2007), in our opinion, requires a systems biological approach, in which the known biochemical, biophysical and cell biological data are integrated into mathematical models. We believe that only the detailed, quantitative, predictions that follow from such models will enable us to effectively select and design experiments aimed at unravelling the complex, collective, effects that underpin cell wall formation.

1.9 Acknowledgements

A.M.C.E. thanks the FOM Institute for Atomic and Molecular Physics (AMOLF), Amsterdam, for financial support for this project. This work was co-funded through EU grant 028974 CASPIC (JL, BM, AMCE). T.K. and J.V. were supported by VENI fellowships 863.04.003 and 863.02.009, respectively, from the Dutch Science Foundation (NWO). The work of B.M. is part of the research program of the ‘Stichting voor Fundamenteel Onderzoek der Materie (FOM)’, which is financially supported by the NWO.

2

Cortical microtubule array initiation

2.1 Abstract

The ordered arrangement of cortical microtubules in growing plant cells is essential for anisotropic cell expansion and hence for plant morphogenesis. These arrays are dismantled when the microtubule cytoskeleton is rearranged during mitosis and reassembled following completion of cytokinesis. The reassembly of the cortical array has often been considered as initiating from a state of randomness, from which order arises at least partly through self-organizing mechanisms. However, some studies have shown evidence for ordering at early stages of array assembly. To investigate how cortical arrays are initiated in higher plant cells, we performed live cell imaging studies of cortical array assembly in tobacco BY-2 cells after cytokinesis and drug-induced disassembly. We found that cortical arrays in both cases initiated non-randomly, but with significant over-representation of microtubules at diagonal angles with respect to the cell axis. A bias that simulation studies indicated could account for the observed evolution of array ordering. Surprisingly, during initiation only about half of the new microtubules were nucleated from locations marked by GFP-GCP2 tagged gamma-nucleation complexes (γ -TuRC), therefore indicating that a large proportion of early polymers was initiated by a non-canonical mechanism not involving γ -TuRC. Consistent with this observation, simulation studies indicate that the initial diagonal ordering of the cortical array is not a barrier to array organization, but rather, that the high rate of non-canonical initiation of new microtubules has the potential to accelerate the rate of array re-population.

2.2 Introduction

Higher plant cells feature ordered arrays of microtubules at the cell cortex (Ledbetter and Porter, 1963) that are essential for cell and tissue morphogenesis, as revealed

by disruption of cortical arrays by drugs that cause microtubule depolymerization (Green, 1962) or stabilization (Weerdenburg and Seagull, 1988), and by loss of function mutations in a wide variety of microtubule associated proteins (MAPs) (Baskin, 2001; Whittington et al., 2001; Buschmann and Lloyd, 2008; Lucas et al., 2011). The structure of these arrays is thought to control the pattern of cell growth primarily by its role in the deposition of cellulose microfibrils, the load-bearing component of the cell wall (Somerville, 2006). Functional relations between cortical microtubules and cellulose microfibrils have been proposed since the early sixties, even before cortical microtubules had been visualized (Green, 1962). Recent live cell imaging studies have confirmed that cortical microtubules indeed guide the movement of cellulose synthase complexes that produce cellulose microfibrils (Paredes et al., 2006) and have shown further that microtubules position the insertion of most cellulose synthase complexes into the plasma membrane (Gutierrez et al., 2009). These activities of ordered cortical microtubules are proposed to facilitate the organization of cell wall structure, creating material properties that underlie cell growth anisotropy.

While organization of the interphase cortical array appears to be essential for cell morphogenesis, this organization is disrupted during the cell cycle as microtubules are rearranged to create the preprophase band, spindle and phragmoplast during mitosis and cytokinesis (reviewed by Wasteney, 2002). Upon completion of cytokinesis, an organized interphase cortical array is regenerated, but the pathway for this reassembly is not well understood.

The plant interphase microtubule array is organized and maintained without centrosomes as organizing centers (reviewed in Wasteney (2002), Bartolini and Gunderson (2006) and Ehrhardt and Shaw (2006) and microtubule self-organization is proposed to play an important role in cortical microtubule array ordering (Dixit and Cyr, 2004). In electron micrographs microtubules have been observed to be closely associated with the plasma membrane (Hardham and Gunning, 1978) and live cell imaging provides evidence for attachment of microtubules to the cell cortex (Shaw et al., 2003; Vos et al., 2004). The close association to the plasma membrane restricts the cortical microtubules to a quasi two-dimensional plane where they interact through polymerization-driven 'collisions' (Dixit and Cyr, 2004). Microtubule encounters at shallow angles (< 40 degrees) have a high probability of leading to bundling, while microtubule encounters at steeper angles most likely result in induced catastrophes or microtubule crossovers (Dixit and Cyr, 2004). Several computational modeling studies have since shown that these types of interactions between surface-bound dynamical microtubules can indeed explain spontaneous co-alignment of microtubules (Allard et al., 2010b; Eren et al., 2010; Hawkins et al., 2010; Tindemans et al., 2010).

The question of how the orientation of the cortical array is established with respect to the cell axis is less well understood. One possibility is that microtubules are selectively destabilized with respect to cellular coordinates (Ehrhardt and Shaw, 2006). Indeed, recent results from biological observations and modeling suggest that catastrophic collisions induced at the edges between cell faces, or heightened catastrophe rates in cell caps could be sufficient to selectively favor microtubules

in certain orientation and hence determine the final orientation of the array (Allard et al., 2010b; Eren et al., 2010; Ambrose et al., 2011; Dhonukshe et al., 2012).

To date, all models of cortical array assembly assume random initial conditions. However, experimental work by Wasteneys and Williamson (1989a, b) in *Nitella tasmanica* showed that, during array reassembly after drug-induced disruption, microtubules were initially transverse. This was followed by a less ordered phase and later by the acquisition of the final transverse order. A non-random initial ordering was also observed in tobacco BY-2 cells by Kumagai et al. (2001), who concluded that the process of transverse array establishment starts with longitudinal order, but did not provide quantitative data for the process of array assembly. The initial conditions for the cortical microtubule array formation are important to consider, as they may strongly influence the speed at which order is established, and could even prevent it from being established over a biologically relevant time scale.

In the present study, we used live cell imaging to follow and record the whole transition from the cortical microtubule-free state to the final transverse array and used digital tracking algorithms to quantify the microtubule order. Nucleation stands out as a central parameter to define during array initiation. Lacking a central body to organize nucleation complexes, the higher plant cell has nucleation complexes Wasteneys and Williamson (1989a,b); Chan et al. (2003); Shaw et al. (2003); Murata et al. (2005); Pastuglia et al. (2006); Nakamura et al. (2010). Therefore we performed high time resolution observations to quantify nucleation complex recruitment, nucleation rates and microtubule nucleation angles. We found evidence for a highly non-random initial ordering state that features diagonal microtubule orientation and an atypical microtubule initiation mechanism. Simulation analysis indicates that these atypical nucleations have the potential to accelerate the recovery of cortical array density.

2.3 Results

2.3.1 After cytokinesis, microtubules reappear with a transient diagonal order

To investigate array initiation, we used tobacco Bright Yellow 2 (BY-2) suspension cells expressing GFP fused to tobacco γ -Tubulin (GFP-TUA). These cells feature highly ordered arrays oriented transversely to the axis of growth, have a relatively high mitotic index, and are ideal for drug treatment in flow cell experiments. Furthermore, the potential crosstalk with neighbors is limited because BY-2 cells generally grow in cell files that break up into individual cells Chan et al. (2011); Crowell et al. (2011); Fujita et al. (2011).

Using point-scanning confocal microscopy, we acquired images from the plane of the cell cortex every 3-5 minutes and measured microtubule length density and ordering after cytokinesis. The first visible microtubules appeared in the cortex after the phragmoplast reached the optical plane of the cell cortex (Figure 2.1a, Figure S2.1

and Movie S1) and within 45 minutes the length density, defined as microtubule length per square micrometer, leveled at around $0.5 \mu\text{m}/\mu\text{m}^2 (= \mu\text{m}^{-1})$, mean of 6 cells; Figure 2.1b). With the increase in length density, the microtubules also became increasingly bundled, as indicated by increases in the fluorescence intensities of individual microtubule structures. As our focus was on microtubule orientation, we treated bundles the same as individual microtubules.

The angles of microtubules with respect to the cell elongation axis were measured and visualized in a contour plot (Figure 2.1c). Time is presented along the x-axis and the angular distribution over the interval from 0° to 180° along the y-axis (20 bins). The color range represents the fraction of the total microtubule length, so that orientation patterns at both low and high microtubule densities can be compared. Surprisingly, the majority of the microtubule length was diagonally oriented at 45° and 135° angles to the elongation axis in the early stages of array reformation, forming two clear peaks in the angular frequency histogram.

To quantify the transition from the diagonal to the transverse cortical microtubule order, the angular distribution data were filtered to produce the weighted diagonal order parameter D and the weighted transverse order parameter T (see Supplementary Information). From the means of the D and T order parameters over time, we infer that the diagonal ordering was dominant for the first 25 minutes after which it was replaced by transverse ordering (Figure 2.1d).

2.3.2 Transient diagonal ordering during recovery from oryzalin treatment

To establish if the mechanism of transverse microtubule ordering via a transient diagonal phase is generic or cell cycle dependent, we immobilized BY-2 cells expressing GFP-TUA in flow cells and treated them for 1 hour with $20 \mu\text{M}$ oryzalin to reversibly depolymerize the cortical microtubule array Morejohn et al. (1987) (Figure 2.2a and Movie S2). This concentration and duration of oryzalin treatment was sufficient to eliminate all detectible GFP-TUA labeled microtubules. Both the microtubule length density increase and the development of ordering after oryzalin wash out were similar as observed after cell division (Figure 2.2b). The average plateau density was reached 25 minutes after appearance of the first cortical microtubules, which is 45 minutes after the start of the oryzalin wash out (mean of 8 cells). The first microtubules reappeared at diagonal angles to the elongation axis (45° and 135° ; Figure 2.2c). On average, the transient diagonal ordering was replaced by the final transverse ordering after 40 minutes (Figure 2.2d). Thus, it appears that both the pattern and kinetics of assembly and ordering are similar whether the array is disassembled by native mechanisms during the cell cycle, or by drug treatment.

2.3.3 Diagonal ordering also occurs during array disassembly

Interestingly, a diagonal bias for microtubule orientation was also observed during late stages of array disassembly as cells exit interphase and form preprophase bands

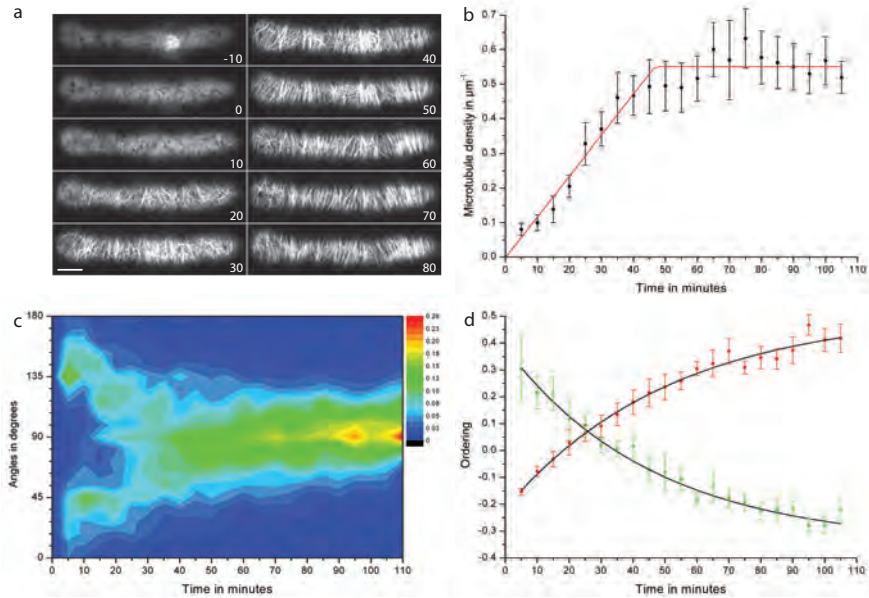


Figure 2.1: Return of cortical microtubules after cell division in BY-2 cells. (a) Cortical microtubules in two daughter cells after cytokinesis. The first frame (T_{-10} minutes) shows the late phragmoplast in the cortex. Time is indicated in minutes, scale bar is $10 \mu\text{m}$. (b) Microtubule length density increase over time after cytokinesis (mean of 6 cells). The mean density plateaus at $0.54 \mu\text{m}^{-1}$ and is reached after 46 minutes, based on linear curve fitting of the individual data points of 6 cells (red line). Bars represent standard error (SE). (c) Angular distribution over time presented as the fraction of the total microtubule length at each measurement (mean of 6 cells). The first microtubules are ordered along the diagonal cell axes of 45° and 135° . (d) Diagonal (green circles) and transverse (red squares) microtubule order parameters, D (green error bars) and T (red error bars), after cell division (means of 6 cells \pm SE) and the exponential curve fittings (black lines, based on all individual data points). At 25 minutes after T_0 (last measurement before microtubules became visible) the transverse microtubule ordering became dominant over the diagonal microtubule order.

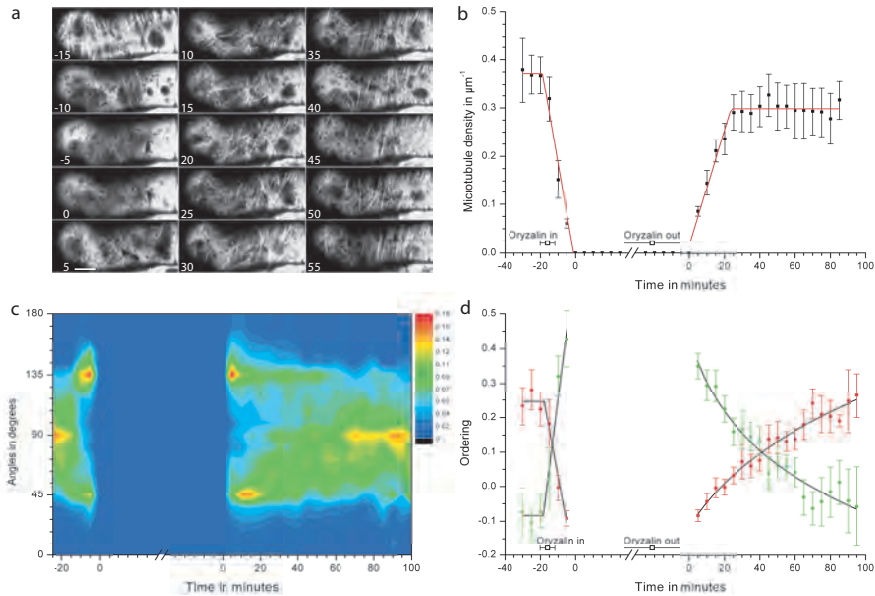


Figure 2.2: Treatment of GFP-TUA expressing BY-2 cells with oryzalin. (a) Cortical microtubules before, during and after incubation with 20 μM oryzalin in a flow cell. Oryzalin was added at T_{-15} minutes and washed out again after 60 minutes by continuous washing with BY-2 culture medium. Scale bar is 10 μm . (b) Microtubule length density in oryzalin treatment over time (mean of 8 cells). The individual cells of the oryzalin treatments were aligned relative to the observation point at which no microtubules were visible after oryzalin addition, and to the point at which no microtubules were yet visible after oryzalin wash out. Both are referred to as T_0 in the text and figures. Imaging was continued during depolymerization and all images were checked for microtubules. At -16 ± 2 minutes (mean \pm SE), 20 μM oryzalin was added and washed out again after 60 minutes. About 21 ± 6 minutes (mean \pm SE) after oryzalin washout, the first cortical microtubules started to reappear. (c) Averaged angular distribution over time presented as the fraction of the total microtubule length at each measurement (mean of 8 cells). Just after addition of oryzalin at the start of recovery after wash out, diagonal microtubules are dominant. (d) Diagonal and transverse cortical microtubule ordering parameters, D (green error bars) and T (red error bars), over time in oryzalin treatment experiments (means of 8 cells \pm SE). Less than 2 minutes after oryzalin addition, D (green circles) became dominant over T (red squares) based on the intercept of the linear curve fittings of the individual data points (black lines). After oryzalin wash out, diagonal ordering became apparent and remained dominant for 36 minutes, based on the intercept of the exponential curve fittings (black lines), followed by dominance of the transverse microtubule array.

(Figure S2.2). Likewise, the same bias was observed in late stages of microtubule depolymerization caused by oryzalin application (Figure 2.2c and d). The microtubule length density started to decrease less than a minute after drug application and reached zero microtubules after 16 minutes. Within 2 minutes after oryzalin addition, a diagonal microtubule order took over the dominant transverse order and lasted until the last microtubules were depolymerized (Figure 2.2d). Thus diagonal biasing of microtubule orientation appears to be a feature both of the last stages of array disassembly and the first stages of array re-assembly, whether arrays are taken apart by cellular mechanisms or by drug treatment.

2.3.4 Microtubule nucleation has a diagonal bias during array initiation

A bias in microtubule orientation might occur because microtubules are preferentially created in specific orientations, or because they are selectively destabilized, or if they are reoriented once initiated. To assess the origin of the diagonal microtubule ordering, we made movies at high time resolution (2s intervals) of BY2 cells expressing GFP-TUA cytokinesis and oryzalin wash out (Movie S3). We observed that in the first 30 minutes the majority of new microtubules were nucleated at the cell cortex at locations free of other detectable microtubules. In fact, the majority of nucleations during this period were free nucleations (274 out of 352, 77%, in 6 cells after cytokinesis, and 73 out of 117, 62%, in 5 cells after oryzalin wash out). These observations are in contrast to those of interphase nucleation, where microtubule-associated microtubule nucleations have been observed to comprise greater than 99% of nucleations in wild type *Arabidopsis* cells Murata et al. (2005); Nakamura et al. (2010); Kirik et al. (2012). We measured the angles of these free nucleations with respect to the cell axis after both cytokinesis (Figure 2.3a) and oryzalin wash out (Figure 2.3b). We did not analyze microtubule nucleations in the same orientation as the microtubule they nucleated on, as they do not give rise to new microtubule orientations. A Bayesian statistical analysis of these data (see Materials and Methods) revealed a significant bias for nucleations to occur along the diagonal directions both after cytokinesis and oryzalin wash out.

2.3.5 A large fraction of nucleations during array initiation are free of labeled γ -tubulin complexes

We found it remarkable that the nucleation bias had the same orientation as the cortical microtubule order just before disappearance. This suggested that a ‘memory’ of the previous array organization might be maintained at the cell cortex. We could imagine three alternative models. First, nucleation complexes recruited to the previous array might persist at the cell cortex, retaining orientational information. Second, there might be other orientational information at the cell cortex that acts to orient newly recruited nucleation complexes as they initiate the next array. Finally, a subset

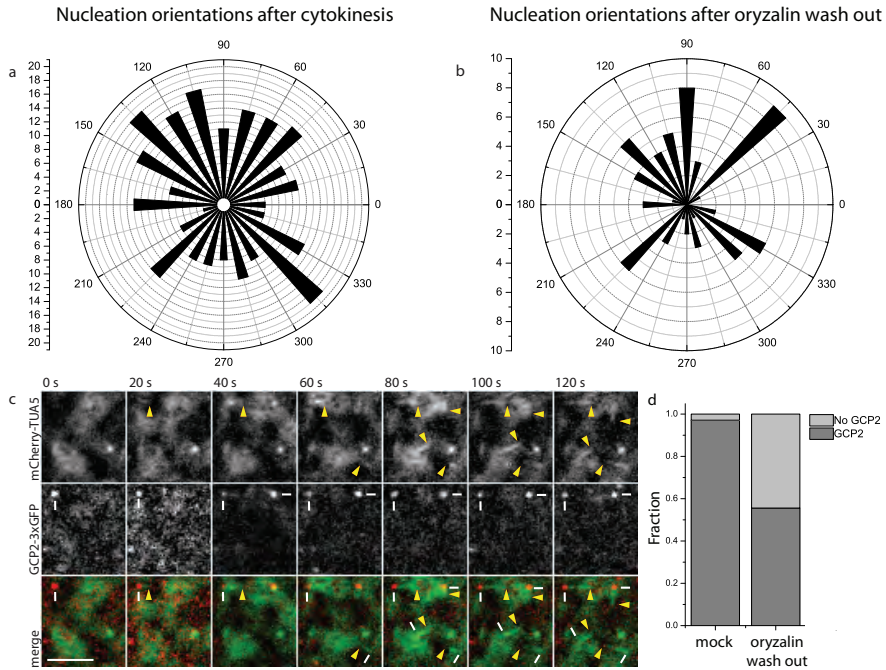


Figure 2.3: Free nucleations after cytokinesis and oryzalin wash out. (a and b) Polar histogram nucleation angles within the 30 minute period after the first cortical microtubules appear after cytokinesis in tobacco BY-2 cells (274 nucleations, 6 cells) (a) and oryzalin wash out (117 nucleations in 5 cells) (b). Angles in degrees, histogram scale is in number of observations. (c) Example of free nucleations after oryzalin wash out in *Arabidopsis* root epidermal cells. Dashes indicate microtubule minus-ends, arrowhead indicate microtubule plus-ends. Two out of four nucleations in this image sequence show a GCP2-3xGFP signal. Scale bar is 3 μm . (d) Bar graph of the fraction of nucleations where GCP2-3xGFP signal was detected or not. Results are shown for untreated cells *Arabidopsis* root epidermal cells (70 nucleations) and after oryzalin wash out (81 nucleations).

of the previous array might be resistant to disassembly either by native mechanisms or by drugs, and they may be either small enough (or be of altered alpha tubulin isoform composition) to evade detection by GFP-TUA6 labeling. These disassembly-resistant remnants might act as orientated seeds for initiating new polymerization during array reassembly.

To distinguish among these hypotheses, we assayed the localization and dynamic behavior of γ -tubulin complexes and their relationship to new nucleations using *Arabidopsis* plants expressing both a γ -tubulin complex marker (GCP2-3xGFP, Nakamura et al., 2010) and a compatible tubulin marker (mCherry-TUA5, Gutierrez et al., 2009, see Movie S4). To facilitate our analysis, we used a 1 hr treatment of 20 μ M oryzalin to disassemble existing cortical arrays. After drug washout, we acquired images of the cell cortex at high time resolution (2s intervals). We observed no evidence for persistent GFP-labeled nucleation complexes at the cell cortex, thus refuting the first hypothesis; that nucleation complexes recruited to the previous array might persist at the cell cortex to initiate the new array.

We then scored all observed nucleation events in the field of view, asking if GCP2-3xGFP was present at the position of microtubule nucleation. As labeled complexes are present and motile in the streaming cytosol Nakamura et al. (2010), we required that punctae GFP signal be present at the position of nucleation for at least two consecutive image frames to be scored positively. In control cells that were not pretreated with oryzalin, we found that 68 out of 70 nucleations (97%) colocalized with the GCP2-3xGFP label (Figure 2.3c and Movie S5, data acquired from 6 cells on 6 plants), a frequency in good agreement with the 98% found by Nakamura et al. (2010) in hypocotyl cells. By contrast, in oryzalin treated cells, only a little over half of the observed nucleations (45 out of 81, 56%) colocalized with the GCP2-3xGFP label in the first 20 minutes after the start of oryzalin wash out, a dramatically lower proportion ($p \ll 0.0001$, one-tailed binomial test, 8 cells). Thus, while only 3% of nucleations was not observed to be accompanied by GCP2-3xGFP in mature arrays, this frequency raised to 44% during early stages of array assembly (Figure 2.3d). The lack of detectable γ -TuRC label at nearly half of the early nucleations argues strongly against the second hypothesis for diagonal nucleation orientation; that orientational information at the cell cortex directs the orientation of new nucleation complexes recruited to the cell cortex during early array assembly. We also found no evidence for involvement of two candidates for such orientational information, the cortical actin cytoskeleton and cellulose microfibrils, by disruption experiments with latrunculin B or isoxaben (Figure S2.3).

On the other hand, the marked reduction in GCP2-3xGFP co-localization was consistent with the third hypothesis; that a large and significant proportion of nucleations during early array recovery arise from seeds not associated with γ -tubulin complexes. We term these nucleation events non-canonical nucleations because they lack association with detectible γ -TuRCs as determined by GCP2-3xGFP labeling, an essential subunit of the core γ -TuRC.

2.3.6 Simulations

We performed mechanistic simulations to ask if the observed prevalence of diagonal microtubule nucleation was sufficient to explain the degree of observed diagonal ordering during the initial stages of array assembly and to ask what affect these non-canonical nucleations might have on the evolution of array density and ordering. In the simulations, cortical microtubules interact on a cylindrical cell-shaped surface of dimensions similar to that of the tobacco BY-2 cells used in our *in vivo* experiments (Figure 2.4a) Tindemans et al. (2010); Deinum et al. (2011). To test for the influence of the non-canonical nucleation events, these nucleations were treated as a separate class, their density and orientations was chosen to match the distributions determined from the live cell experiments (see the Materials and Methods section for further details on the simulation technique and the parameters employed). In simulations that include all nucleation events the length density initially rises steeply, reaching 80% of the final density in just 10 minutes, then transiently leveling off (Figure 2.4b and illustrated in Figure 2.4a at 15 min.). By contrast, in simulations without the non-canonical nucleation class, the length density rises more gradually and steadily, reaching 80% of the final density only after about 40 minutes (Figure 2.4b). Thus, the non-canonical nucleations appear to have the potential to significantly accelerate the recovery of array density during array re-assembly.

When simulations were run without the non-canonical nucleation class there was no initial bias of the angular distribution (Figure 2.4c). As expected, when these nucleations were added to the simulation, a clear initial bias at 45 and 135 degrees is created (Figure 2.4d), markedly similar to our experimental observations (Figure 2.1c). The diagonal and transverse order parameters D and T as a function of time for the simulations with the non-canonical nucleation class (Figure 2.4e) both qualitatively and quantitatively match the values we found experimentally (Figure 2.1d). Thus, the inclusion of the diagonally biased nucleation events observed in living cells have the potential to explain both the initial diagonal ordering and the observed evolution of array ordering in these cells. While non-canonical nucleations had the effect of lowering the initial transverse ordering state of the simulated arrays, the difference is not significant and the order parameters level off to the same value (Figure 2.4f), indicating that biased non-canonical nucleations did not present a barrier to array ordering.

2.4 Discussion

The transverse arrangement of the cortical microtubule array is essential for anisotropic growth, yet little was known about how it arises from a disassembled state, a situation that arises at each cell division during the life of the cell. The currently accepted self-organization models for transverse cortical microtubule array establishment, based on microtubule interactions (Allard et al., 2010b; Eren et al., 2010; Hawkins et al., 2010; Tindemans et al., 2010), assume random initial conditions. We found that

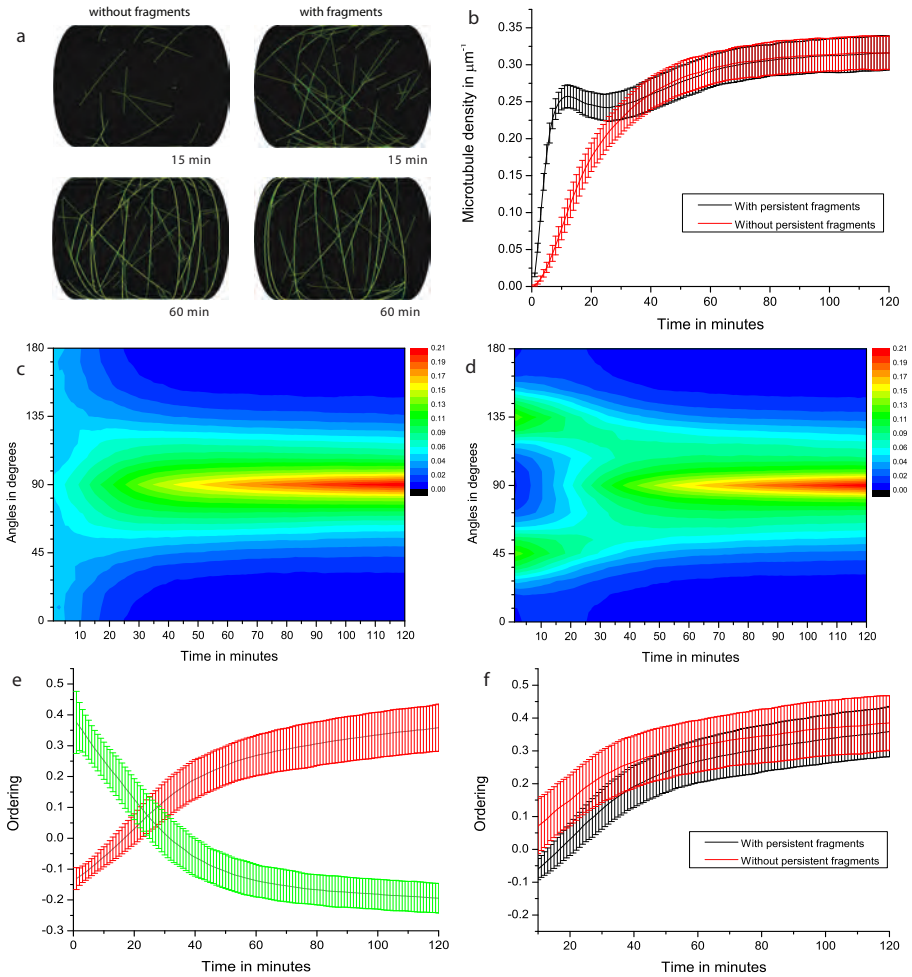


Figure 2.4: Results of the simulations. (a) Snapshots of representative microtubule configurations at 15 and 60 minutes after the start of the simulation both with (right) and without (left) persistent fragments. (b) The time evolution of the average diagonal D (green error bars) and transverse T (red error bars) cortical microtubule ordering parameters. The gray lines represent the average value and the error bars represent one standard deviation. (c and d) Averaged angular distribution over time presented as the fraction of the total (optical) microtubule length from simulations without (c) and with (d) persistent microtubule fragments. (e). The time evolution of the average (optical) density of microtubules for the simulations with and without persistent fragments, error bars show standard deviation. (f) All simulation results are combined for 500 individual simulations.

the first microtubules in new arrays of tobacco BY-2 cells were in fact not randomly oriented but showed significant ordering, at orientations of both 45 and 135 degrees. This was true both for array assembly during the cell cycle as well as reassembly of arrays after oryzalin washout. Organization in these arrays did not evolve by gradual ordering from a disorganized, random state, but by a transition from one ordered state to another.

Exploration of the cause for the non-random initiation of array establishment revealed that there was a significant bias in the orientation of early microtubule nucleations, sharing the same 45° and 135° bias relative to the cell axis that was observed for array ordering. Results from simulation studies incorporating these oriented nucleations matched experimental observations very closely, indicating that this population of directionally biased nucleations is sufficient to explain the fast-forming initial diagonal ordering state of new arrays, and together with self-ordering based on microtubule interactions, is sufficient to explain the transition from this array into the final transverse array.

We considered several alternative ideas for the mechanism of nucleation orientation. In interphase cells, the majority of nucleations at the cell cortex occurs from the sides of existing microtubules with a major peaks at about 40° Murata et al. (2005) and a secondary peak at 0° (parallel to the mother polymer) Chan et al. (2003); Nakamura et al. (2010); Kirik et al. (2012). Thus, in the interphase arrays studied to date existing microtubules largely determine the orientation of new microtubule nucleation. The vast majority of the nucleation events occur at gamma tubulin nucleation complexes as visualized with tagged components of the core complex (>98%, Nakamura et al., 2010; Kirik et al., 2012). However, at the start of array assembly there are no obvious existing microtubules (this study, Wasteney and Williamson, 1989, 1989) to recruit and position nucleation complexes Nakamura et al. (2010), therefore it was necessary to consider other mechanisms for nucleation orientation. One possibility was that oriented γ -TuRC complexes are simply retained at the cell membrane from the previous cortical array, an idea that was contradicted by our observation that γ -TuRCs in *Arabidopsis* root cells were not retained at the cell cortex from the previous array. A second possibility was that newly recruited γ -TuRCs are positioned by cryptic orientational information at the cortex. Surprisingly, however, we found that labeled γ -TuRC complexes failed to be detected at 44% of the nucleation events observed during array initialization compared to 3% at steady state microtubule density. This result both effectively eliminated a mechanism based solely on oriented γ -TuRCs and revealed that many early nucleations apparently arise from non-canonical nucleation sites that lack a γ -TuRC.

The above results, together with the observation that cortical microtubules were oriented diagonally not only during the buildup of the cortical microtubule array but also during the last stages of breakdown during oryzalin treatment and preprophase band formation, were consistent with a third possible mechanism - that segments of the previous array survive or are resistant to disassembly, whether by oryzalin or by native mechanisms during mitosis. Segments that could then act as oriented seeds that participate in initiation of the next array. Consistent with the

idea of disassembly-resistant microtubule seeds, deactivation of γ -tubulin complexes in several organisms does not abolish all microtubule nucleation *in vivo* (reviewed by Job et al., 2003) and nucleation free of γ -TuRCs is well known to occur *in vitro* at high enough concentrations of free tubulin dimers Fygenon et al. (1994). Previous studies by Wasteneys and Williamson (1989b) in *Nitella* are also consistent with this possibility. These investigators observed that while *Nitella* microtubules returned in their original transverse orientation during recovery from oryzalin, orientation was random after longer, and presumably more complete, oryzalin treatment (Wasteneys and Williamson, 1989, 1989). In our studies, incomplete drug action cannot explain observations of array re-assembly following cytokinesis, since there was no drug treatment in these cells and the extremely similar mode and kinetics of array reassembly we observed between these cells and those recovering from oryzalin treatment suggest that similar mechanism are responsible in both situations.

If the latter hypothesis is true, a couple of puzzles remain. First, microtubule seeds from the previous cell cycle were not readily detected by imaging of GFP-TUA. However, this might be easily explained if the seeds are small enough to contain only a few labeled subunits (only a portion of alpha subunits in the cell are tagged), a degree of labeling that may well lie below the high background of unpolymerized subunits in the cytosol. It is also formally possible that the seeds may have a composition that does not include the labeled tubulin isoform used for imaging. A second puzzle is why the presumed source of the oriented seeds - the last cohort of microtubules at the end of array disassembly - has a diagonal bias to the cell axis. One possibility is that the bias arises from the normal formation of the newest microtubules by branching nucleation at about 40 degrees to their mother polymers Wasteneys and Williamson (1989a,b); Murata et al. (2005); Chan et al. (2009); Nakamura et al. (2010). In a transversely oriented array, these nucleations would lie approximately at 45 μ m and 135 μ m to the cell axis, and would have a high likelihood of interacting with the dominant population of transverse microtubules. These interactions can lead to incorporation into bundles by treadmilling motility Shaw et al. (2003); Dixit and Cyr (2004), or catastrophe (Dixit and Cyr (2004), both of which would tend to diminish the population of diagonally oriented polymers. However, as the microtubule array is broken down and microtubule density drops, encounters would be predicted to be less frequent and therefore the likelihood of aligning or eliminating branching microtubules will be reduced.

Whether the source of oriented nucleation in early array assembly is due to seeds from the previous array or another mechanism, our observations reveal the existence of a substantial class of non-canonical nucleations not associated with γ -TuRCs that contribute to the initiation of the cortical array. In simulation studies we explored how these non-canonical nucleations may affect array reassembly and found this class of oriented nucleations to have the potential to significantly accelerate recovery of array density without significantly impeding the acquisition of ordering driven by microtubule interactions. The existence of this mechanism may address a fundamental dilemma the plant cell faces in rebuilding an array from scratch. In interphase cells, nucleation from γ -TuRC complexes was observed to be approximately 10-fold

more likely when they are localized to microtubules than to other locations at the cell cortex Nakamura et al. (2010). If this reflects a fundamental property of γ -TuRC activation, then the cell may face limitations in how fast it can initiate new arrays when there are no existing cortical microtubules to recruit γ -TuRCs and contribute to their activation. Our live cell observations and simulation studies reveal a class of nucleations that do not require γ -TuRC recruitment and activation at cortical microtubules may act as a primer to accelerate the assembly of the new array.

2.5 Materials and methods

2.5.1 Plant material

Tobacco (*Nicotiana tabacum* L.) Bright Yellow-2 (BY-2) suspension cultured cells were grown according to standard protocols (Nagata et al., 1992). We stably transformed BY-2 cells using *Agrobacterium tumefaciens* LBA4404 mediated procedures with a reporter construct consisting of the enhanced green fluorescent protein fused to tobacco α -tubulin (sGFP-TUA) under control of the CaMV 35S promoter, kindly provided by Dr. S. Hasezawa, University of Tokyo, Japan (Kumagai et al., 2001). The BY-2 cell line expressing eGFP-FABD was generously provided by Dr. T. Ketelaar (Wageningen University) Ketelaar et al. (2004). We used *Agrobacterium tumefaciens* to transform the pGCP2-GCP2-3xGFP construct, kindly provided by Masayoshi Nakamura and Takashi Hashimoto (Nara Institute of Science and Technology, Ikoma, Japan), into an *Arabidopsis thaliana* Col-0 expressing 35S-mCherry-TUA5 Gutierrez et al. (2009).

2.5.2 Specimen mounting

Transformed cells were imaged in thin 10 to 20 μ L gas permeable micro-chambers lined on one side with Biofoil (VivaScience, Hannover, Germany) and a 24 x 24 mm coverslip on the other side as described earlier (Vos et al., 2004). Slides were sealed with VALAP (1:1:1 Vaseline : lanolin : paraffin). For oryzalin treatments, cells were immobilized in plastic flow cells (1 channel of 100 μ L with a height of 0.4 mm; Ibidi, Munich, Germany) that were pretreated with 1 mg/mL poly-L-lysine solution in dH₂O for 30 min at room temperature. Ten flow cell volumes of 20 μ M oryzalin (from 20 mM stock in DMSO) in BY-2 medium were perfused through the channel with cells and after 1 hour, washed out with constant perfusion of BY-2 medium at a flow rate > 0.1 mL/min. For latrunculin B and isoxaben experiments, 10 mL of a BY-2 culture was incubated for at least 3 hours in 0.5 or 1.0 μ M latrunculin B or at least 24 hours in 10 μ M isoxaben before adding 20 μ M oryzalin and cell immobilization in a flow cell. Washes with latrunculin B or isoxaben were initiated after 1 hour to allow the microtubule cytoskeleton to recover, but not the actin cytoskeleton or the cellulose microfibril production. The immobilization, the perfusion of medium with 0.1% DMSO, 0.1% ethanol and the confocal imaging did not influence the cytoarchitecture

or microtubule organization of the tobacco BY-2 cells (data not shown).

The *Arabidopsis* plants were grown on standard Hoagland's medium and gently mounted between an objective slide and coverslip spaced by two strips of double sided Scotch tape. For the oryzalin treatment, the plants were transferred to a six well plate containing 1.0 μM oryzalin for an hour to depolymerize the microtubules. Oryzalin was washed out at a flow rate of 0.5 mL $\text{dH}_2\text{O}/\text{min}$.

2.5.3 Microscopy

For the long-term microtubule analysis we used confocal laser scanning microscopy (CLSM). Images and time-lapse movies were produced with a 63x / 1.4 NA oil immersion DIC lens on an Axiovert 200M microscope equipped with a Pascal CLSM unit (Zeiss, Jena, Germany). The GFP was excited with the 488 nm argon laser and a 505 nm long-pass emission filter. To see all microtubules in the cortex, a pinhole of 1.5 to 2 airy disc units (1.0 to 1.4 μm in the Z-axis) was used. The scan time was 4 to 8 $\mu\text{sec}/\text{pixel}$ and the temporal resolution was 3 to 5 minutes. Alternatively, time-lapse Z-series of 2.5 μm thickness were made on a Leica DM IRB microscope equipped with the perfect focusing system, a CSU22 spinning disk set up (Yokogawa, Tokyo, Japan) and a C9100 EM-CCD camera (Hamamatsu Photonics, Hamamatsu City, Japan). We used a 100x / 1.4 NA objective lens and excited the GFP with a 488 nm argon laser. Five 0.5 μm optical sections, each taking 250 ms, were typically obtained at 3-minute intervals. The visible area with cortical microtubules varied from about 200 to 600 μm^2 .

For the nucleation analysis we used a confocal spinning disk microscope described earlier Gutierrez et al. (2009), except that a Nikon Eclipse Ti microscope with the perfect focusing system and a 100x 1.45 NA oil objective replaced the Zeiss Axiovert 200. Alternatively, we used a total internal reflection fluorescence (TIRF) microscopy on a Nikon Eclipse Ti microscope with the perfect focusing system. We used a 100x 1.49 NA TIRF oil objective and excited with a solid-state 478 nm laser (Cobolt AB) and using a Semrock 535/39 emission filter. The microscope was equipped with a manual Nikon TIRF arm and a QuantEM EM-CCD camera (Photometrics). We used 800 ms exposure time and a 2 or 2.14 s time interval for the spinning disk and TIRF microscope respectively.

2.5.4 Data analysis

Time-lapse images were converted into 8-bit tiff file stacks with ImageJ (W. S. Rasband, U. S. National Institutes of Health, Bethesda, Maryland, USA, <http://rsb.info.nih.gov/ij/>, 1997-2007). Z-stacks were converted to average or maximum projections of 3 to 5 sections. The ImageJ StackReg plug-in was used to align the images of a stack Thevenaz et al. (1998). All visible microtubules in the images were traced using the semi-automatic ImageJ plug-in NeuronJ (v1.01) Meijering et al. (2004). The microtubule tracings were stored as a series of x and y pixel coordinates with a maximum distance of 5 pixels in both the x and y direction between subsequent points. A Perl script was

used to extract the line segments and distribute their lengths over 20 evenly spaced bins according to their angle with the x-axis. The script corrects for the uneven distribution due to discrete pixel values of possible segment angles produced by NeuronJ (see Supplementary information and Figure S2.4 for the verification procedure). As we could not distinguish between the plus and minus ends of microtubules, every line segment was assigned an angle in the interval from 0° to 180° . The bins had a width of 9° and were centered on 0° , 9° , etc., up to 171° .

For each image, the microtubule length density was obtained by dividing the total microtubule length by the area of the cortical section in the images. The angular distribution data are presented in contour plots produced with Origin (OriginLab, Northampton, MA, USA) as the fraction of microtubule length at each time point. For clarity, an extra 180° bin is depicted as a copy of the 0° bin in each graph. The angle bins are along the y-axis and time along the x-axis, and a rainbow color gradient indicates the cumulative microtubule length or fraction in 20 equal sized steps, ranging from blue (few microtubules) to red (maximum length or fraction). Plots of mean distributions of several experiments were produced by aligning the timing of individual cells to the moments of zero microtubules after breakdown or before re-polymerization, and averaging the fractions.

To calculate the increase in microtubule density after cytokinesis and oryzalin wash out, and the final plateau value, data from individual experiments were fitted with the linear function: if $t > T_p$, then density = $P_1 + P_2 T_p$, else density = $P_1 + P_2 t$, with T_p as the time to reach the plateau density. The time of emergence of diagonal (45° and 135°) and transverse (90°) microtubule ordering was analyzed by filtering the angle bins with two test functions: T for transverse ordering and D for diagonal ordering (see Supplementary Information and Figure S2.5). Both functions have the property that a randomized system yields a value of zero. A system that is perfectly ordered (in the transverse direction for T and the diagonal direction for D) produces a value of 1.

For the nucleation analysis we determined the position in the cell, the time point, the angle with respect to the cell axis, whether the nucleation was free or microtubule bound and the angle of the seed microtubule in case of branching nucleation. For further analysis we only used the microtubule nucleations that were unbound. To assess whether a bias exists for nucleation along diagonal directions, we defined 15° bins around the 45° , 135° , 225° and 315° degree directions, and scored microtubules in these bins as being diagonal. We introduced a diagonal biasing parameter δ by equating the probability of a diagonal nucleation to a non-diagonal nucleation.

$$P_{diag}(\delta) = \frac{\frac{1}{6}\delta}{\frac{1}{6}\delta + \frac{5}{6}(1-\delta)} \quad (2.1)$$

This parameter is normalized such that $\delta = 0$ implies there are no diagonal nucleations, $\delta = 1$ implies all nucleations are diagonal, while $\delta = \frac{1}{2}$ is the neutral case in which there is no bias, in which case the proper unbiased weight $\frac{1}{6} = \frac{60^\circ}{360^\circ}$ is accorded to the diagonal bins. We then performed a maximum likelihood estimate of δ by

evaluating the likelihood ratio

$$\frac{L(\delta)}{L_{\frac{1}{2}}} = \frac{P_{diag}(\delta)^M (1 - P_{diag}(\delta))^{N-M}}{\left(\frac{1}{6}\right)^M \left(\frac{5}{6}\right)^{N-M}} \quad (2.2)$$

where M is the number of diagonal microtubules observed out of a total of N . For the nucleations after cytokinesis we have $M = 66$ and $N = 274$, yielding $\delta = 0.61$. For the nucleations after oryzalin washout we have $M = 26$ and $N = 73$, yielding $\delta = 0.73$ (see Figure S6 a and b). Note that a standard one-tailed binomial analysis also rejects the null hypothesis of no bias with $p < 0.001$ for the post-cytokinesis case and $p < 0.0001$ for the oryzalin washout case.

2.5.5 Simulation methods

We performed simulations of interacting cortical microtubules using the event-based algorithm Tindemans et al. (2010). The simulations are implemented on a cylindrical cell geometry with a length of $80 \mu\text{m}$ and a radius of $40 \mu\text{m}$. Microtubules that impinge on the edges of the cylinder undergo catastrophes, a boundary condition that was shown to robustly select a transverse orientation of the steady-state array (Allard et al., 2010; Eren et al., 2010).

The kinetic parameters for the dynamics of the microtubule plus-ends are based on Vos et al. (2004): growth speed $v^+ = 0.08 \mu\text{m s}^{-1}$, shrinkage speed $v^- = 0.16 \mu\text{m s}^{-1}$, spontaneous catastrophe rate (switch from growing to shrinking state) $r_c = 0.003 \text{ s}^{-1}$ (a value slightly lower than that of Vos et al. 2004, consistent with a likely overestimation of this quantity in that work due to undetected collision-induced catastrophes), and rescue rate (switch from shrinking to growing state) $r_r = 0.007 \text{ s}^{-1}$. The minus-ends of microtubules shrink with a constant treadmilling speed of $v_t = 0.01 \mu\text{m s}^{-1}$, following Shaw et al. (2003) and identical to Deinum et al. (2011).

The results of angle-dependent collisions between growing microtubules and obstructing ones, follow the simplified scheme also employed by Allard et al. (2010), Eren et al. (2010) and Deinum et al. (2011). All collisions with an incidence angle below 40° result in collision induced bundling, where the incoming microtubule changes direction and continues to grow along the obstructing one. The outcomes of steep angle encounters vary greatly from cell type and stage Wasteneys and Ambrose (2009), therefore we measured these outcomes in our 2s dataset after cytokinesis in BY-2 cells. We found that of 70 encounters $> 40^\circ$ in 4 cells, 14 (20%) encounters induced a catastrophe and 56 (80%) resulted in a crossover. Therefore in our simulations collisions with an incidence angle larger than 40° have a 20% probability of undergoing an induced catastrophe, where they switch to a shrinking state, and a 80% probability of simply crossing over the obstructing microtubule.

New microtubules are nucleated at a constant overall rate of $r_n = 0.0002 \text{ s}^{-1} \mu\text{m}^{-2}$, which we estimated from our observations of the nucleations after cytokinesis Deinum et al. (2011). Nucleations occur either at an arbitrary location in the model cortex or from a microtubule. We modeled the portioning of nucleation events between

microtubule-free and microtubule-bound by a density-dependent chemical equilibrium, which accounts for the affinity of nucleation complexes for the microtubules. The fraction of microtubule-bound nucleations is given by

$$f_{bound} = \frac{\rho}{\rho + \rho_{\frac{1}{2}}} \quad (2.3)$$

where ρ is the (time-dependent) length density ($\mu\text{m } \mu\text{m}^{-2}$) of the microtubules, and the cross-over density $\rho_{\frac{1}{2}} = 0.1 \mu\text{m } \mu\text{m}^{-2}$, determines the location of the equilibrium, which we chose in order to match the observed timescale of the crossover towards the final transversely ordered state. The microtubule-bound nucleations have an orientational distribution with respect to the parent microtubule, which is a coarse-grained representation Deinum et al. (2011) of the experimentally observed patterns Chan et al. (2009). We have reduced the rate of unbound nucleations by the factor of 10 to $r_{n \text{ free}} = 0.00002 \text{ s}^{-1} \mu\text{m}^{-2}$, following the data presented by Nakamura et al. (2010) for a steady state microtubule array.

At the start of the simulations we add a finite pool of microtubule fragments with the density of $ds \ 0.1 \mu\text{m}^{-2}$ and an activation rate of $r_s \ 0.003 \text{ s}^{-1}$. These values were based on the free nucleation rate of BY-2 cells after cytokinesis. Only these reactivating microtubule fragments have a bias towards the diagonal directions of 45° and 135° . This bias was implemented by drawing the direction of nucleation with respect to the parent microtubule from the following distribution

$$\psi(\theta) = \frac{1}{2\pi I_0 \alpha} \exp\left(\alpha \cos 4\left(\theta - \frac{\pi}{4}\right)\right) \quad (2.4)$$

where the angle θ is expressed in radians, α is a parameter that sets the degree of bias, and I_0 is a modified Bessel function of the first kind (see e.g. Abramowitz and Stegun, 1970). We chose $\alpha = 1.5$, which reproduces the experimentally determined ratio between the nucleations in 15° bins around the diagonal directions and those in the remaining directions, for the case after cytokinesis. In the control simulations, this pool of microtubule nucleations was not present.

All simulations were started from an initially empty cortex. The time evolution of the angular distributions of microtubules was analyzed using the same filters also used for the experiments (see Figure S2.5). The microtubule density is reported in terms of an ‘optical density’ in which overlapping microtubules in bundles do not separately contribute to the density, but only the bundle as a whole, mimicking the values measured in the experiments. All simulation results are the average of 500 independent simulations performed with the same parameters. The results were also used for subsequent calculations of D and T and Figure 4c.

2.6 Acknowledgements

We thank Seiichiro Hasezawa (University of Tokyo) for the generous gift of the tobacco GFP-TUA construct and Tijds Ketelaar (Wageningen University) for the BY-2 cell line

expressing the GFP-FABD. We also thank Tijs Ketelaar for helpful discussions.

2.7 Supplementary information

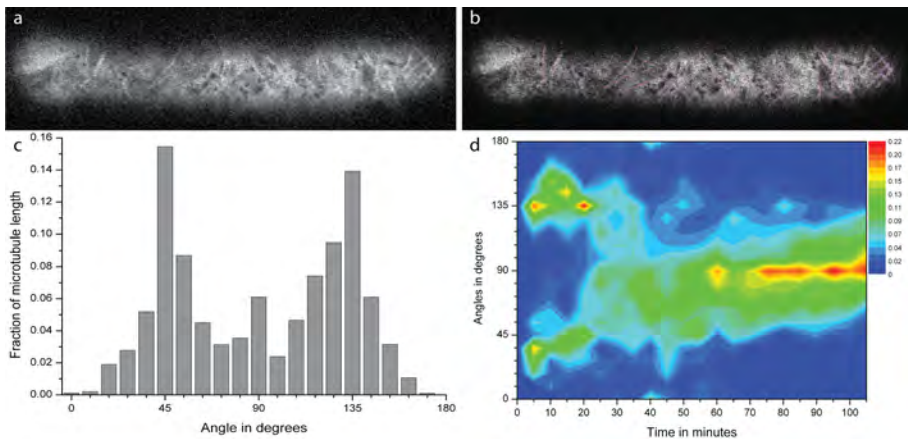


Figure S2.1: Microtubule ordering after cell division in two daughter cells. (a) Snapshot of the two cells at T_{20} , and (b) the same image with the tracings of the microtubules in purple (see also Movie S1). Scale bar is $10 \mu\text{m}$. (c) Angle distribution histogram of the microtubules in the two daughter cells at T_{20} (as indicated in c with an arrow). The fraction of microtubule segments that is diagonally oriented (at 45° and 135°) is larger than that at 90° . (d) Angle distribution plot of cortical microtubules over time of the left daughter cell in a. In this cell, diagonal ordering is visible when the first microtubules appear in the cortex. After 30 minutes, the transverse ordering becomes dominant and increases in strength.

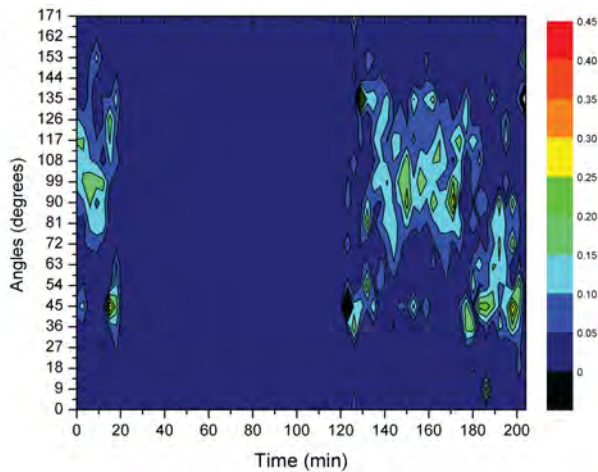


Figure S2.2: Contour plot with the angular distribution of the microtubule length fractions over time of a BY-2 cell expressing 35s-GFP-TUA that progresses into prophase after oryzalin washout. The oryzalin wash-in started at T_0 , after which the microtubules depolymerized. During this depolymerization, the 45° and 135° angles emerged as dominant angles. This was also the case during recovery from the oryzalin treatment, which started at T_{120} . The cell formed a transverse cortical microtubule array at about T_{140} . At about T_{170} the interphase cortical array started to breakdown as the cell entered prophase, again, microtubule angles of 45° and 135° became dominant (T_{180}). The microtubules inside the forming preprophase band were not measured.

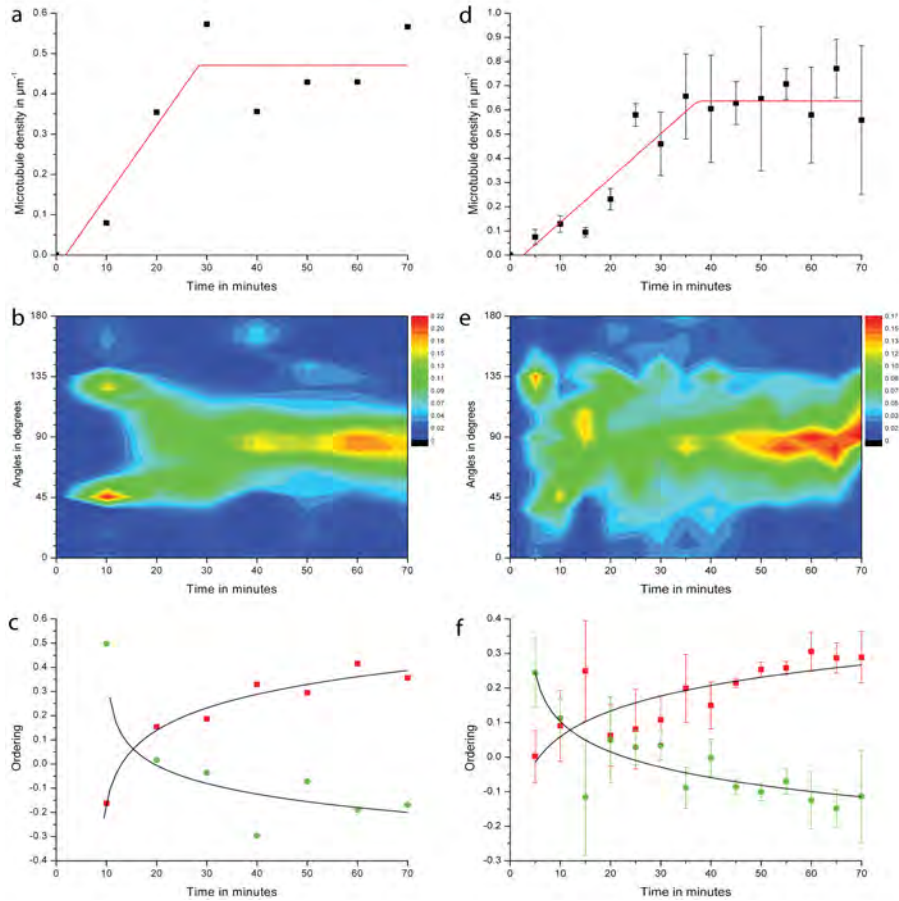


Figure S2.3 Cortical microtubule density and angle distribution after oryzalin treatment in the presence of latrunculin B (a, b and c) or isoaxaben (d, e and f). (a and d) The microtubule length density increased to a plate density (red line). (b and e) The angular distribution of the microtubule length fractions over time. In the absence of filamentous actin or functional cellulose synthase complexes, the diagonal ordering of the first cortical microtubules is still visible. (c and f) The transverse order parameter (red squares) surpassed the diagonal one (green circles) after 15 ± 10 minutes.

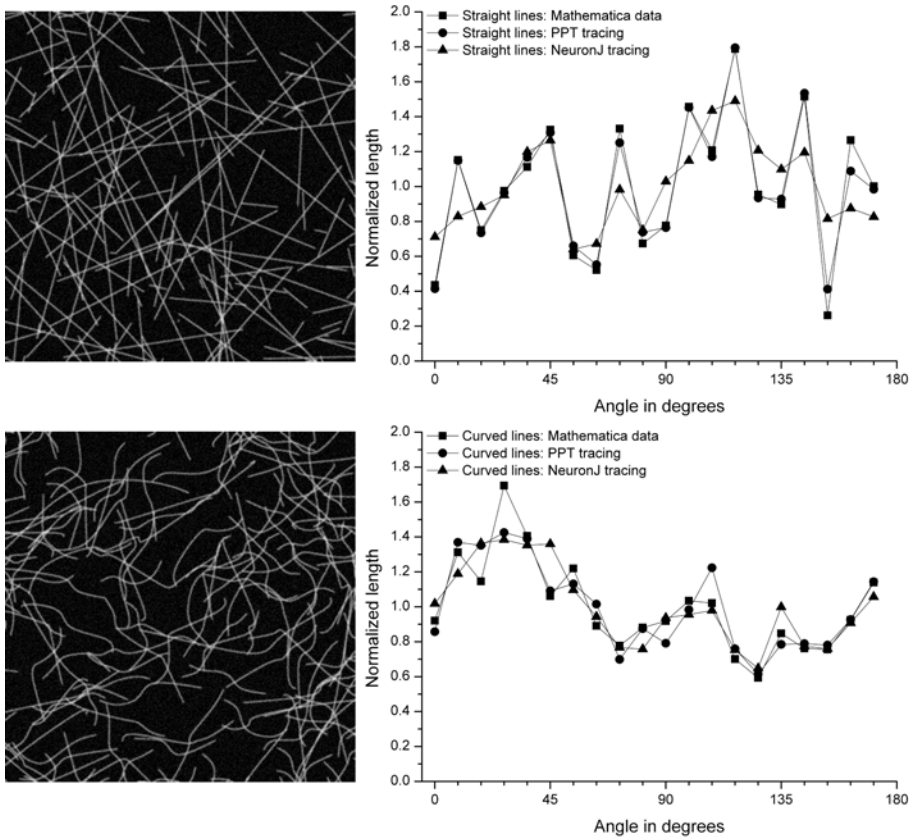


Figure S2.4: Verification of the Perl script through two different line drawings. In black the 'original' angle distribution of the vector drawing of straight lines (a) and curved lines (b) that were produced with Mathematica (black squares in the graphs); tracings of the Mathematica image using PowerPoint (red circles in the graphs) and the NeuronJ-Perl script tracing results (blue triangles in the graphs).

To confirm the accuracy of our analysis methods, we have generated three randomized line graphs using Mathematica (Wolfram Research, Inc., Champaign, IL, USA) containing straight lines and random curves. Gaussian noise was added using Photoshop (Adobe Systems Inc., San Jose, CA, USA). The images were analyzed by different people using two different methods. First, they were manually traced with curved lines using Microsoft PowerPoint. The traced curves were digitally extracted from a PDF document and analyzed using Mathematica to obtain a normalized length distribution in 20 bins. The generated images were also analyzed using NeuronJ and the subsequent processing steps as used for the experimental data and as described in the Materials and Methods. In Figure S2.4, the results from both methods are compared to the reference values that were computed directly from the

original data. From this comparison, we conclude that the results stemming from the semi-automated NeuronJ tracing closely resemble the true distribution. We estimate the error of the NeuronJ tracings to be around 1 bin in the angle direction and $\pm 14\%$ in amplitude. In addition, we rotated a movie in ImageJ by 27 degrees and did the microtubule tracking again. The pattern after rotation was similar as before, but shifted 27 degrees. The differences found were within the error margin mentioned before.

To analyze the appearance and disappearance of the diagonal and transverse microtubule orderings, we defined two filter functions: T for transverse ordering and D for diagonal ordering. A numerical value for the degree of transverse (T) or diagonal (D) ordering was obtained by multiplying the normalized density data by the relevant filter function and summing over all bins. Both filters were constructed such that an isotropic orientation distribution yields a value of zero, whereas a distribution that is fully contained within the three bins surrounding the target direction returns a value of one. The filter functions have a value of one over a width of 27° (3 bins), centered on 90° in the case of the transverse filter and centered on 45° and 135° in the case of the diagonal filter. The remaining values were chosen such that the sum of all weights is zero (Figure S2.5).

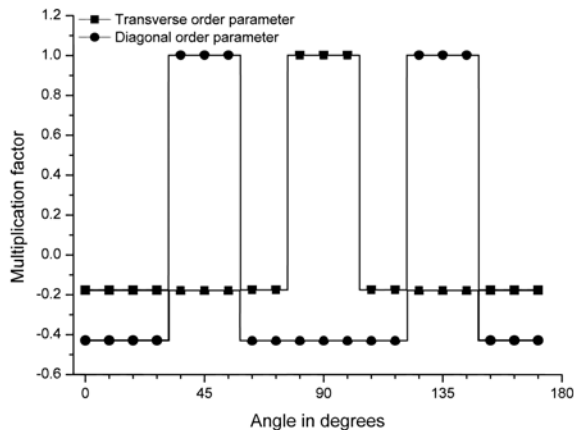


Figure S2.5: Depiction of the filter functions used to calculate the weighted ordering parameters, D and T , from the microtubule density angle fractions.

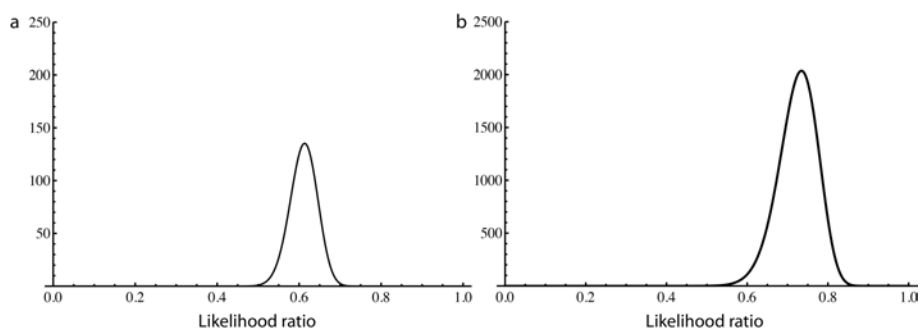


Figure S2.6: Plot of the likelihood ratio for a biased versus an unbiased model of diagonal nucleations as a function of the bias parameter δ on the basis of the data for cytokinesis (a), and oryzalin washout (b), showing significant contrast for selecting the maximum likelihood estimate of δ .

3

Cellulose synthase complex trafficking

3.1 Abstract

Plant cell morphogenesis relies on the organization and function of two polymer arrays separated by the plasma membrane: the cortical microtubule cytoskeleton and cellulose microfibrils in the cell wall. Studies using *in vivo* markers confirmed that one function of the cortical microtubule array is to drive organization of cellulose microfibrils by guiding the trajectories of active cellulose synthase (CESA) complexes in the plasma membrane, thus orienting nascent microfibrils. Here we provide evidence that cortical microtubules also position the delivery of CESA complexes to the plasma membrane and interact with small CESA-containing compartments by a mechanism that permits motility driven by microtubule depolymerization. The association of CESA compartments with cortical microtubules was greatly enhanced during osmotic stress and other treatments that limit cellulose synthesis. On recovery from osmotic stress, delivery of CESA complexes to the plasma membrane was observed in association with microtubule-tethered compartments. These results reveal multiple functions for the microtubule cortical array in organizing CESA in the cell cortex.

3.2 Introduction

Plant cells have microtubule arrays that are organized without a centrosome or other central organizing body. Acentrosomal arrays are common in many organisms, including mammals, but the mechanisms by which these arrays are organized and their precise cellular functions are often poorly understood Bartolini:2006bt. In plant cells undergoing axial growth, interphase microtubules form highly organized arrays at the cell cortex, with microtubules lying in parallel to the plasma membrane and transverse to the cell's axis of elongation, as both single and bundled polymers

(Barton et al., 2008; Ehrhardt, 2008). New polymers arise from dispersed nucleation sites in the cell cortex and show dynamics at both polymer ends that result in net migration of microtubules in the direction of their plus ends, thus creating a highly dynamic array that undergoes constant remodelling (Ehrhardt, 2008; Shaw et al., 2003). Disruption of microtubule organization by genetic or pharmacological means has demonstrated that these arrays are essential for acquisition of differentiated cell shape (Paradez et al., 2006). A central question in plant cell development is how these distinctive microtubule arrays function to guide cell morphogenesis.

It has long been hypothesized that one essential function of the cortical microtubule array is to control the material anisotropy of the cell wall by interacting with CESA complexes to guide the orientation of cellulose microfibrils, the key load-bearing constituent of the cell wall (Green, 1962; Heath, 1974; Staehelin and Giddings, 1982). CESA complexes are molecular machines thought to be composed of 36 catalytic subunits and arranged in symmetrical rosettes with diameters of 25-30 nm, as observed in freeze-fractured plasma membranes (Emons, 1985; Herth, 1983; Kimura et al., 1999; Mueller and Brown Jr., 1980; Somerville, 2006). In *Arabidopsis thaliana*, genetic studies have suggested that simultaneous expression of at least three of ten isoforms is necessary for a functional complex, with CESA1, 3 and 6 being involved in primary cell wall synthesis (Desprez et al., 2007; Persson et al., 2007; Taylor et al., 2003). A functional YFP-CESA6 fusion protein revealed a patterned distribution of active CESA complexes in the plasma membrane, which localized to and tracked along individual elements of the cortical microtubule array (Paradez et al., 2006). Changes in microtubule organization were observed to precede changes in the organization of CESA complexes in the plasma membrane, confirming the microtubule guidance hypothesis for cellulose deposition.

Although dynamic YFP-labelled CESA complexes are observed to be positioned along cortical microtubules (Paradez et al., 2006), it is not known how CESA is delivered to the plasma membrane and how this association is established. Are CESA complexes delivered at addresses defined by cortical microtubules, or are they delivered at random locations, subsequently forming associations with cortical microtubules? Rosettes have been observed by freeze-fracture electron microscopy in the membranes of vesicles and Golgi cisternae, suggesting that CESA complexes are assembled before they reach the plasma membrane (Haigler and Brown, 1986). Consistent with this observation, YFP-CESA6 protein prominently labels Golgi bodies and also labels a population of smaller compartments (Paradez et al., 2006) henceforward termed small CESA compartments (SmaCCs). Here we have used live-cell imaging of labelled CESA and tubulin proteins to investigate the role of the cortical microtubule cytoskeleton in the spatial control of CESA trafficking and delivery to the plasma membrane of *Arabidopsis*.

3.3 Results

3.3.1 Observation of CESA complex delivery events to the plasma membrane

Epidermal cells in the upper hypocotyl of seedlings expressing pCESA3-GFP-CESA3 to label cellulose synthase complexes, and either 35S-mCherry-TUA5 or 35S-mCherry-MAP4-MBD to label cortical microtubules, were observed by spinning disk confocal microscopy (Figure 3.1). To more easily reveal newly delivered CESA complexes, we bleached existing GFP-CESA3 in a large region of the plasma membrane. Delivery events had to meet two criteria: first, de novo appearance of a GFP-CESA3 puncta in the optical plane of the plasma membrane that could not be attributed to migration of existing plasma membrane localized complexes or a focal shift, and second, steady movement in subsequent frames consistent with active CESA complexes (Desprez et al., 2007; Haigler and Brown, 1986; Paredez et al., 2006; Debolt et al., 2007a,b) (Figure 3.1; Movie S1). On the basis of these criteria, 4.8 ± 0.7 CESA-complex delivery events $\mu\text{m}^{-2} \text{h}^{-1}$ were observed.

Individual delivery events typically showed three phases of behavior. First, in most events (37 of 60), a labelled particle appeared in the focal plane and showed erratic motility with rapid and short dislocations (Figure 3.1b, f; Movies S2, S3). Second, the particle stabilized and remained in a fixed position for 62 ± 23 s ($n = 60$ events). Finally, the particle was observed to move at a slow and steady velocity of approximately $200\text{-}400 \text{ nm min}^{-1}$, typically on a linear path. In some cases (7 of 60), a bifurcation of signal was seen to coincide with the onset of steady motility (Figure 3.1f), with daughter particles moving in opposite directions and with approximately half the intensity each of the initial, stabilized particle (Figure 3.1g). We interpret these events to be consistent with arrival of a trafficking compartment with erratic motility behavior in the optical plane and the subsequent delivery of one or two CESA complexes with slow and steady motility behavior. From these observations alone, it is not known whether the static phase represents stabilization of the delivering compartment adjacent to the plasma membrane or whether it represents CESA complexes that have been inserted into the plasma membrane but have yet to synthesize enough cellulose to drive complex motility (Paredez et al., 2006; Debolt et al., 2007a).

3.3.2 CESA complexes are delivered at sites coincident with microtubules

The positions of all delivery events within a sub-region of the bleached area were determined for the first 10 min of fluorescence recovery. These positions were defined as the centroids of GFP-CESA3 particles during the static phase of delivery (Figure 3.1e). Sixty delivery events were then mapped onto segmented images of mCherry-MAP4-MBD (Figure 3.1d, e). Forty-seven events (78%) were observed to be coincident with microtubules, a frequency significantly greater than the 30 events expected by chance alone ($P < 0.001$, binomial test). Thus, CESA complexes are preferentially

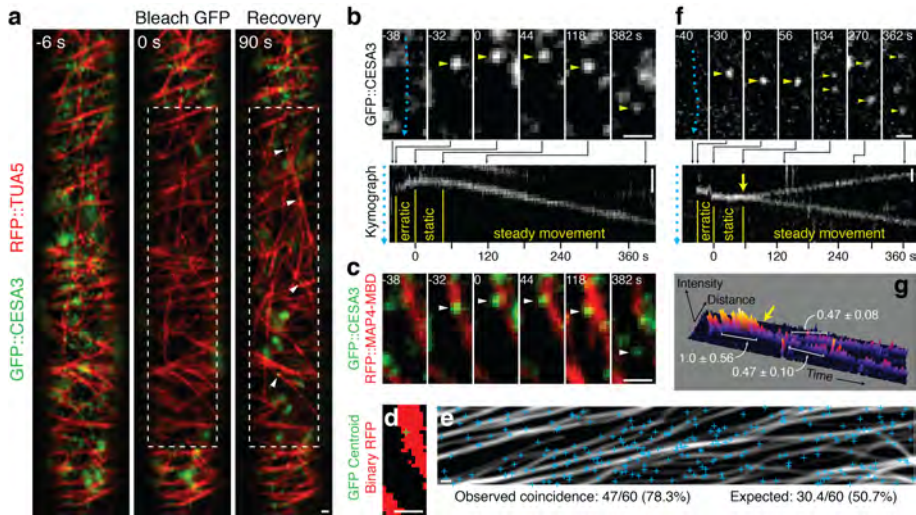


Figure 3.1: Delivery of CESA complexes to the plasma membrane is coincident with microtubules. Three day old dark grown *Arabidopsis* seedlings expressing GFP-CESA3 and mCherry-TUA5 or mCherry-MAP4-MBD were imaged at 2-s intervals. (a) Photobleaching was used to visualize delivery of GFP-labelled CESA complexes (arrowheads). A delivery rate of $4.8 \text{ events } \mu\text{m}^{-2} \text{ h}^{-1}$ was measured from observations of 811 events in 3 cells from 3 seedlings. (b) Delivery of a GFP-CESA3 particle. The CESA particle (arrowhead) undergoes three stages of behavior seen on a kymograph taken along its path of movement (cyan line): erratic motility, static localization and steady movement. (c) Colocalization of the GFP-CESA3 particle in b with a microtubule. (d) Determination of coincidence between a CESA complex delivery site and microtubules. At the start of the static phase ($t = 0$), the centroid of the particle (cross) is coincident with the thresholded microtubule signal. (e) Map of CESA complex delivery sites in one cell overlaid on a 10-min average projection of microtubule signal (mCherry-MAP4-MBD). This panel illustrates the relationship of the two patterns without correction for microtubule dynamics. Sixty delivery events (from 3 cells) were analyzed for colocalization of CESA insertion into the plasma membrane with cortical microtubules as in d; results are summarized in the panel. Events of CESA complex appearance were associated with microtubules at a frequency significantly higher than chance ($P < 0.001$, binomial test). (f) Delivery of multiple CESA particles at the same time and position. A GFP-CESA3 particle arrives at the plasma membrane and splits into two punctae, seen as bifurcation of signal (yellow arrow) on the kymograph taken along the cyan line.

Figure 3.1: (g) Surface plot of kymograph in f. Mean intensity above background was measured along the trunk (before split) and both branches (after split) and reported as relative values \pm s.d. Each daughter particle contains roughly half the intensity of the original particle. A yellow arrow marks the bifurcation point. Scale bars, μm .

delivered to the plasma membrane at sites coincident with microtubules.

To determine whether CESA delivery to the plasma membrane requires microtubule function, we measured the rate of delivery events in cells treated with the microtubule depolymerizing drug oryzalin. A delivery rate of 4.2 ± 1.3 events $\mu\text{m}^{-2} \text{h}^{-1}$ was observed ($n = 3$ cells from 3 seedlings), a rate not significantly different from that in controls ($P = 0.57$, t-test). Therefore, cortical microtubules seem to guide CESA complex delivery, but they are not required for the act of delivery.

3.3.3 Perturbation of actin disrupts the global distribution of CESA at the plasma membrane

Wightman and Turner (2008) reported recently that in xylem vessels, actin filaments - not microtubules - mark CESA delivery sites at the cell surface. To investigate the role actin might have in CESA distribution in epidermal cells, we treated seedlings with $1 \mu\text{M}$ latrunculin B to disassemble the actin cytoskeleton. Cytoplasmic streaming was severely inhibited, as assayed by Golgi body motility, but YFP-CESA6 punctae characteristic of active complexes remained visible in the plasma membrane (Figure 3.2b, c) indicating that delivery to the plasma membrane was not prevented. However, the global distribution of CESA complexes was severely disrupted and many cells showed large areas bereft of signal (Figure 3.2a, b). A clumped distribution of Golgi bodies was observed in these cells, which showed close correlation with the patchy CESA signal at the plasma membrane (Figure 3.2b). In control cells, patchy distribution of Golgi bodies was also observed occasionally for short periods lasting 1-3 min. Photobleaching recovery experiments revealed that CESA delivery in these cells was biased to regions of higher Golgi body density (Figure 3.2d,f). Taken together, these results suggest that motility and distribution of Golgi bodies by the actin cytoskeleton (Nebenführ et al., 1999) may be required for proper global organization and distribution of CESA complexes in the plasma membrane, whereas the microtubule cytoskeleton seems important for fine-scale positioning of CESA delivery.

3.3.4 Isoxaben and osmotic stress cause cortical tethering of SmaCCs

To explore CESA trafficking further, we examined the behavior of Golgi bodies and SmaCCs. Golgi bodies, SmaCCs and active CESA complexes were distinguished by characteristic motility, morphology and localization (Figure 3.3a,c). We had previously shown that the cellulose synthesis inhibitor isoxaben caused the rapid disap-

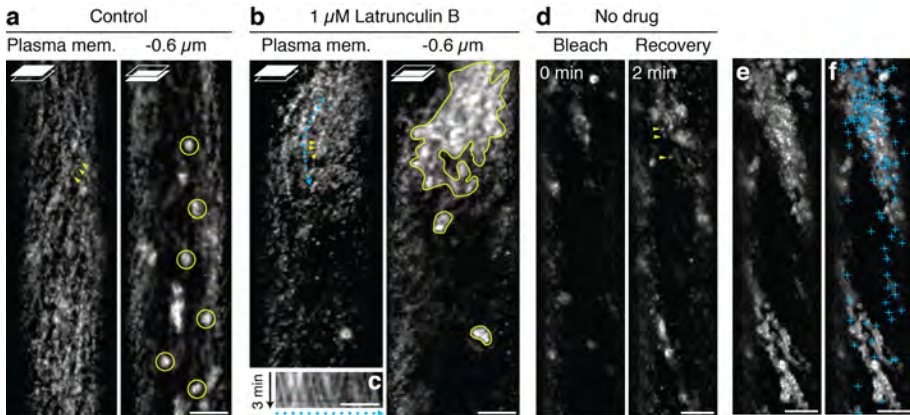


Figure 3.2: CESA complex delivery is correlated with cortical Golgi body distribution. (a, b) Latrunculin B induces stable clustering of Golgi bodies and active CESA complexes. Seedlings expressing YFP-CESA6 were treated with 0.05% DMSO (a) or latrunculin B (1 μM) in 0.05% DMSO (b) for 4 h. After latrunculin B treatment for 4 h, cytoplasmic streaming was severely diminished. Focal planes at the plasma membrane and lower cell cortex are shown. In cells treated with latrunculin B, the non-uniform distribution of CESA complexes (arrowheads) in the plasma membrane coincided with underlying Golgi bodies (circled) in the cell cortex. (c) Kymograph along the cyan trace in b. Particles show slow (300 nm min^{-1}) and steady velocities, consistent with motility of active CESA complexes. (d,f) Transient clustering of Golgi bodies in the cell cortex leads to spatially concentrated delivery of CESA complexes to the plasma membrane. (d) GFP-CESA3 signal in a cell was bleached. After 2 min, labelled CESA complexes (arrowheads) accumulated non-uniformly. (e) A 2-min brightest point projection (61 frames) of GFP signal in d. (f) Map of CESA complex delivery sites overlaid on e. Cortical regions visited by Golgi bodies (light areas) show a higher density of deliveries (crosses) than regions bereft of Golgi bodies (dark areas). Scale bars, 5 μm .

pearance of YFP-CESA6 complexes from the cell surface (Paredes et al., 2006). When isoxaben treatment was carried out for longer periods of time, a striking additional response was observed: SmaCCs accumulated in the cell cortex (Figure 3.3a,e) and showed a marked reduction in motility, with sustained episodes of positional stability (Figure 3.3; Movie S4). Golgi bodies in the cell cortex (labelled with YFP-CESA6 or YFP-SYP32; (Uemura et al., 2004)) also showed reduced motility (Figure 3.3g; Movie S4). The disappearance of YFP-CESA6 punctae was accompanied by a quantitative loss of YFP signal from the plasma membrane (Figure S3.1), indicating that isoxaben caused net removal of YFP-CESA6 from the membrane rather than simply dispersing the protein by disruption of complex structure (Somerville, 2006). The cellular pathology of isoxaben treatment described above was mimicked by several other small molecules that disrupt cellulose biosynthesis (data not shown), including AE F150944 ((Kiedaisch et al., 2003); Figure 3.3f; Figure S3.2).

As isoxaben and other cellulose synthesis inhibitors are pharmacological agents, we sought to determine whether there are physiological conditions that perturb CESA complex trafficking. Previous studies have shown that osmotic stress downregulates synthesis of cell wall polysaccharides, including cellulose (Iraki et al., 1989), and rosettes were depleted in the plasma membrane of freeze-fractured plant cells that were not turgid (Emons, 1985). Treatment with 200 mM mannitol, a concentration of osmoticum that did not induce plasmolysis (Figure S3.3), caused cortical accumulation and tethering of SmaCCs (Figure 3.3; Figure S3.2, Movie 4). The density of punctae in the plasma membrane was also reduced, but the extent of this clearing was variable.

Although both isoxaben and osmotic stress caused tethering of SmaCCs and Golgi bodies in the cell cortex, the motility of endosomes labelled with YFP-RabF2a (Preuss et al., 2004b) was not affected by isoxaben and was slowed but not stopped by mannitol treatment (Figure 3.3g). Furthermore, isoxaben did not alter the localization of the brassinosteroid receptor BRI1 (Friedrichsen et al., 2000) and the t-SNARE NPSN12 ((Zheng et al., 2002); Figure S3.3), suggesting that the drug neither disrupts trafficking of plasma membrane proteins in general nor causes bulk internalization of plasma membrane proteins. Similarly, both of these markers remained at the plasma membrane during treatment with 200 mM mannitol, although some evidence for internalization of label was observed (Figure S3.3). The effects of isoxaben and osmotic stress were reversible after a washout with water (Figure S3.2). Together, these results suggest that isoxaben causes a specific perturbation in the localization and motility of compartments involved in the trafficking of CESA6, whereas osmotic stress causes a similar syndrome of responses but may affect membrane trafficking more generally.

Treatment with brefeldin A, which blocks secretion and other membrane trafficking events by inhibiting the Sec7/BIG class of guanine nucleotide exchange factors (Nebenführ et al., 2002), also caused cortical SmaCC accumulation and tethering (Figure 3.3; Figure S3.2, Movie 4), suggesting that the responses observed with isoxaben and osmotic stress might be caused by specific disruption of membrane trafficking.

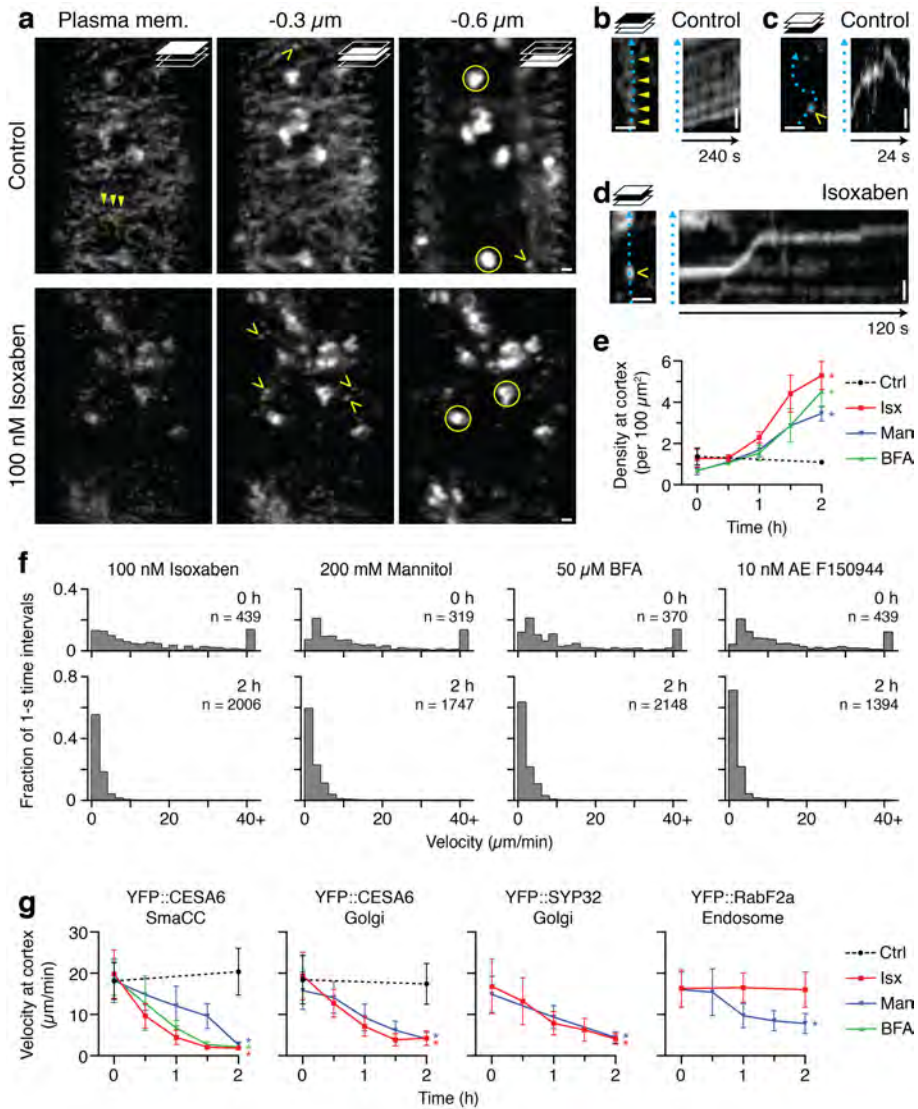


Figure 3.3: Isoxaben, osmotic stress and brefeldin A redistribute CESA protein and alter the location and dynamics of compartments containing CESA. (a,f) Seedlings expressing YFP-CESA6 were treated with 0.05% DMSO (control), 100 nM isoxaben in 0.01% DMSO, 200 mM mannitol, 50 μM brefeldin A in 0.05% DMSO or 10 nM AE F150944 in 0.01% DMSO for 2 h. *Figure caption continued on next page...*

Figure 3.3: (a) Confocal z-series of the cell cortex. Propidium iodide staining of the cell wall provided a fiducial marker for the start of the series. In controls, YFP punctae (closed arrowheads) corresponding to active CESA complexes are visible in the plasma membrane. Lower optical planes reveal Golgi bodies (circled) and small CESA compartments (SmaCCs, open arrowheads). Isoxaben removed most punctae from the plasma membrane and caused accumulation of labelled organelles in the cell cortex. (b,d) Kymographs of YFP-CESA6 structures taken along cyan traces. In controls, punctae (b) travel at slow and constant rates, whereas SmaCCs (c) move at higher velocities and change directions frequently. (d) With isoxaben treatment, changes in SmaCC velocity and direction were less frequent, compared with c. (e) SmaCCs accumulate in the cortex under treatment with isoxaben, mannitol or brefeldin A. Measurements (mean \pm s.e.m.) were taken from 3 cells (from 3 seedlings). (f) Histograms of SmaCC velocity in the cell cortex before and after chemical treatment, measured in the same 3 seedlings per treatment. (g) Organelle velocity in the cell cortex. Seedlings expressing the indicated fluorescent protein fusion were imaged, and velocity was measured for the indicated organelle. Time courses show the weighted average of $n = 18$ organelles in 3 cells from 3 seedlings (data are mean \pm s.e.m.). Linear regression slopes significantly different than zero are marked with asterisks ($P < 0.05$). Scale bars, $1 \mu\text{m}$.

3.3.5 Osmotic stress inhibits CESA delivery to the plasma membrane

The disappearance of CESA label at the plasma membrane and the cortical accumulation of SmaCCs might be caused by a reduction in the rate of CESA complex insertion into the plasma membrane, stimulation of CESA complex recycling from the plasma membrane, or both. CESA delivery rate was reduced over 100-fold in cells treated with 200 mM mannitol for 3 h: 0.04 ± 0.04 events $\mu\text{m}^{-2} \text{h}^{-1}$ (5 cells, 5 seedlings), compared with 4.8 ± 0.7 events $\mu\text{m}^{-2} \text{h}^{-1}$ for controls (3 cells, 3 seedlings). Addressing the rate of internalization is more challenging, but experiments using the lipophilic tracer dye FM4-64 (Bolte et al., 2004) showed that dye endocytosed after initial mannitol treatment did not label SmaCCs, although SmaCCs could be labelled after the dye had time to redistribute to other internal membranes, including Golgi bodies (Figure S3.4).

3.3.6 Tethered SmaCCs colocalize with cortical microtubules

Time-lapse imaging revealed that cortically localized SmaCCs, which were often stationary, also showed saltatory movement along linear paths (Figure 3.3d; Movie S4), a pattern of movement consistent with cytoskeletal motility. Imaging of cells

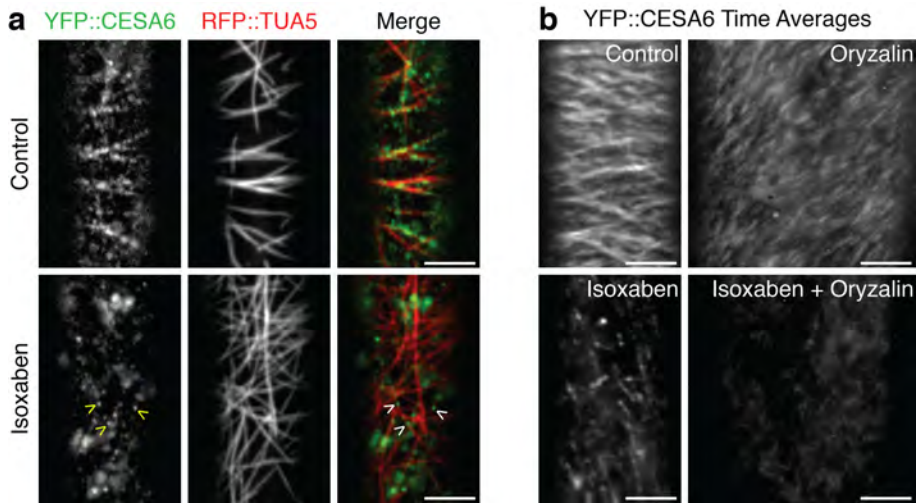


Figure 3.4: SmaCCs associate with cortical microtubules in cells treated with isoxaben. (a) Seedlings expressing YFP-CESA6 and mCherry-TUA5 were treated with 0.01% DMSO (control) or 100 nM isoxaben in 0.01% DMSO. SmaCCs (arrowheads) colocalize with microtubules. (b) Depolymerization of microtubules by oryzalin prevents cortical accumulation of CESA6 under isoxaben treatment. Seedlings expressing YFP-CESA6 were incubated in 0.01% DMSO + 0.1% methanol alone (control) or together with 100 nM isoxaben, 20 μ M oryzalin or 100 nM isoxaben + 20 μ M oryzalin for 8 h. Averages of 61 frames representing 5 min. Scale bars, 5 μ m.

expressing markers for both CESA and microtubules revealed that during treatment with isoxaben, mannitol or brefeldin A, cortically tethered SmaCCs were substantially colocalized with microtubules (Figure 3.4a; Figure S3.5a, Movies S5,8). Oryzalin treatment prevented accumulation of SmaCCs at the cell cortex (Figure 3.4b), indicating that microtubules are also necessary for cortical tethering of SmaCCs.

3.3.7 SmaCC motility is driven by depolymerizing microtubule ends

To further elucidate SmaCC behaviour, we analysed the joint dynamics of microtubules and 50 SmaCCs from 8 cells treated with isoxaben. Only SmaCCs that were traceable for at least five continuous frames (that is, 20 s) were analysed. SmaCCs moved along paths defined by microtubules 43.0% of the time, were stationary and coincident with a labelled microtubule for 55.1% of the time (frame-to-frame displacement $<50 \text{ nm s}^{-1}$), and were not associated with microtubules 1.9% of the time. Of the SmaCCs observed to move, 37 moved processively in coincidence with depoly-

merizing ends (Figure 3.5a; Supplementary Information, Movie S9). Of the remaining 14, 9 were stationary and the other four showed movement along microtubule bundles where individual polymers and polymer ends could not be distinguished (see below). In this data set and others, comprising at least 100 observations, SmaCCs were never observed to move along the lattice of an unambiguously single microtubule - a behavior characteristic of translocation by motor proteins such as kinesins - or to track with growing polymer ends. To further test whether SmaCC motility was driven by microtubule depolymerization, microtubules were stabilized by taxol. SmaCC velocity was reduced significantly (Supplementary Information, Figure S3.5b, c), indicating that SmaCCs require dynamic ends for microtubule-dependent motility. Observation of tip-tracking motility suggests that tethered SmaCCs are physically associated with microtubules.

Multiple SmaCCs associated with the same microtubule were observed to be collected by depolymerizing ends (Figure 3.5b; Supplementary Information, Movie S10), with total signal increasing in a stepwise fashion with the addition of each SmaCC. The movement of SmaCCs associated with depolymerizing ends was not confined to single cortical microtubules, but was also observed within microtubule bundles (Figure 3.5c; Supplementary Information, Movie S11), suggesting that the architecture of bundles does not prevent this form of organelle motility. Finally, SmaCCs were observed to track both plus and minus ends of microtubules (Figure 3.5b), indicating that these organelles use a mechanism of microtubule end tracking motility that is independent of polarity.

Observation of sustained interaction of SmaCCs with cortical microtubules was uncommon in cells under normal conditions, but close examination of image sequences acquired at 2-s intervals revealed brief microtubule tip-tracking events (6 events in 4 cells from 4 seedlings; Figure 3.5d, e; Supplementary Information, Figure S3.6, Movie S12).

3.3.8 CESA delivery is associated with microtubule-tethered SmaCCs

To explore the functional nature of tethered SmaCCs, we followed the fate of CESA protein as osmotic stress was lifted. We observed two classes of events in these experiments. First, we observed CESA complex delivery associated with microtubule-tethered SmaCCs ($n = 18$ events in 7 cells; Figure 3.6; Supplementary Information, Figure S3.7, Movie S13). These SmaCCs could show microtubule tip-tracking behavior before complex delivery (Figure 3.6). Second, we observed the successive break-up of SmaCCs into more numerous and less bright cytoplasmic components. These break-up products did not show the slow, steady and constrained trajectories of active CESA complexes but rather, the more erratic motility behavior of SmaCCs (Figure 3.7; Supplementary Information, Movie S14). As 'collection' behaviour of SmaCCs was often observed (Fig. 5b), it is possible that these break-up events represent the dispersal of tethered SmaCC aggregates.

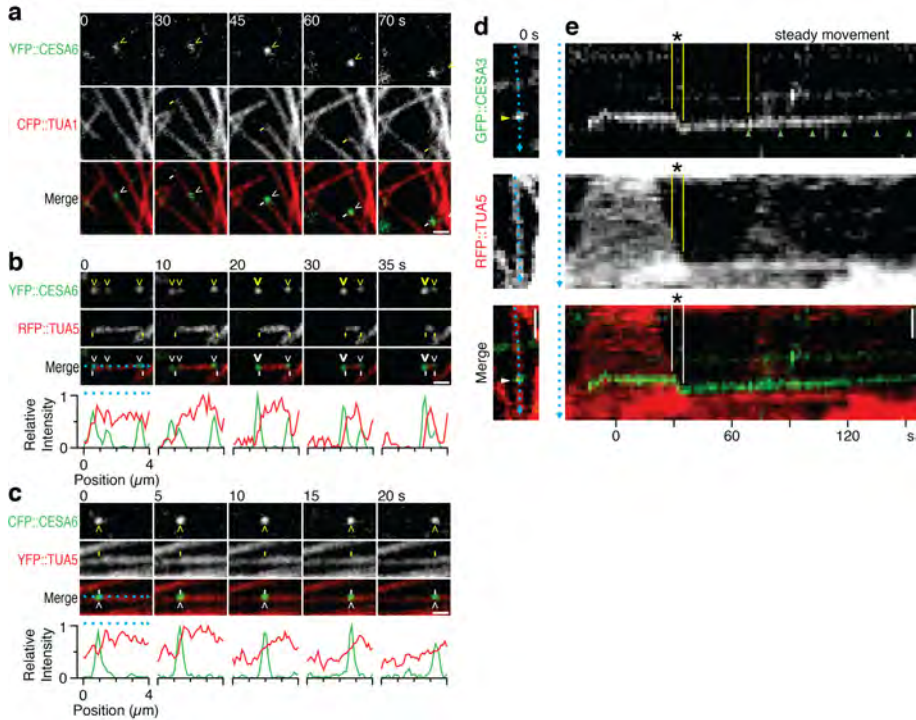


Figure 3.5: CESA tracks depolymerizing microtubule ends. (a,c) Cortically tethered SmaCCs frequently show tip-tracking behavior during isoxaben treatment or osmotic stress. Time series showing dynamic association between SmaCCs (arrowheads) and microtubule ends (dashes). Seedlings expressing markers for CESA (green) and microtubules (red) were treated with 100 nM isoxaben or 200 mM mannitol. (a) A microtubule-associated SmaCC is initially stationary and then moves along the microtubule when encountering a depolymerizing microtubule end. (b) SmaCCs track with the depolymerizing plus and minus ends of the same microtubule. Two SmaCCs on the left are collected on the depolymerizing end. The increase in CESA signal suggests that both compartments maintain association with the depolymerizing end. (c) A SmaCC moves with a shrinking microtubule end in a microtubule bundle. For b and c, intensity from both channels was measured along the cyan trace for each time point. (d, e) CESA undergoes brief tip-tracking events under normal conditions. A labelled CESA complex is delivered to the plasma membrane in the absence of drugs. (d) Still images at $t = 0$ showing GFP-CESA3 (arrowhead) and an associated microtubule.

Figure 3.5: (e) Kymograph along the cyan trace in a. The static phase of CESA complex delivery is interrupted by a depolymerizing microtubule end. GFP-CESA3 moves with the depolymerizing end for several frames (*), becomes static again and then moves steadily. Green arrowheads mark the position of GFP-CESA3 where steady movement starts. The transitory nature of the tip-tracking event makes it difficult to identify the tracking object as a SmaCC or possibly a membrane-embedded CESA complex, although the former possibility is the more parsimonious hypothesis. Scale bars, 1 μm .

3.3.9 Microtubule-associated SmaCCs are heterogeneous in identity

The observations consistent with quantitative delivery of one or two CESA complexes under normal conditions (Figures 3.1, 3.5d, e) suggest that these compartments are large enough to contain 1 or 2 CESA complexes and thus are probably vesicular. Some Golgi bodies were observed to associate with SmaCCs under normal conditions and to show physical tethering to microtubule-associated SmaCCs during osmotic stress or isoxaben treatment (Supplementary Information, Figure S3.8, Movie S15). Consistent with these observations, three putative markers for the trans-Golgi network - SYP41, SYP42 and SYP61 (Uemura et al., 2004; Bassham et al., 2000) - showed significant overlap with freely motile SmaCCs under both normal conditions and during osmotic stress or isoxaben treatment. However, the population of cortically-tethered SmaCCs showed no significant colocalization with SYP41 or SYP42, although a minority (20 of 60 in 3 cells) colocalized with SYP61 (Figure 3.8; Supplementary Information, Figure S3.9). Thus, microtubule-associated SmaCCs seem to constitute a heterogeneous population of organelles. A survey of 9 additional fluorescent markers for various endomembrane structures did not reveal a definitive marker for most of the tethered SmaCCs (Supplementary Information, Table 1 and data not shown). Further elucidation of SmaCC diversity will probably require isolation of SmaCCs and analysis of constituent proteins other than CESA.

3.4 Discussion

Interphase microtubule arrays have important roles in the vectorial trafficking of membranes and proteins in many organisms, but the function of the acentrosomal cortical array of higher plant cells in trafficking and targeting has remained little explored. Bundles of cortical microtubules have long been observed to underlie thickenings in specialized secondary cell walls (Hepler and Newcomb, 1964; Oda et al., 2005) and recently were shown to colocalize with mucilage secretion in seed coat cells (McFarlane et al., 2008). Here we assayed protein delivery by observing single delivery events of CESA complexes to the plasma membrane and found that

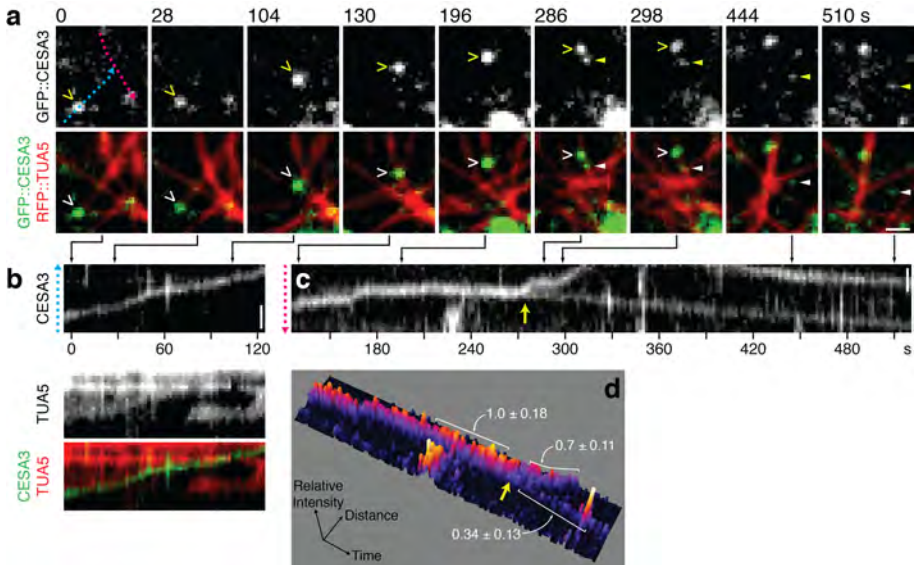


Figure 3.6: SmaCCs are associated with CESA complex delivery to the plasma membrane. (a,c) Seedlings were treated with 200 mM mannitol for 3 h and then washed with water for 0.5 h. (a) A SmaCC (open arrowhead) tracks a depolymerizing microtubule end for the first 120 s and then jumps to an adjacent microtubule. At 274 s, the SmaCC begins to split into two structures of unequal intensity. The brighter compartment (open arrowhead) leaves the focal plane (at 314 s) in a manner consistent with SmaCC motility. The dimmer compartment (closed arrowhead) moves at a slow and steady velocity, consistent with CESA complex motility in the plasma membrane. (b) Kymograph along the cyan line in a, showing prolonged tip-tracking by the SmaCC. (c) Kymograph along the magenta line in a, showing the SmaCC-associated delivery event. A yellow arrow marks the bifurcation point. (d) Surface plot of c. Mean intensity above background was measured in the indicated regions and reported as relative values \pm s.d. A yellow arrow marks bifurcation. The sum of signal intensity from both branches roughly equals the trunk, suggesting both daughter particles originated from the same structure. Scale bars, 1 μ m.

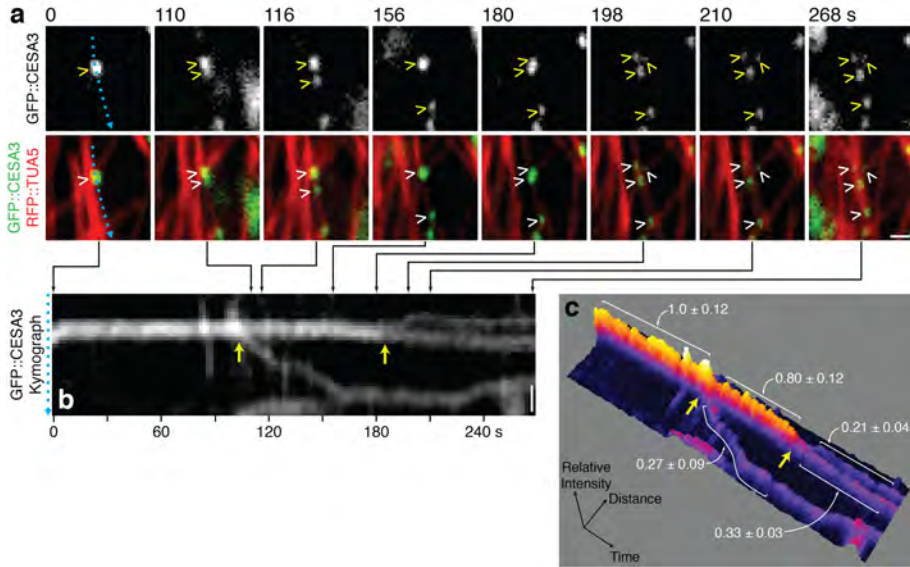


Figure 3.7: Successive break-up of one SmaCC into multiple cytoplasmic compartments. Seedlings were treated with 200 mM mannitol for 3 h and then washed with water for 0.5 h. (a) A SmaCC (arrowhead) splits into two compartments, clearly visible at 116 s. The brighter daughter SmaCC then proceeds to split into 3 compartments, clearly visible at 198 s. All structures show motility characteristic of SmaCCs. (b) Kymograph along the cyan trace in a. Yellow arrows mark the bifurcation events. (c) Surface plot of b. Mean intensity above background was measured in the indicated regions and reported as relative values \pm s.d. Yellow arrows mark the bifurcation points. The sum of intensity values after each bifurcation event roughly equals the intensity of the originating compartment. The second break-up event has three daughter particles, only two of which move along the kymograph trace in a. Mean intensity for the third daughter particle, measured along a different kymograph line, is 0.18 ± 0.05 . Scale bars, 1 μ m.

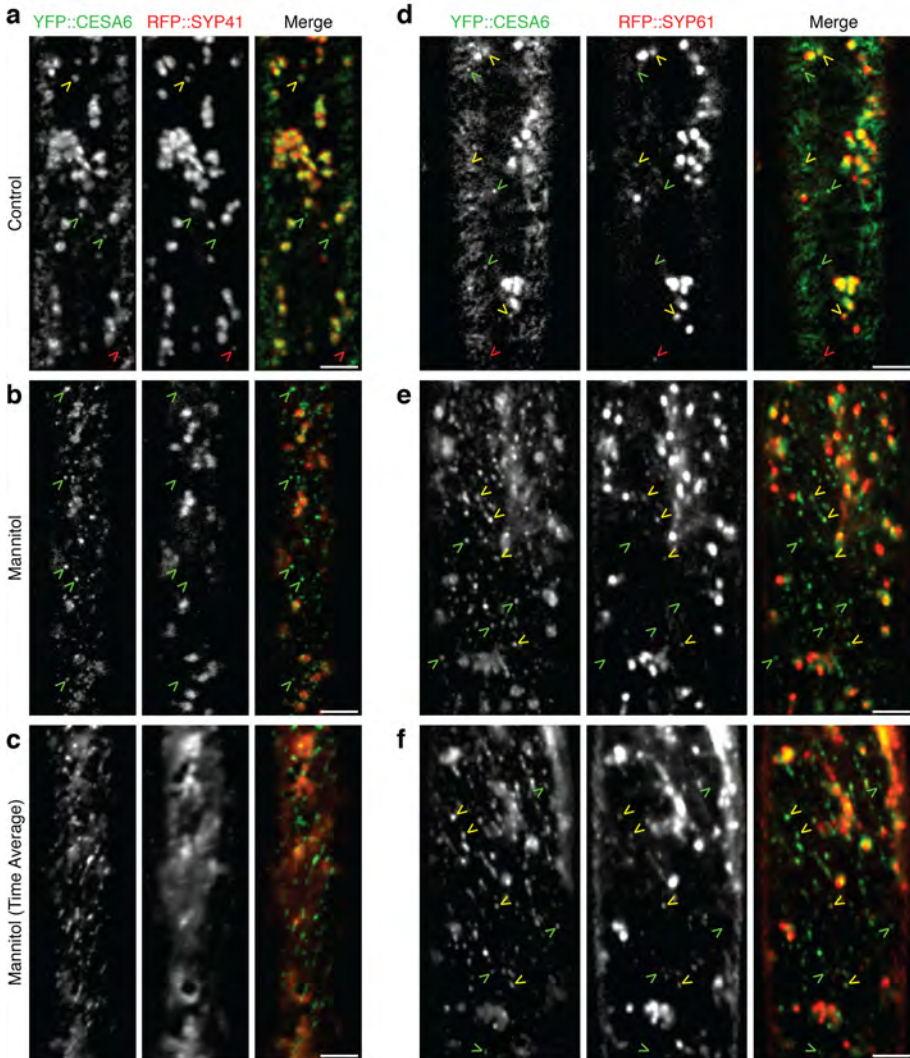


Figure 3.8: SYP41 and SYP61 label a subset of SmaCCs. (a,f) Seedlings expressing YFP-CESA6 and mCherry-SYP41 (a,c) or mCherry-SYP61 (d,f) were incubated in water (a, c) or 200 mM mannitol (b, c, e, f) for 3 h and imaged at the cell cortex. (a, d) Some small compartments are labelled with YFP only (green arrowheads), mCherry only (red arrowheads) or both (yellow arrowheads). (b, c) SYP41 fails to label cortically tethered SmaCCs (green arrowheads) after mannitol treatment.

Figure 3.8: (e, f) SYP61 labels some tethered SmaCCs (yellow arrowheads) but not all (green arrowheads). Of 60 tethered SmaCCs, 20 were labelled by mCherry-SYP61 (observations from 3 cells from 3 mannitol-treated seedlings). These results suggest that SmaCCs are a heterogeneous population of membranous compartments, with one class being identified by SYP41 colocalization, a second by SYP61 colocalization and microtubule association, and a third class by the absence of SYP41/61 colocalization but with microtubule association. This latter class makes up the majority of observed SmaCCs that show sustained microtubule interaction. (a, b, d, e) Still images. (c, f) Averages of 61 frames representing 1 min. Scale bars, 5 μm .

most of the newly arrived complexes were optically coincident with labelled microtubules. This result suggests two possible mechanisms. First, microtubules might interact with and organize exocytotic machinery, creating a pattern of vesicle docking sites that is coincident with the microtubule array. Second, CESA-containing delivery compartments might preferentially dock and pause at microtubules, as actinomyosin-driven cytoplasmic streaming carries them through the cortex, thus promoting interaction with export sites located adjacent to microtubules. These models are not mutually exclusive. Support for the latter mechanism is provided by our observations of SmaCC interaction with cortical microtubules and of CESA delivery events coinciding with microtubule-associated SmaCCs during recovery from osmotic stress. Although sustained pausing of SmaCCs on microtubules was not observed in untreated cells, observation of brief tip-tracking events suggest that perturbations of CESA activity might cause prolongation of a SmaCC-microtubule interaction that is normally short-lived.

Two classes of hypotheses can be envisioned for the function of microtubule-dependent positioning of CESA delivery to the plasma membrane. Positioning of CESA delivery might ensure efficient association of CESA with cortical microtubules at the time of microfibril initiation. This mechanism would ensure that most microfibrils are initiated in the appropriate positions and orientations as determined by cortical microtubule array organization. Alternatively, microtubules might help to coordinate the location or timing of CESA delivery with other proteins or polysaccharides required for cell wall biogenesis.

The mechanism for SmaCC tethering to microtubules and tip-tracking motility seems to be unusual for a membranous compartment. SmaCC motility could possibly be driven by a tip-tracking kinesin (Wu et al., 2006); however, the observation that both polymer ends are tracked would require two such motors with opposite polarity, each activated by depolymerization. The tip-tracking behaviour of SmaCCs more closely resembles the behaviour of the DAM1 complex in yeast (Westermann et al., 2006), a part of the kinetochore required for chromosome segregation. The Dam1

complex forms a ring structure around microtubules, which move processively on depolymerizing microtubule ends *in vitro* (Westermann et al., 2006). Non-encircling Dam1 oligomers are also observed to track shrinking microtubule ends (Grishchuk et al., 2008). However, a search of the *Arabidopsis* genome reveals no clear DAM1 homologues. Biochemical and genetic investigations will be required to reveal if there are in fact dual motors acting on the same cargo, if there are other proteins that function similarly to DAM1, or if there is a new mechanism for microtubule-based motility waiting to be discovered.

Microtubule tip-tracking motility might help to distribute SmaCCs on the cell cortex, although prolonged cytoskeletal association of SmaCCs does not seem to be prevalent during normal cell growth. Another possibility is that motility is simply a consequence of a more fundamental microtubule attachment mechanism. Cortical microtubules are highly dynamic polymers that show treadmilling behaviour (Shaw et al., 2003). To maintain attachment to this dynamic substrate, an organelle or vesicle must either be able to remain associated with a shrinking end or undergo quick re-association with another microtubule when depolymerization destroys the site of attachment. SmaCC movement on shrinking ends may therefore represent a mechanism for maintaining attachment to a treadmilling array.

The observation that cellulose biosynthesis inhibitors, osmotic stress and brefeldin A all caused cortical accumulation and tethering of SmaCCs suggests that these treatments may impinge on a common pathway regulating CESA trafficking. Previous work on osmotic stress provides a physiological context for this distinctive response. During severe osmotic stress, soluble sugars and amino acids accumulate at high intracellular concentrations to counteract water efflux (Handa et al., 1983), and the biosynthesis of cellulose and hemicellulose is reduced (Iraki et al., 1989). Our observations suggest that the CESA complex itself is depleted from the plasma membrane during this metabolic shift and that its insertion into the plasma membrane is inhibited. Sequestration of either recycled or outgoing CESA in cytoplasmic reservoirs adjacent to the cell surface might provide an effective mechanism of blocking cellulose biosynthesis to increase the cytosolic concentration of sugar precursors, as well as allow for efficient redeployment of CESA to the plasma membrane on relief from the stress. Evidence for such deployment was in fact observed during recovery from osmotic stress.

Here we present evidence that, in addition to guidance of CESA complexes, the cortical microtubule array also acts to position delivery of CESA complexes to the plasma membrane and interacts with CESA trafficking compartments. The relative contributions of these cortical array functions to plant cell growth and morphogenesis can now be investigated through use of the expanding collection of mutants and small molecule effectors that perturb cellulose synthesis and cell growth.

3.5 Materials and methods

3.5.1 Transgenic lines

All *Arabidopsis* lines were ecotype Columbia. Five lines were used for dual imaging of CESA and microtubules: 1) pCESA3-GFP-CESA3 and 35S-mCherry-TUA5, 2) pCESA3-GFP-CESA3 and 35S-mCherry-MAP4-MBD, 3) pCESA6-YFP-CESA6 and 35S-mCherry-TUA5, 4) pCESA6-CFP-CESA6 and 35S-YFP-TUA5 and 5) pCESA6-YFP-CESA6 and 35S-CFP-TUA1 (Paredes et al., 2006). All lines produced similar results.

To generate all mCherry constructs, mCherry was amplified from a donor vector (Shaner et al., 2004) with primers 5'-TTGGATCCATGGTGAGCAAGGGCGAGGA-3', and 5'-GGTCC GGACTTGACAGCTCGTCCATGC-3', which contained Bam HI and Bsp EI sites, respectively. This fragment was cut with Bam HI and ligated to an HA tag containing a linker sequence. The HA tag was made using complementary oligonucleotides 5'-GGCCATGGGCTACCCATACGATGTTCCAGATTACGCTTCACTAGGAGGACCTTCAG-3' and 5'-GATCCTGAAGGTCCTCTAGTGAAGCGTAATCTGGAACATCGTATGGGTAGCCCATGGCC-3', which featured flanking Nco I and Bam HI sites. The YFP sequence in the pEG104 binary vector (Earley et al., 2006) was then exchanged with the HA-mCherry fragment via NcoI and Bsp EI sites. TUA5, SYP41, SYP42 or SYP61 was amplified from Col-0 genomic DNA and inserted into the resulting vector using Gateway cloning technology (Invitrogen) as described previously (Kirik et al., 2007). The microtubule-binding domain (MBD) of MAP4 was amplified from the genomic DNA of GFP-MAP4-MBD plants (Marc et al., 1998). The mCherry fusion constructs were then introduced into YFP-CESA6 plants (Paredes et al., 2006) or GFP-CESA3 plants (Desprez et al., 2007) by *Agrobacterium*-mediated transformation to generate the double-labelled lines. CFP-CESA6 plants were constructed as described previously (Paredes et al., 2006) and crossed with YFP-TUA5 plants (Debolt et al., 2007a) to create a double-labelled line.

GFP-CESA3 (Desprez et al., 2007) and GFP-KOR1 (Robert et al., 2005) seeds were provided by S. Vernhettes (Institut National de la Recherche Agronomique, Versailles, France). YFP-RabF2a, YFP-RabA4b and YFP-RabG3c (Preuss et al., 2004b) seeds were provided by E. Nielsen (University of Michigan, USA). YFP-SYP32, YFP-RabF2b, YFP-RabC1, YFP-RabA1g, YFP-RabA5d and YFP-RabG3f seeds were provided by N. Geldner (Salk Institute, CA, USA; Geldner and Chory, unpublished data).

3.5.2 Growth

Seeds were surface sterilized, stratified for 3 days at 4 °C, and sown on 0.8% agar containing 0.5x Murashige and Skoog (MS) salts and 1x Gamborg's vitamin solution (Sigma-Aldrich) at pH 5.7. After 1 h of light exposure, the seedlings were grown in darkness for 60-72 h at 22 °C.

3.5.3 Specimen mounting

Seedlings were mounted between a 24 x 60 mm cover glass and a 1-mm thick 0.8% agar pad affixed to a 22 x 22 mm cover glass. The agar cushion stabilized the specimen for sustained time-lapse imaging, minimized compression and mechanical damage, and allowed greater reproducibility in mounting conditions.

3.5.4 Drug treatments

For time-courses, seedlings were mounted in solution containing the chemical agent(s) and imaged at various time points. For other experiments, seedlings were submerged in 2 ml of solution in 12-well cell culture plates (Becton Dickinson) and incubated in darkness. Isoxaben, brefeldin A, latrunculin B, taxol, oryzalin (Sigma-Aldrich) and AE F150944 (Bayer CropScience) were dissolved in dimethyl sulfoxide (DMSO) or methanol to create stock solutions. Working solutions of chemicals were freshly diluted in water from these stocks immediately before use. Propidium iodide (PI) and FM4-64 were dissolved in water and used at a concentration of $10 \mu\text{g ml}^{-1}$ and $20 \mu\text{M}$, respectively

3.5.5 Confocal microscopy

Imaging of plants expressing GFP:CESA3 and mCherry-TUA5 or MAP4-MBD was performed on a system featuring a CSU-X1 spinning disk head (Yokogawa), Axiovert 200 inverted microscope (Zeiss), x100/1.4 NA oil immersion objective, QuantEM:512SC CCD camera (Roper Scientific) and x1.2 lens between the spinning disk unit and camera. Excitation switching and shuttering was performed by a multi-channel AOTF device (AA Opto-Electronic Company), and emission filtering was accomplished with band pass filters (530/50 nm for GFP, and 640/50 nm for mCherry; Chroma Technology). GFP and mCherry were excited at 491 nm and 561 nm, respectively, by solid-state lasers. Typical exposure times were 600 ms for GFP and 300 ms for mCherry.

Photobleaching was performed by a FRAP/PA system (Roper Scientific) integrated into the setup above. Focused laser light was scanned on the image plane by a pair of galvometer-driven mirrors inside the FRAP/PA unit. Scanner positions were calibrated to image coordinates using an automated procedure. GFP photobleaching was performed with a 491 nm laser (5 ms per scan point of 4 pixels in diameter) for plants expressing GFP-CESA3 and mCherry-MAP4-MBD or a 405 nm laser (10 ms per scan point) for plants expressing GFP-CESA3 and mCherry-TUA5.

Imaging of seedlings expressing YFP-CESA6 and mCherry-SYP41/42/61 or labelled with FM4-64 was performed on a system similar to the one described above, except a DMI6000 B inverted microscope (Leica) was used and an AOTF from Crystal Technologies was used to select and attenuate excitation light. YFP was imaged using the same settings as GFP, and FM4-64 used the same settings as mCherry.

All other imaging was performed on a system as described previously (Paredes et al., 2006). Fluorescent markers were excited at 442 nm (CFP), 488 nm (GFP/YFP), 514 nm (YFP) or 568 nm (PI). Emission was collected through band-pass filters (Chroma Technologies): 480/40 nm (CFP), 525/50 nm (GFP/YFP), 570/65 nm (YFP) and 620/60 nm (RFP and PI). Acquisitions were typically performed with 500-ms exposures (with two-frame averaging).

For all imaging experiments, focal shift was monitored by tracking other objects in the same focal plane as the object under study.

3.5.6 General image processing

All image processing was performed using ImageJ software (Rasband, 2012). For analyses involving measurement of signal intensity, only linear adjustments to pixel values were made. For other images, background signal was reduced using the 'Subtract Background' tool (rolling ball radius of 20 - 30 pixels) in ImageJ. Image drift was corrected using ImageJ plugins: StackReg (Thevenaz et al., 1998) and MultiStackReg (<http://www.stanford.edu/~bbusse/work/downloads.html>). Post-acquisition frame averaging (http://valelab.ucsf.edu/nico/IJplugins/Running_ZProjector.html) was applied to time series where indicated.

3.5.7 Colocalization analysis of CESA delivery sites and cortical microtubules

GFP signal in seedlings expressing GFP-CESA3 and mCherry-MAP4-MBD was bleached at the plasma membrane and imaged at 2-s intervals. The CESA channel was scanned for delivery events defined by punctae appearing at the plasma membrane and then moving steadily. Sixty events from 3 cells were selected arbitrarily and analysed. For each putative delivery event, previous frames were studied to ensure that the puncta of interest appeared *de novo* and could not be attributed to other particles nearby. At the start of the static phase ($t = 0$), the centroid of the particle was determined by eye. A 3-frame running average was applied to the microtubule channel. The frame representing $t = 0$ was then thresholded using the Isodata algorithm in ImageJ to create a binary image of microtubule signal. The particle centroid was then mapped onto the binary image to determine colocalization.

A binomial test was used to determine whether CESA delivery was coincident with microtubules at a frequency higher than chance. The expected colocalization between delivery events and microtubules, according to the null hypothesis, was dependent on the optical coverage of microtubule signal at the cell cortex. To calculate this value, the microtubule channel was converted into a binary image stack, and averaged over the time series. The mean pixel intensity in this time average projection represented the optical coverage. Overall, microtubules occupied approximately 50.7% of the cell cortex. From our analysis, 47 of 60 delivery events were coincident with microtubules. The observed frequency is significantly higher than chance according to the binomial test ($P < 0.001$).

3.5.8 Delivery rate analysis of CESA complexes

Seedlings expressing GFP-CESA3 and mCherry-MAP4-MBD or TUA5 were treated with control, oryzalin (20 μM) or mannitol (200 mM) for 308 h and bleached as described above. All observable CESA delivery events within a large area (277-569 μm^2) of the bleach region were counted over a 3- to 10-min window per cell. For control, 811 events in 1031 μm^2 were observed in 3 cells over a combined 30 min. For oryzalin, 1011 events in 1458 μm^2 were observed in 3 cells over a combined 30 min. For mannitol, 8 events in 1778 μm^2 were observed in 5 cells over a combined 22 min.

3.5.9 Measurement of particle intensity in kymographs

CESA-labelled particles occasionally appeared to split into two or more daughter particles. To confirm that the CESA signal was conserved before and after putative splitting events, individual particle intensities were measured in a background-subtracted kymograph. For each time-point, a 5-pixel (0.67 μm) portion of the kymograph line, centered on the particle, was measured. Mean intensity from multiple time points was then calculated. Surface plots of kymographs were generated using the Interactive 3D Surface Plots plugin (<http://rsbweb.nih.gov/ij/plugins/surface-plot-3d.html>).

3.5.10 Measurement of SmaCC density at cell cortex

Time series imaging of YFP-CESA6 labelled cells was performed in the optical plane of the cell cortex. SmaCCs in the first frame of the time series were tallied. SmaCCs were identified by optical size and dynamic behaviour as revealed in subsequent frames. The area of the visible cortex was also measured, and density was calculated (number of compartments per 100 μm^2).

3.5.11 Organelle velocity analysis

Frame-to-frame velocities of objects were measured using the ImageJ SpotTracker plugin (Sage et al., 2005). A Gaussian blur filter (2 pixel radius) was applied to time series of Golgi body images to identify centroids with greater ease. For each time point, multiple objects were tracked in at least 3 cells in 3 plants. The set of frame-to-frame velocities for one object was treated as a statistical subgroup. The weighted average of subgroups for each time point was calculated, as well as the standard error of this value. Linear regression was performed using Prism 5 (GraphPad software) to determine whether organelle velocity decreased significantly over time (that is, slope less than zero). Two-level nested ANOVA was also performed to determine whether organelle velocity differed significantly between two treatments.

3.6 Acknowledgements

We thank S. Vernhettes, E. Nielsen and N. Geldner for providing transgenic Arabidopsis seeds; V. Kirik for help with vector construction; B. Busse for modifying the ImageJ frame alignment plugin; and S. Debolt, V. Kirik, R. Brown, T. Ketelaar and H. Höfte for helpful discussions. This work was supported by grants from the National Science Foundation (0524334) and the EU Commission (FP6-2004-NEST-C1-028974).

3.7 Supplementary information

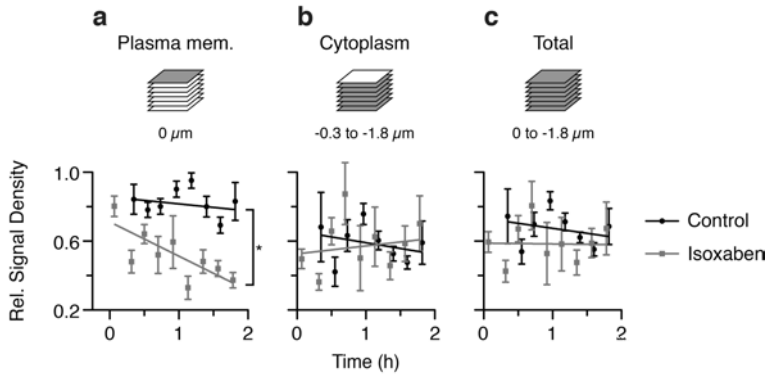


Figure S3.1: Isoxaben causes loss of YFP-CESA6 signal from the plasma membrane. Seedlings expressing YFP-CESA6 were treated with 0.01% DMSO (control) or 100 nM isoxaben in 0.01% DMSO. Z-series of 10 optical planes, spaced $0.3 \mu\text{m}$ apart, were acquired. Propidium iodide was used to stain the cell wall, providing a fiducial marker for the start of the z-series. Based on examination of many images, we determined that the outer three planes ($z = +0.3$ to $+0.9 \mu\text{m}$) represented the extracellular space and the fourth ($z = 0 \mu\text{m}$) represented the plasma membrane. The next six planes ($z = -0.3$ to $-1.8 \mu\text{m}$) sampled the cellular space interior to the plasma membrane. Relative YFP-CESA6 signal densities were measured in background-subtracted images representing the plasma membrane (a), cytoplasm (b) and total (c). Each data point represents signal density (relative intensity per unit volume) from at least 3 cells from 3 unique plants. Isoxaben significantly decreases YFP-CESA6 signal at the plasma membrane (a) compared to control ($P = 0.027$, F-test for equality of slopes of regression lines). Total integrated signal does not change significantly (c), suggesting there is no net loss of CESA6. Since most of the total CESA6 protein resides in cytoplasmic organelles, and measured values for cytoplasmic signal have high variance (b), it is not possible to determine if the protein lost at the plasma membrane could be accounted for in cytoplasmic pools. Measurements in a were corrected for out-of-focus signal caused by Golgi bodies and small compartments. First, the planes representing the cytoplasm were summed and thresholded by eye. Structures larger than 12 square pixels were identified using the 'Analyze particles' tool in ImageJ. Regions of the plasma membrane that were directly above these structures were eliminated from analysis. Thus the reported intensities in a primarily represent signal from CESA punctae in the plasma membrane. Error bars represent s.e.m.

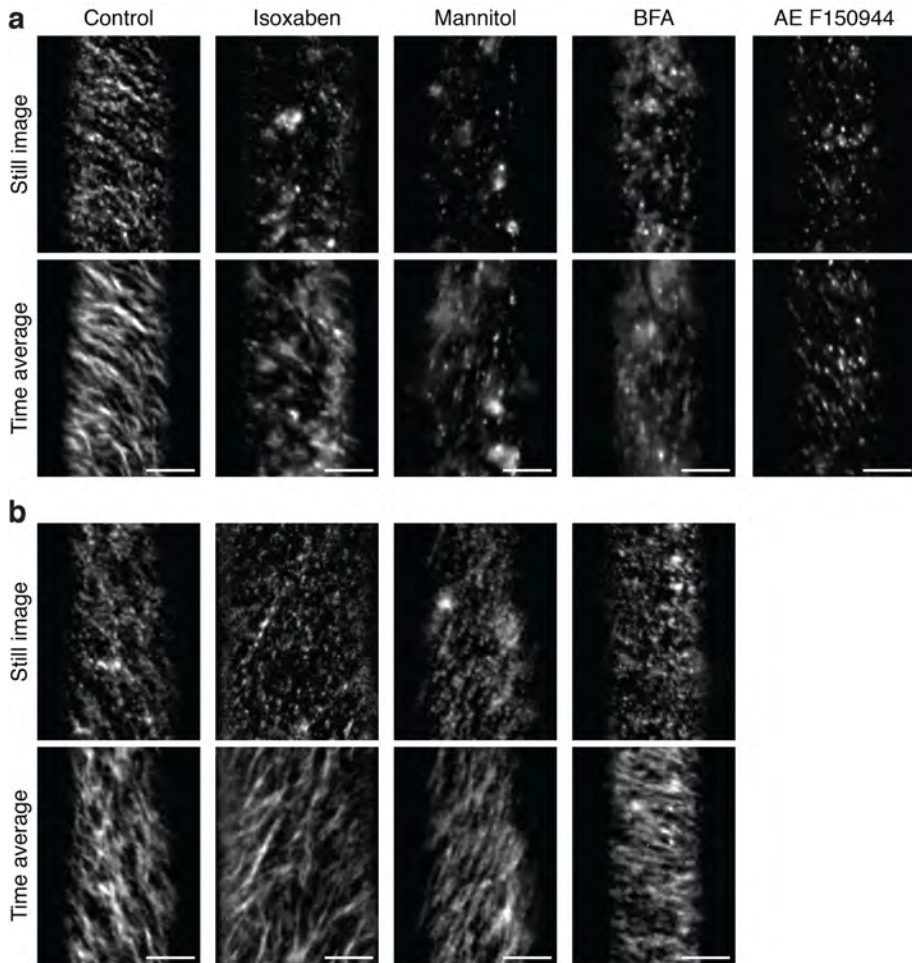


Figure S3.2: Effects of isoxaben, mannitol or BFA treatment on CESA6 are reversible. Seedlings expressing YFP-CESA6 were treated with 0.05% DMSO (control), 100 nM isoxaben in 0.01% DMSO, 200 mM mannitol, 50 μ M BFA in 0.05% DMSO or 10 nM AE F150944 in 0.01% DMSO for 3 h (a). In all non-control treatments, few punctae are visible in the plasma membrane, and many SmaCCs are observed in the cell cortex. The plants were then incubated in water for 5 h. After washing, CESA6 complexes accumulate in the plasma membrane and are motile in all treatments (b). Observations were performed on three plants per treatment. Representative images are shown. Washout was not performed for AE F150944-treated plants. Time-averaged projections were made from 61 images collected over 5 min. Scale bar, 5 μ m.

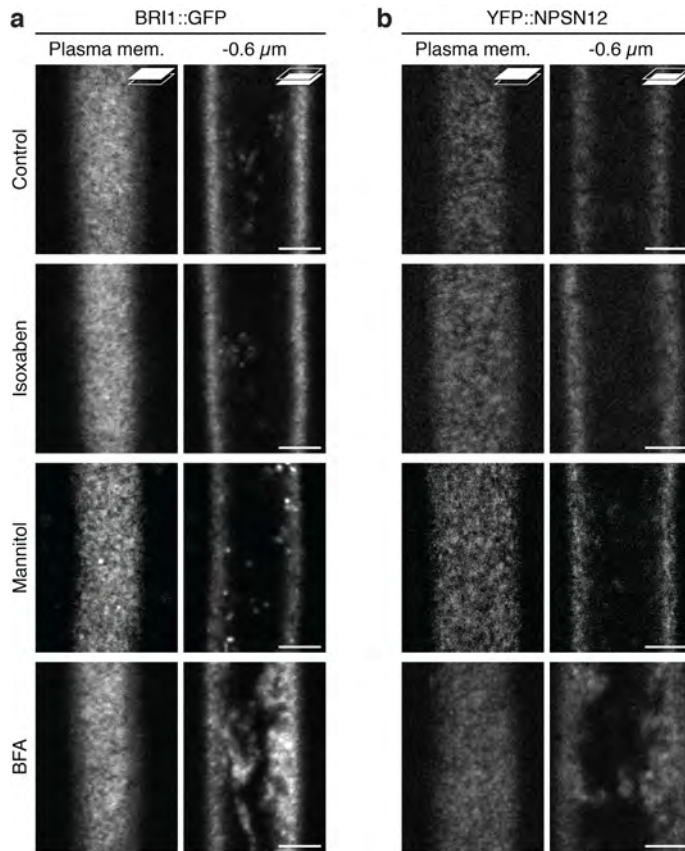


Figure S3.3: Isoxaben does not generally affect the localization of plasma membrane proteins. Seedlings expressing plasma membrane markers BRI1-GFP (a) or YFP-NPSN12 (b) were treated with 0.05% DMSO (control), 100 nM isoxaben in 0.01% DMSO, 200 mM mannitol or 50 μ M BFA in 0.05% DMSO. Focal planes at the plasma membrane and lower cell cortex are shown. Isoxaben does not noticeably disrupt localization of either labeled protein. Mannitol causes some detectable internalization of BRI1 signal but does not induce plasmolysis at the concentration used. BFA causes intracellular accumulation of labeled BRI1 and NPSN12. Scale bar, 5 μ m.

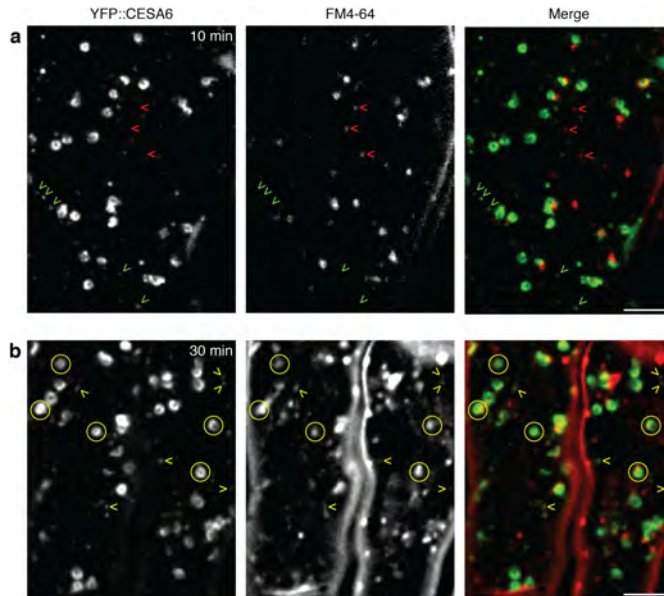


Figure S3.4: FM4-64 dye is internalized into SmaCCs slowly. YFP-CESA6 seedlings were light-grown for 3 days and incubated in 200 mM mannitol and 20 μ M FM4-64 for 10 min (a) or 30 min (b). Epidermal hypocotyl cells were imaged. (a) At 10 min, the dye labels endosomes (Bolte et al., 2004) (red arrowheads) that are not coincident with cortically tethered SmaCCs (green arrowheads), which were identified based on their dynamics. (b) After 30 min, the dye labels Golgi bodies (circles) and some SmaCCs (yellow arrowheads), indicating that it is possible to eventually load enough dye into SmaCC membranes for positive detection. The fact that dye is not detected in SmaCCs at earlier time points, although the plasma membrane is well labeled, suggests that most observed SmaCCs are not directly formed by endocytosed plasma membrane. Scale bar, 5 μ m.

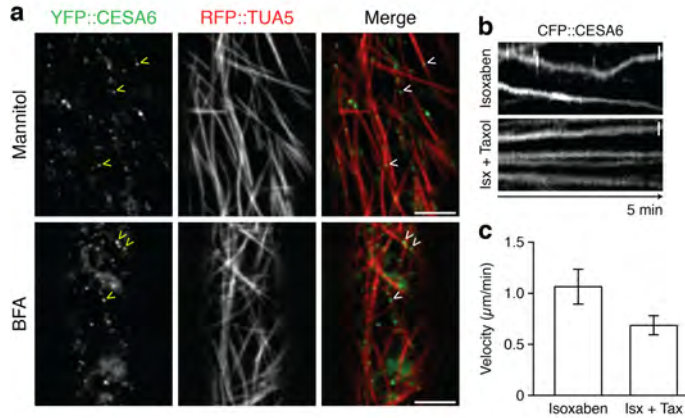


Figure S3.5: SmaCCs colocalize with cortical microtubules in cells treated with BFA or mannitol. Seedlings expressing YFP-CESA6 and mCherry-TUA5 were treated with 200 mM mannitol or 50 μ M BFA for 3 h. SmaCCs (arrowheads) show colocalization with microtubules. Scale bar, 5 μ m. (b, c) Stabilization of cortical microtubules by taxol lowers SmaCC velocity under isoxaben treatment. Seedlings expressing CFP-CESA6 and YFP-TUA5 were treated with 100 nM isoxaben in 0.11% DMSO or 100 nM isoxaben + 20 μ M taxol in 0.11% DMSO for 2 h. Visualization of labeled microtubules confirmed that taxol slowed down depolymerization of microtubules. (b) Representative kymographs of SmaCCs. (c) Velocities of SmaCCs in the cell cortex. For each treatment, $n = 24$ SmaCCs from 4 cells (from 4 seedlings). Application of isoxaben and taxol together reduces SmaCC velocity more than isoxaben does alone ($P < 0.001$, two-level nested ANOVA). Error bars represent s.e.m. Scale bar, 1 μ m.

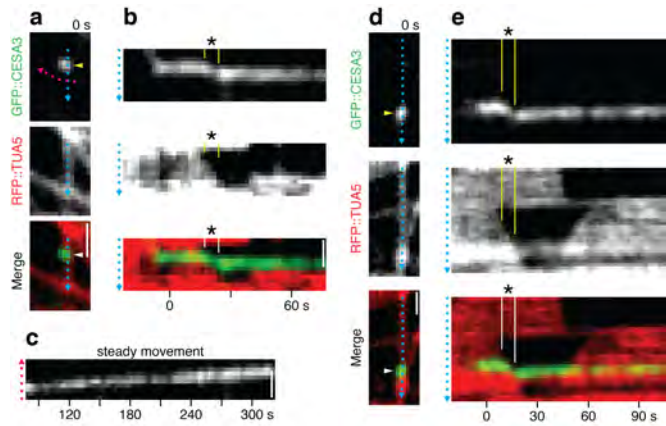


Figure S3.6: Two additional examples of CESA tip tracking under normal conditions. Seedlings expressing GFP-CESA3 and mCherry-TUA5 were imaged in the absence of drugs. (a,c) First example. (a) Still images at $t = 0$ showing GFP-CESA3 (arrowhead) and an associated microtubule. (b) Kymograph along cyan trace in a. A CESA particle appears in the focal plane of the plasma membrane and becomes stationary. This static behavior is interrupted by a depolymerizing end. GFP-CESA3 tracks with the end for several frames (*) and then becomes static again. (c) Kymograph along magenta trace in a. At 78 s, the CESA particle moves steadily. (d, e) Second example. (d) Still images at $t = 0$ showing GFP-CESA3 (arrowhead) and an associated microtubule. (e) Kymograph along cyan trace in d. As in b, GFP-CESA3 tracks on a depolymerizing end (*). Scale bar, $1 \mu\text{m}$.

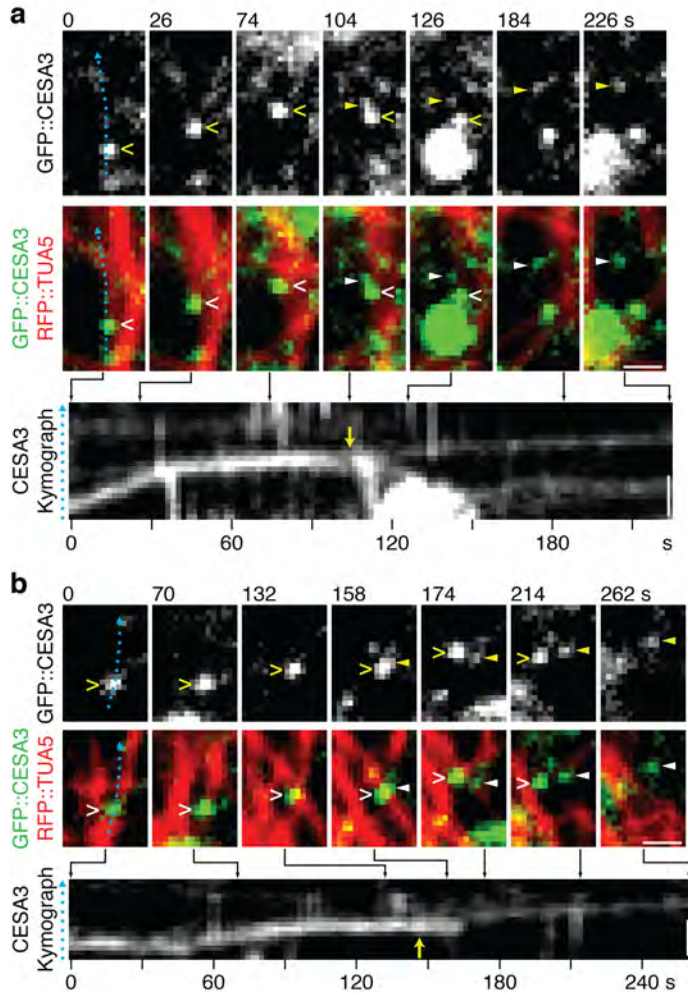


Figure S3.7: Two additional examples of CESA delivery events that are associated with SmaCCs. Seedlings were treated with 200 mM mannitol for 3 h and then washed with water for 0.5 h. Kymographs were taken along the cyan trace. Yellow arrows mark bifurcation on the kymographs. (a) First example. A SmaCC (open arrowhead) tracks on a depolymerizing end before splitting into two structures of unequal intensity at 104 s. The brighter particle (open arrowhead) moves in a manner consistent with SmaCC motility. The dimmer particle (closed arrowhead) moves at a slow and steady rate, consistent with CESA complex motility in the plasma membrane. (b) Second example. A similar event occurs in a different cell. The splitting event occurs at around 146 s. Scale bar, 1 μm .

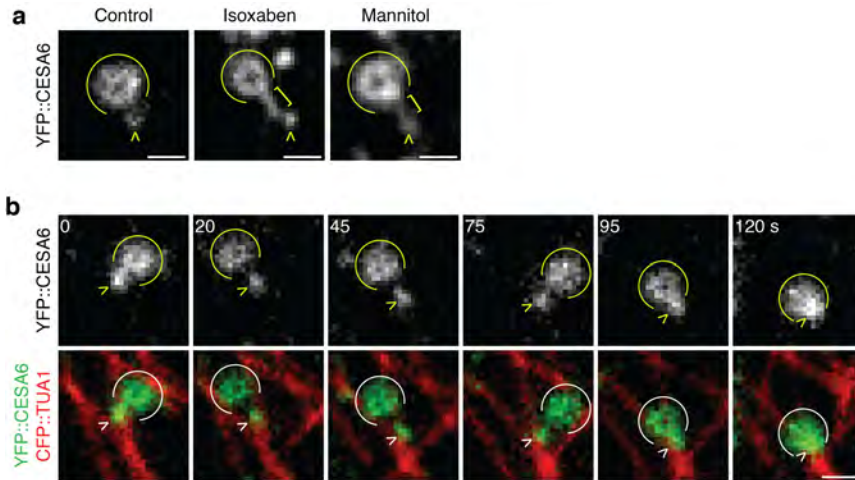


Figure S3.8: Golgi bodies associate with SmaCCs. (a) YFP-CESA6 seedlings were treated with 0.01% DMSO (control), 100 nM isoxaben in 0.01% DMSO or 200 mM mannitol for 3 h. In the control, physical association between Golgi bodies (arcs) and SmaCCs (arrowheads) is frequently observed. With isoxaben or mannitol treatment, this association is more conspicuous: the two structures are sometimes observed to be connected by a detectable strand of YFP-CESA6 signal (bracket), which may represent a membrane bridge. (b) Association between Golgi bodies and cortically localized SmaCCs persists for up to several minutes in the presence of cytoplasmic streaming. Seedlings expressing YFP-CESA6 and CFP-TUA1 were treated with 100 nM isoxaben for 2 h. A short distance ($< 1.3 \mu\text{m}$) is maintained between a Golgi body and a moving SmaCC for 120 s, suggesting the two are physically tethered. These observations suggest that some SmaCCs can form tight associations with Golgi bodies, which might be the case if these SmaCCs are derived from them or interact closely with them to exchange cargo. Scale bar, $1 \mu\text{m}$. See Movie 15.

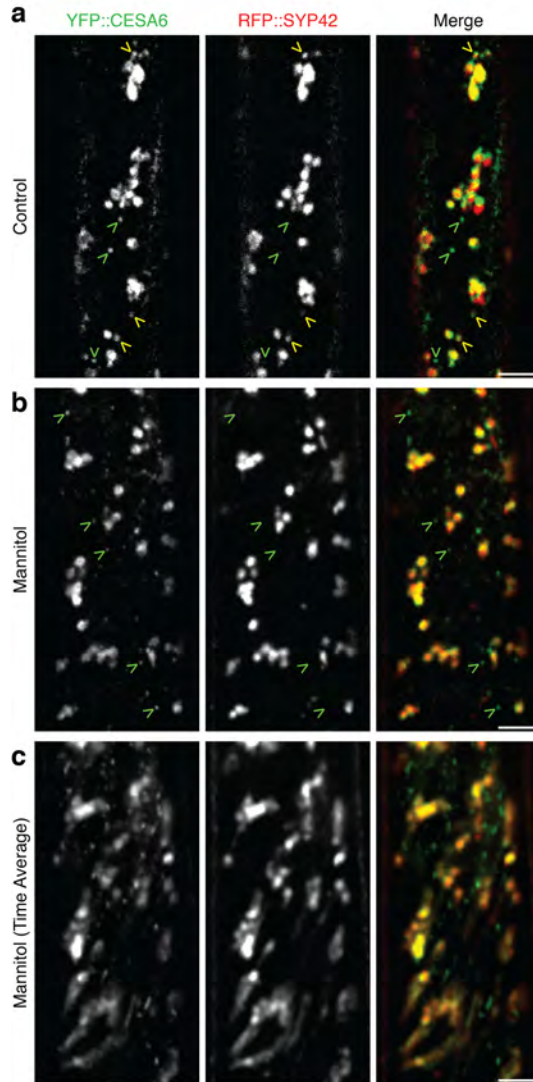


Figure S3.9: SYP42 labels a subset of SmaCCs. Seedlings expressing YFP-CESA6 and mCherry-SYP42 were incubated in water (a) or 200 mM mannitol (b, c) for 3 h and imaged at the cell cortex. (a) Some small compartments are labeled by YFP only (green arrowheads) or both YFP and mCherry (yellow arrowheads). (b, c) SYP42 fails to label cortically tethered SmaCCs (green arrowheads) after mannitol treatment. (a, b) Still images. (c) Averages of 61 frames representing 1 min. Scale bar, 5 μm .

Associations between the actin and microtubule cytoskeleton

4

4.1 Abstract

In eukaryotic cells, the actin and microtubule (MT) cytoskeletal networks are dynamic structures that organize intracellular processes and facilitate their rapid reorganization. In plant cells, actin filaments (AFs) and MTs are essential for cell growth and morphogenesis. However, dynamic interactions between these two essential components in live cells have not been explored. Here, we use spinning-disc confocal microscopy to dissect interaction and cooperation between cortical AFs and MTs in *Arabidopsis thaliana*, utilizing fluorescent reporter constructs for both components. Quantitative analyses revealed altered AF dynamics associated with the positions and orientations of cortical MTs. Reorganization and reassembly of the AF array was dependent on the MTs following drug-induced depolymerization, whereby short AFs initially appeared colocalized with MTs, and displayed motility along MTs. We also observed that light-induced reorganization of MTs occurred in concert with changes in AF behavior. Our results indicate dynamic interaction between the cortical actin and MT cytoskeletons in interphase plant cells.

4.2 Introduction

The cytoskeleton supports many fundamental cellular processes, including morphogenesis, cell division, and vesicle trafficking (Goode et al., 2000; Fu et al., 2005; Collings, 2008; Gutierrez et al., 2009; Petrásek and Schwarzerová, 2009; Szymanski and Cosgrove, 2009). The actin filaments (AFs) and microtubules (MTs) were formerly viewed as two distinct networks with separate functions, but were found to cooperate in yeast (*Saccharomyces cerevisiae*) and animal cells (Goode et al., 2000). For example, coalignment of AFs and MTs was observed in *Taricha granulosa* (newt) lung epithelial cells (Salmon et al., 2002), and MTs were transported in association

with AFs to sites of induced wounding in *Xenopus laevis* oocytes (Mandato and Bement, 2003). Whereas AFs and MTs are common to eukaryotic organisms, structural and functional differences are evident in plant species; perhaps due to the presence of a rigid cell wall and a large central vacuole, and also due to the absence of the cytoskeleton-organizing centers referred to as centrosomes in animal cells and as spindle pole bodies in yeast cells (Ehrhardt and Shaw, 2006)

Reports of AF and MT associations in plants are scarce, but are supported by imaging of fixed tissues, pharmacological studies, and the existence of common binding partners (Collings, 2008). In fixed tissues, fine transverse AFs have been observed as an ordered array, reminiscent of the transverse arrangements of MTs (Collings and Wasteneys, 2005), and AFs and MTs have been observed to coalign (Traas et al., 1987; Blancaflor, 2000; Collings and Wasteneys, 2005; Barton and Overall, 2010). MT depolymerization resulted in partial loss of the fine transversely oriented cortical AFs in *Arabidopsis thaliana* and carrot (*Daucus carota*) cells, leading to the proposal that associations between the AFs and MTs may occur (Traas et al., 1987; Collings and Wasteneys, 2005). In addition, environmental or developmental cues have been documented to induce changes in MTs and AFs, hinting at coordinate action. For example, reorientation of the MT array was concurrent with changes in AF organization in tracheary elements of developing *Zinnia elegans* cells (Kobayashi et al., 1988), and disruption of the AFs impaired MT reorganization, an effect that also was observed in azuki bean (*Vigna angularis*) cells (Takesue and Shibaoka, 1998).

The use of electron and confocal microscopy has allowed for a basic understanding of the behavior of the individual cytoskeleton components (Traas et al., 1987; Shaw et al., 2003; Sheahan et al., 2004; Staiger et al., 2009). Because the AFs and MTs are highly dynamic (Shaw et al., 2003; Staiger et al., 2009), a plausible scenario is that interactions occur only briefly, which would make them challenging to capture in static images by electron microscopy. Monitoring both components in real time using stably transformed cells with dual-labeled reporter constructs may provide a powerful tool for revealing coordinate behavior and elucidating the underlying principles. Only two previous reports, one focusing on trichomes (Saedler et al., 2004) and the other on root hairs (Timmers et al., 2007), have used dual-labeled probes for AFs and MTs in plants, but evidence for or against heterotypic interaction remains needed.

We have investigated coordinated AF and MT activities, using spinning disc confocal microscopy of dual-labeled lines, coupled with pharmacological studies. We deduce quantitatively that AFs and MTs interact dynamically, and that the AFs depend on the MTs to recover following drug-induced depolymerization events and for reorganization following light stimulus.

4.3 Results

4.3.1 Stabilization of the actin cytoskeleton leads to aberrant MT organization

Several studies have assessed MT behavior after AF disruption via pharmacological agents such as latrunculinB (latB) and cytochalasinB (Collings, 2008). Here, we tested whether a more stable actin configuration had an impact on the organization of MTs using the drug jasplakinolide (Bubb et al., 1994). Because jasplakinolide has not been extensively employed in plant cell biology, we first grew *Arabidopsis* seedlings on different concentrations of the drug and assessed the impact on growth (see Figures S4.1A to 4.1E). From these experiments, and subsequent experiments using seedlings expressing green fluorescent protein (GFP)-F-actin binding domain of fimbrin1 (FABD) (Ketelaar et al., 2004), we determined that 5 μM was a suitable concentration for short-term jasplakinolide treatments. Short-term treatment of 5-d-old seedlings with jasplakinolide (5 μM for 3 h) revealed that actin bundles and filaments became fragmented, rigid, and less dynamic in hypocotyl cells (Figures 4.1A and 4.1B; see MovieS4.1 online). To investigate whether this behavior was reversible, we performed washout experiments for a period of 48 h, and we observed that the AFs recovered (see FigureS4.1F). To assess the impact of this treatment on the MTs, we exposed 5-d-old seedlings expressing mCherry- α -tubulin 5 isoform (TUA5) (Gutierrez et al., 2009) to the same treatment conditions. Interestingly, MT orientation was less ordered after short-term treatment of jasplakinolide compared with controls (Figures 4.1C and 4.1D). As previously observed (Paredez et al., 2006), cortical MTs in elongating cells were transversely or obliquely oriented to the cell axis in arrays with marked parallel ordering (Figures 4.1C and 4.1E). Treatment with jasplakinolide caused a striking loss of array order (Figures 4.1D and 4.1E). To check whether MT dynamics were influenced by jasplakinolide treatment, we measured the growth (v_g) and shrinkage velocities (v_s) of the plus end of single MTs. No significant differences were found between the jasplakinolide- and mock-treated cells (Figure 4.1F).

Because the mode of action of jasplakinolide as an actin-stabilizing drug in plant cells was not established prior to this study, it was important to test whether the drug cross-reacted with MTs, thereby disturbing MT organization. To test this hypothesis, we generated *Arabidopsis* plants coexpressing mCherry-TUA5 and GFP-FABD. Dual-labeled 5-d-old seedlings were treated with 1 μM latB for 6 h, and 5 μM jasplakinolide was added for an additional 6 h. As expected, the latB treatment completely removed the actin cytoskeleton and only free GFP-FABD was observed (see Figure S4.1G). In the absence of AFs, the MTs in jasplakinolide-treated cells remained arranged as observed in control-treated seedlings (see FigureS4.1G and 1H online), i.e., the latB/jasplakinolide-treated seedlings displayed MTs with parallel orientation (see Figure S4.1G). Thus, the effect of jasplakinolide on cortical MT organization was dependent on actin assembly and was not due to action of the drug on a second target.

To assess the organization of the fragmented actin cytoskeleton relative to MTs,

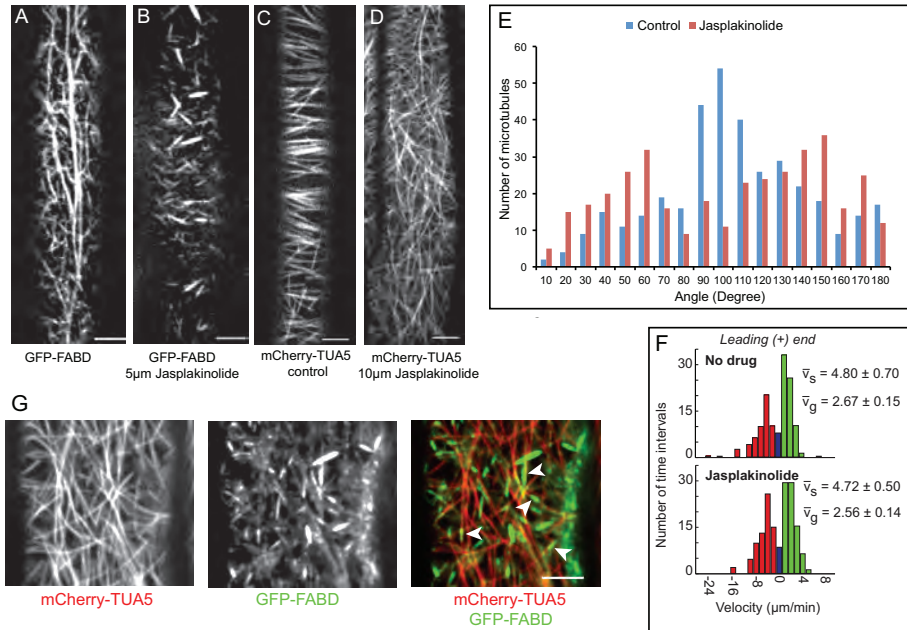


Figure 4.1: Jasplakinolide affects MT orientation through stabilization of the actin cytoskeleton. (A) and (B) Organization of the actin cytoskeleton in mock-treated (A) and jasplakinolide-treated (B) hypocotyl cells of GFP-FABD-expressing 5-d-old etiolated seedlings. (C) and (D) MT organization in control (C) and jasplakinolide-treated (5 μM for 3 h [D]) hypocotyl cells of YFP-TUA5-expressing 5-d-old etiolated seedlings. (E) Histogram documenting distribution of MT angles with regard to the growth axis. (F) v_g and v_s were measured for the leading ends of single MTs (\pm SE). Histograms are presented showing shrinkage (red), growth (green), and pause (blue). (G) Actin fragments reside in transient coincidence with cortical MTs after jasplakinolide treatment (5 μM for 6 h). White arrowheads indicate actin fragments aligned with MTs. Scale bars, 5 μm .

we treated 5-d-old GFP-FABD and mCherry-TUA5 dual-labeled seedlings with jasplakinolide. Interestingly, static AFs, which were present throughout the cortical focal plane, appeared to align with MTs (Figure 4.1G; Movie S2). In addition, a fraction of small actin fragments was observed to align with and move along paths defined by MTs (see Movie S2).

Together, these results suggested the possibility of crosstalk between the actin and MT cytoskeletons in that alteration of actin assembly or turnover, as perturbed by jasplakinolide, was correlated with loss of MT organization, and stabilized AFs were found to align with and move along MTs.

4.3.2 Cortical AFs transiently coalign with MTs

The alignment between fragmented AFs and MTs in the jasplakinolide-treated cells prompted us to investigate whether the two cytoskeletal structures also interact under normal conditions. Confocal observation of dual-labeled hypocotyl cells of 3-d-old etiolated seedlings revealed numerous sites where cortical AFs and MTs were colocalized and coaligned (Figures 4.2A to 4.2C; see Movies S3 and S4). Coalignment between the MTs and AFs was observed mainly between transversely or obliquely oriented AFs and MTs at the cell cortex; however, in some instances, we also observed alignment between longitudinal cortical actin bundles and MTs. The AFs emerged from lower focal planes or moved across the cortical optical plane, and aligned with MTs (Figures 4.2D and 4.2E; see Movies S3 and S4). Straightening and bending events of cortical AFs, as reported by Staiger et al. (2009), were also observed to coalign with MTs in some cases (Figure 4.2E; see Movie S4).

Some degree of colocalization and coalignment of the two labeled cytoskeletal structures would be expected by chance alone if the two systems were independent. We analyzed the dynamics of coalignment to determine if it was non-random. We observed that sections of dynamic AFs that aligned with MTs were frequently stabilized in this configuration over short periods of time (Figures 4.2D and 4.2E). We refer to these stabilized AF configurations as AF pauses. We surveyed AF pausing that occurred for 30 s or longer using linear transects and kymograph analysis along the entire cell length and we found that the majority of AF pauses coincided with MTs. Of the 114 pause events observed in four cells, 78 (or 68.4%) coincided with MTs (Figures 4.2F and 4.2G), which is significantly higher than the 53 events expected by chance based on MT signal coverage in the images ($P < 0.001$, binomial test, see materials and methods). The majority of the non-pausing AFs in the kymograph did not align with the MTs. Hence, changes in AF dynamics were associated with MT juxtaposition.

4.3.3 Coordinated changes to AFs and MT organization upon light induction

We observed that 35% of the AF pausing events (see Figure 4.2) occurred during the first 50 s of imaging (Figure 4.3A; see Figure S4.2A). The other pausing events were

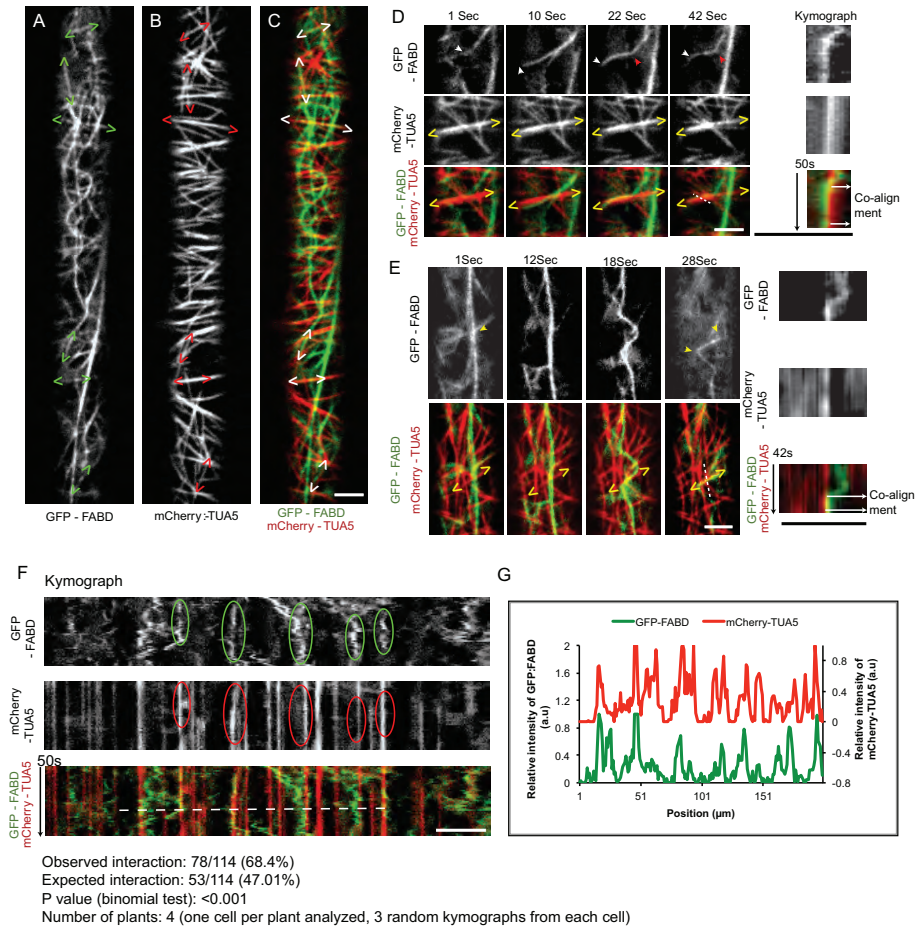


Figure 4.2: Coalignment between cortical AFs and MTs in *Arabidopsis* hypocotyl cells. (A) to (C) Dual-labeled GFP-FABD (A) and mCherry-TUA5 (B), and merge of A and B (C), observed in hypocotyl cells of 3-d-old etiolated seedlings. Carets enclose regions of co-occurrence of the two channels. (D) Selected frames from a time series of a GFP-FABD and mCherry-TUA5 dual-labeled line. Red arrowheads indicate regions where AFs appear static after MT alignment. White arrowhead indicates that AFs emerge from a lower focal plane, and yellow carets enclose the region of MT and AF coalignment. The far right panel shows a kymograph corresponding to the dashed white line, with time on the vertical axis.

Figure 4.2: (E) AF bending and straightening events facilitate alignment between AFs and MTs. Yellow arrowheads indicate the region of the AF that exhibits bending, and yellow carets enclose the region of the coaligned MT and AF. The far right panel shows a kymograph corresponding to the white dashed line, with time on the vertical axis. (F) Kymograph covering the entire cell length showing multiple static AF events (green enclosure) that coincided with MTs (red enclosure). Only AFs that were static for more than 30 s were considered. (G) A fluorescence intensity plot of a transect of the kymograph shown in (F) [white dashed line]). a.u., arbitrary units. Scale bars, 5 μm .

observed during the remaining 10 min of imaging. Thus, observation of pausing was significantly biased to the beginning of the observation interval, indicating that the act of observation may influence the frequency of pausing. This was reminiscent of previous observations that transversely oriented MTs in etiolated hypocotyl cells rearrange in response to light during observation (Ueda and Matsuyama, 2000; Paredes et al., 2006). However, comparable analyses for light-induced changes in AFs are lacking. Consistent with previous studies, we confirmed that MTs rearranged from a largely transverse orientation to a more oblique array under our imaging conditions (Figures 4.3B and 4.3C). We then observed the organization and behavior of the AFs and MTs in 3-d-old dual-labeled dark-grown hypocotyls (Figure 4.3C; see Movie S5). Intriguingly, time-series images revealed that the cortical and mainly transversely oriented AFs became progressively less prevalent during imaging (Figures 4.3C and 4.3D). The altered behavior of AF distribution at the cell cortex occurred in tandem with the light-induced rearrangement of the MT array (Figures 4.3B and 4.3D). To investigate whether the changes in behavior of AFs were influenced by the MT cytoskeleton, we treated seedlings expressing mCherry-TUA5 with 20 μM oryzalin (an MT-depolymerizing drug) overnight to ensure complete depletion of MTs (see Figure S4.2B). The spatial distribution of the AF signal remained nearly constant throughout the imaging process in the absence of the MT cytoskeleton (see Figures S4.2C and S4.2D). These results indicate that the organization of MTs may, directly or indirectly, influence the distribution of AFs at the cortex.

4.3.4 AFs Recover along MTs following washout of LatB

To investigate further the dynamic interactions between AFs and MTs, we assessed reassembly behavior of both structures after depolymerization. We treated 3-d-old dual-labeled GFP-FABD and mCherry-TUA5 seedlings with latB overnight, and then allowed for actin recovery after washout of the drug. The overnight latB treatment resulted in complete removal of the labeled actin cytoskeleton in hypocotyl cells. At about 3 h after latB washout, short fragments of actin label began to appear at the cell cortex (Figure 4.4A, Figure 5.4A; Movie S6). These nascent foci of actin label

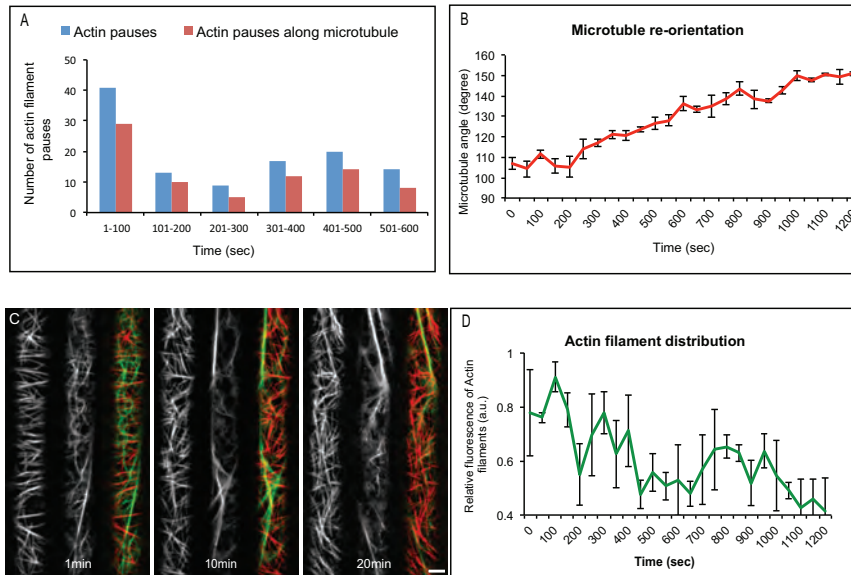


Figure 4.3: Light-induced rearrangements of the cytoskeleton. (A) Histogram showing actin-MT interaction over time ($n = 4$ cells). (B) Changes in average MT angle over time during the process of imaging ($n = 3$ cells). Error bars represent SE. (C) Selected frames from a time series of a GFP-FABD and mCherry-TUA5 dual-labeled line at the hypocotyl cell cortex in etiolated 3-d-old seedlings after light exposure. (D) Changes in relative fluorescence intensity of AFs over time ($n = 3$ cells). Error bars represent SE. a.u., arbitrary units. Scale bars, $5 \mu\text{m}$.

appeared in linear arrays that coincided with MTs in image overlays and line scan analyses (Figures 4.4A and 4.4B; Movie S6). These observations indicate that new actin polymerization can be initiated at positions coinciding with cortical MTs.

The labeled AFs increased in size during recovery from an average of $0.85 \pm 0.30 \mu\text{m}$ (3 h after latB washout) to $2.15 \pm 0.75 \mu\text{m}$ and $4.18 \pm 2.03 \mu\text{m}$, after 5 and 8 h of recovery, respectively ($n = 100$, three cells from three seedlings). Intriguingly, 5 h after latB washout, reformed AF fragments were observed traveling along cortical MTs with varying velocities, i.e., 7.4 to $17.3 \mu\text{m}/\text{min}$ ($n = 37$; Figure 4.4C; see Movie S7). From time series taken from three cells, we observed 12 incidences of reformed actin fragments that migrated together with dynamic MT plus ends (Figures 4.4C to 4.4E; see Movie S8). It is important to note that the actin cytoskeleton had almost completely recovered 24 h after latB washout, indicating that the pharmacological effects were reversible (Figure 4.5B; see Movie S9). Together, these results corroborate interaction and coalignment between AFs and MTs in vivo.

The observed re-emergence of AFs along MTs suggests that AF polymerization can occur at MT sites in *Arabidopsis* cells. We investigated time series images of mCherry-TUA5 and GFP-FABD dual-labeled lines, and observed instances of polymerization of new AFs emanating from existing actin bundles that were colocalized with MTs (see Figure S4.2E and Movie S10). However, reliable quantitative analysis of such events was not possible due to the highly crowded and dynamic nature of the cytoskeleton arrays under steady state conditions.

4.3.5 Mutual dependence of the actin and MT cytoskeleton assayed by recovery after depolymerization

The experiments above present evidence for actin regeneration along MTs. To test if the MTs are needed for AF recovery, we depolymerized both cytoskeleton components by treating them with latB and oryzalin overnight. We then washed out latB, but maintained the oryzalin treatment. After 6 h of recovery in the presence of oryzalin, only diffuse GFP-FABD signal and sparse punctae of actin label were observed. These fragments were neither fixed in position like the nascent punctae in cells with intact MTs, nor did they show rapid long range movement consistent with cytosolic streaming; rather, they displayed limited and erratic movement (Figure 4.5C; see Movie S11) consistent with Brownian motion. After 20 h of recovery, most cells showed a similar punctate pattern of actin foci as observed after 6 h. However, we also observed single straight actin rods, or bundles, which were stationary over the time of observation (Figure 4.5D; see Movie S12). Thus, recovery of actin structures labeled by GFP-FABD was sensitive to oryzalin treatment, suggesting that MTs or an MT-dependent cell function is required for reassembly of the actin cytoskeleton after depolymerization.

To investigate the influence of AFs on MT recovery, we also performed oryzalin washout experiments in the absence or presence of the actin cytoskeleton. In the absence of latB, MTs began to recover 5 h after oryzalin washout (Figure 4.5E; see Movie S13), and treadmilling MTs were present throughout the cell cortex after 20 h

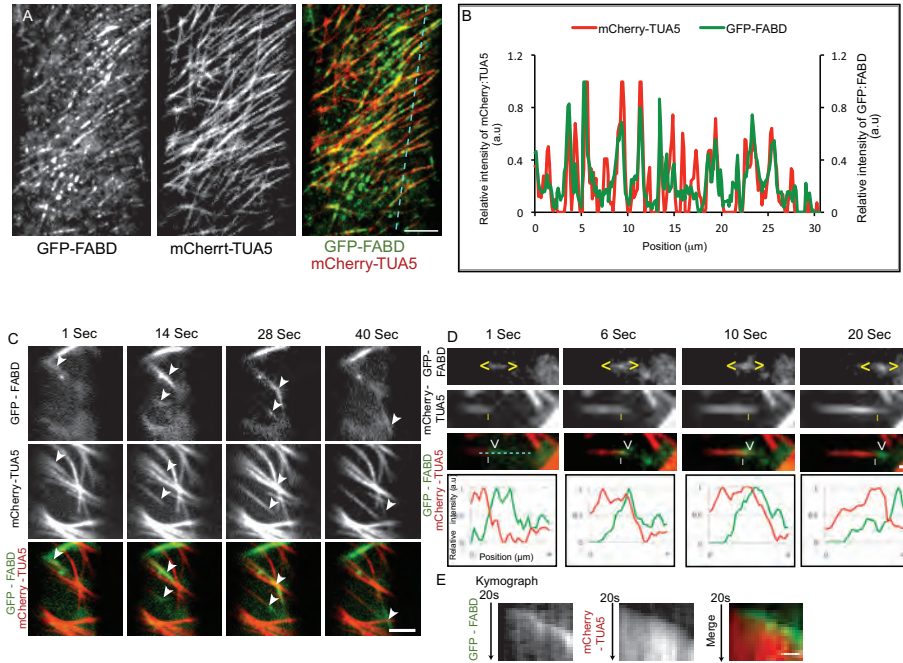


Figure 4.4: Recovery of the actin cytoskeleton following latB treatment and washout requires MTs. (A) Newly formed AFs coincide with MTs 3 h after latB washout. (B) Fluorescence intensity plot of the GFP-FABD and mCherry-TUA5 signals across a transect of an elongating hypocotyl cell (cyan line shown in [A]). a.u., arbitrary units. (C) Selected frames from a time series of a GFP-FABD and mCherry-TUA5 dual-labeled line at the hypocotyl cell cortex in etiolated 3-d-old seedlings 5 h after latB washout. White arrowheads indicate the movement of small AF fragments along MTs. Scale bar, $5 \mu\text{m}$. (D) Selected frames from a time series of a GFP-FABD and mCherry-TUA5 dual-labeled line at the cell cortex 5 h after latB washout. Yellow carets enclose small actin structures that move along the MT plus end (yellow vertical line). Bottom panel, fluorescence intensity plot of the GFP-FABD and mCherry-TUA5 signals along the cyan line in top panel. (E) Kymograph of the cyan line in image (D). Scale bars, $1 \mu\text{m}$.

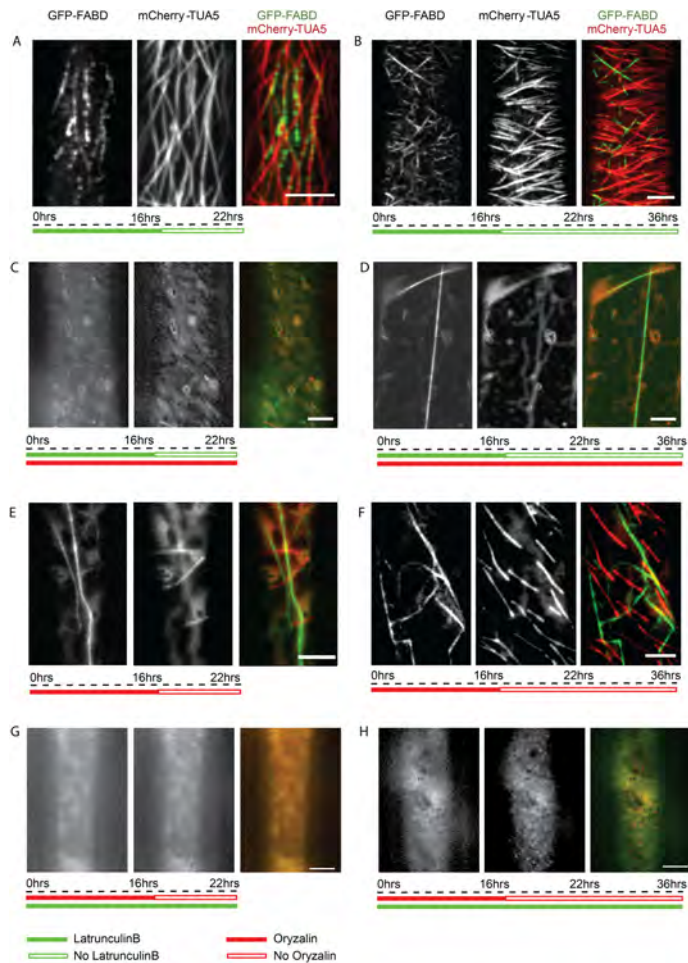


Figure 4.5: Mutual dependence of the actin and MT cytoskeleton as-sayed by recovery after depolymerization. (A) and (B) One μM latB treatment of GFP-FABD and mCherry-TUA5 dual labeled etiolated 3-d-old seedlings for 16 h followed by washout of latB and recovery of the actin cytoskeleton for 6 h (A) and 20 h (B). (C) and (D) One μM latB and 20 μM oryzalin treatment for 16 h followed by washout of latB and recovery of the actin cytoskeleton for 5 h (C) and 20 h (D). (E) and (F) Oryzalin treatment of GFP-FABD and mCherry-TUA5 dual labeled lines for 16 h followed by washout of oryzalin and recovery of MTs for 5 h (E) and 20 h (F). (G) and (H) LatB and oryzalin treatment for 16 h followed by washout of oryzalin and recovery of MTs for 5 h (G) and 20 h (H). Scale bars, 5 μm .

(Figure 4.5F; Movie S14). However, in cells pretreated with latB, only small punctae of MT label were visible 6 h after oryzalin washout (Figure 4.5G; see Movie S15). In addition, apart from the punctate patterns of fluorescence, the majority of the cells lacked conspicuous MT polymers 20 h after washout in the absence of the actin cytoskeleton (Figure 4.5H; see Movie S16).

It is important to note that cells treated overnight with both cytoskeleton inhibitors for up to 16 h could recover 48 h after transfer to media without the drugs (see Figure S4.3A and Movie S17). Although similar recovery analysis of seedlings in long-term treatments (20 h with an additional 16-h treatment) did not recover, seedlings that underwent 6-h treatments with either one of the inhibitors after the overnight treatment with both inhibitors were able to recover (see Figures S4.3B and S4.3C, and Movies S18 and S19). Taken together, these observations indicate that MT and AF recovery following inhibitor treatments depends on the presence or function of the other cytoskeleton component.

4.4 Discussion

Dynamic interactions between AFs and MTs have been reported in animal systems (Goode et al., 2000). In plants, proximity of AFs and MTs has been observed only in fixed tissues (Traas et al., 1987; Blancaflor, 2000; Collings and Wasteneys, 2005; Barton and Overall, 2010). We present evidence based on live-cell imaging that cortical AFs and MTs interact and that cortical MT or MT function is required for re-establishing the cortical actin cytoskeleton after disassembly. Previous studies speculated that MTs could influence the orientation of newly formed AFs (Hussey et al., 1998), an idea consistent with our observations that emerging actin fragments coincided with, and traveled along, MTs during reassembly.

Several studies have shown that perturbations of one cytoskeletal component can change the organization of the other (for review, see Collings, 2008). For example, disruption of the AF array using cytochalasinD affected MT organization in developing *Zinnia elegans* tracheary cells (Kobayashi et al., 1988). Jasplakinolide has previously been reported to cause delayed self-incompatibility-induced MT depolymerization in pollen tubes of *Papaver rhoeas* (Poulter et al., 2008). Our observations show that jasplakinolide induced changes in F-actin assembly and turnover, and affected the orientation and parallel ordering of MTs in etiolated hypocotyl cells. Whereas the mechanism of jasplakinolide action on MT organization is not known, one possible class of mechanism is steric interference by stabilized AFs, which could inhibit MT-MT interactions (Dixit and Cyr, 2004; Ehrhardt and Shaw, 2006), MT membrane attachment (Ehrhardt and Shaw, 2006; Ambrose and Wasteneys, 2008), or recruitment and function of MT-associated nucleation complexes (Murata et al., 2005; Nakamura et al., 2010).

To study these interactions further, we made use of a physiologically driven change in cytoskeletal organization (Ueda and Matsuyama, 2000; Chan et al., 2007). In agreement with previous studies (Paredes et al., 2006), we observed that the

transverse MT organization gradually changes to a longitudinal organization upon light exposure and resulted in a reduction of coalignment between AFs and MTs. These changes were accompanied by a decrease in cortical AF density. Thus, in addition to the light-induced MT reorganization showed previously (Paredes et al., 2006; Chan et al., 2007), we showed that the actin cytoskeleton was also affected. Whereas reorientation of cortical MTs has been shown to drive reorientation of cellulose synthase trajectories (Chan et al., 2010), it remains to be determined what functions associated with cell growth might be altered by the observed changes in actin distribution.

The light-induced changes in actin distribution appeared to be dependent on the presence of an intact MT cytoskeleton. Whereas this could signify a direct relationship between the two cytoskeletal arrays, it is important to note that removal of the MTs also affects cell growth (see Figure S4.1D; Baskin et al., 1994). Therefore, it is difficult to deduce whether the MTs orchestrate the changes of the AF array directly, or whether these changes are due to alterations in growth. In plant cells, the photoreceptor proteins cryptochrome (Chaves et al., 2011) and/or phototropin (Christie, 2007) are involved in blue light-induced inhibition of hypocotyl cell elongation, and could be involved in triggering the orchestrated changes of the cytoskeleton components. The proteins that communicate light perception from plant cell photoreceptors to MT rearrangements have yet to be identified, but studies of chloroplast movements in *Arabidopsis* have revealed targets of blue light photoreceptors associated with the actin cytoskeleton, including THRUMIN1, a protein that mediates movement of chloroplasts via changes in actin bundling in response to blue light (Whippo et al., 2011), and KAC1/2, newly discovered kinesins that may interact with AFs rather than MTs (Suetsugu et al., 2010). Identification of additional proteins that are involved in transduction of light signals to the cytoskeleton is required for understanding how signaling to both cytoskeletons may be coordinated.

Pharmacological studies have increased our understanding of interactions and crosstalk between the two cytoskeleton components (Collings, 2008). AF recovery after microinjection of a pollen-specific actin depolymerization factor in *Tradescantia blossfeldiana* stamen hairs showed that AFs reappeared as transverse arrays, similar to the orientation of MT arrays rather than the longitudinal AF arrays found in untreated cells (Hussey et al., 1998). Similarly, injection of an antiserum against an actin bundling protein resulted in the dispersal of thick actin bundles into fine AFs at the same cortical plane as the MTs in root hair cells of *Hydrocharis bubia* (Tominaga et al., 2000). The authors speculated that MTs could influence the orientation of newly formed AFs. Our observations of AFs after latB washout provide direct evidence of AF polymerization along cortical MTs and indicate that cortical MTs may play a role in positioning actin nucleation.

Supporting the possibility that cortical MTs may position actin nucleation, Deeks et al. (2010) reported that the *Arabidopsis* FORMIN4 colocalized with MTs and could interact with the actin and MT cytoskeleton through a MT binding domain. Similarly, another formin, *Arabidopsis* FORMIN14, was found to interact with MTs and AFs during the process of cell division (Li et al., 2010). Such proteins could position actin

nucleation at MTs. Some MT plus end tracking proteins associate with formins in yeast and animals (Wen et al., 2004; Martin and Chang, 2005), and MT plus ends have also been shown to play a role in deploying regulatory factors for actin nucleation in fission yeast and animal tissue culture cells (reviewed in Basu and Chang, 2007). It remains to be determined if plus end tracking proteins also interact with formins or other actin nucleation factors in plant cells. Whereas new actin growth is easily observed following latB washout, it has proved challenging to quantify locations of new AF growth under normal conditions of cell growth, in large part due to the density and dynamics of the cortical actin cytoskeleton. It is anticipated that future studies in which actin nucleating proteins can be observed in concert with labeled AF will help to address these challenges, much as observation of MT nucleation complexes has improved analysis of MT nucleation (Nakamura et al., 2010).

One of the more intriguing observations in this study is the movement of actin fragments along cortical MTs in jasplakinolide-treated cells and during recovery from latB treatment. Kinesin motors, such as the cotton (*Gossypium hirsutum*) kinesins KCH1 and KCH2, have been described that localize to MTs and to fine AFs, possibly through the presence of a unique calponin homology domain (Preuss et al., 2004a; Xu et al., 2009). Perhaps a similar mechanism is acting during the transport of the newly formed AFs along the MTs observed in our study.

AF recovery after latB washout revealed actin fragments colocalizing with MTs, indicating that MTs could serve as a scaffold for actin nucleation. The mechanism by which MT recovery is dependent on the actin cytoskeleton is less clear. AFs, along with actin binding proteins, may be required for the early stages of cortical MT array establishments. On the other hand, and unlike the AF recovery experiments, the recovery of MTs after oryzalin washout did not reveal any physical association between AFs and MTs. Further, live cell imaging studies of MT nucleation complexes did not reveal any changes in cortical association of the complexes, or any difference in MT nucleation dynamics, after AF depolymerization (Nakamura et al., 2010). Whereas this does not rule out a direct interaction between the AFs and re-emerging MTs after the oryzalin washout, it may suggest that other mechanisms are responsible for our observation. One plausible explanation is that the washout of oryzalin may be dependent on actin-based cytoplasmic streaming. Washout of oryzalin, which has a high affinity for free tubulin dimers (Strachan and Hess, 1983; Morejohn et al., 1987), is heavily dependent on the rate of transport of already internalized oryzalin molecules from the cytoplasm to sites at the plasma membrane to exit the cell. The presence of a cuticle could further act as a barrier and reduce efflux of oryzalin from hypocotyl cells. Therefore, the depolymerization of AFs could drastically decrease the speed at which oryzalin molecules are being removed from the cytosol.

In summary, we show that cortical AFs and MTs interact at the cortical focal plane of plant cells, and that these interactions are altered during coordinated array reorganization. Reassembly experiments suggest dependence of the AF cytoskeleton on the MT cytoskeleton for nucleation of the AFs, which may be facilitated by formins and other factors perhaps analogous to those involved in MT-associated actin nucleation in yeast and animal cells.

4.5 Materials and methods

4.5.1 Plant materials, growth conditions and genetic analysis

Arabidopsis thaliana Columbia seedlings were surface sterilized, stratified for 3 d, and grown vertically on plates containing Murashige and Skoog media (1x Murashige and Skoog salts, 8 g L⁻¹ agar, 1x B5 vitamins, and 10.8 g L⁻¹ sugar) in light (16-h photoperiod) or dark conditions at 21 °C for 5 d for light microscopy, and 3 d for confocal microscopy. The FABD-GFP and mCherry:TUA5 constructs were as described in Ketelaar et al. (2004) and Gutierrez et al. (2009), respectively.

4.5.2 Drug treatments

Seedlings were immersed in 2 mL of solution with drugs or control solution in 12-well cell culture plates in the dark and were subsequently imaged. Stock solutions of LatB and oryzalin were dissolved in methanol or in DMSO, respectively, and working stocks were made fresh by further dilution in water. For drug washout and recovery experiments, the seedlings were washed in water three times, after which they were transferred to a fresh solution for recovery.

4.5.3 Specimen mounting

The seedlings were mounted between a cover glass and a 1-mm thick 1% agar pad affixed on a circular cover slip, thus stabilizing the sample and preventing it from compression and mechanical damage.

4.5.4 Microscopy

Light microscopy was performed using a Leica Stereomicroscope (Leica MZ12.5 and Leica DFC420 digital camera). Seedlings expressing GFP-FABD, mCherry-TUA5, and dual-labeled lines of GFP-FABD and mCherry-TUA5 were imaged on a confocal microscope equipped with a CSU-X1 Yokogawa spinning disc head fitted to a Nikon Ti-E inverted microscope, a CFI APO TIRF x100 N.A. 1.49 oil immersion objective, an evolve charge-coupled device camera (Photometrics Technology), and a x1.2 lens between the spinning disc and camera. GFP was excited at 491 nm and mCherry at 561 nm using a multichannel dichroic and an ET525/50M or an ET595/50M band pass emission filter (Chroma Technology) for GFP and mCherry, respectively. Image acquisitions were performed using Metamorph online premier, version 7.5. Typical exposure times were 600 ms for GFP and 300 ms for mCherry.

4.5.5 General image processing and analysis

All images were processed using ImageJ software (Rasband, W.S., National Institutes of Health). Background correction was performed using 'Subtract Background' tool

(rolling ball radius 30-40 pixels), and StackReg (Thevenaz et al., 1998) was used to correct focus drift. Linear adjustments in pixel values were made when measuring signal intensities.

4.5.6 Rates of cortical MT dynamics

v_g and v_s were measured for the leading ends of single MTs derived from hypocotyls of etiolated seedlings expressing mCherry-TUA5 and treated with jasplakinolide (5 μ M for 3 h), or with a mock control. Data were derived from three independent seedlings for control and treated lines, and the number of ends measured for control cells was $n = 51$ (v_s) and 76 (v_g), and for jasplakinolide-treated seedlings was $n = 43$ (v_s) and 71 (v_g). The Multiple Kymograph plug-in in ImageJ (National Institutes of Health) using a line width of 3 was used to calculate MT velocities in micrometers per minute. Histograms and statistical comparisons were collated in GraphPad Prism-5 and were presented as shrinkage (red), growth (green), and pause (blue).

4.5.7 Colocalization analysis of AFs and MTs

Three random kymographs that stretched the entire length of the cell were generated ($n = 4$ cells). The kymograph (line width 3) generated from the actin channel was first analyzed, and only AF pauses (i.e., AFs appeared static) that occurred for more than 30 s were considered for further analyses. The AF pauses were subsequently mapped over the kymograph from the MT channel to determine colocalization. MT coverage was estimated by using a binary image of the MT channel, which was thresholded, and mean pixel intensity was measured using ImageJ (MTs occupied 47% of the area). Statistical estimates of whether the observed colocalization occurred by chance were calculated using a binomial test.

4.5.8 MT angles and fluorescence intensity of AFs

Three cells each from different seedlings were used for the analysis in all cases. Every 25th image of the time series was taken from a total of 600 images for the analysis. MT angles were measured with regard to the growth axis and always in a clockwise direction, using the angle tool in ImageJ. AFs were manually thresholded with ImageJ to avoid detection of free GFP-FABD, and histograms were generated to determine the total number of pixels occupied by the thresholded regions, which was then taken as the value for total fluorescence intensity.

4.6 Acknowledgments

We thank Olivier Hamant and Markus Grebe for the critical comments on the manuscript, Anne Mie C. Emons, Zoran Nikoloski, and Florian Hollandt for stimulating discussion

about the topic, and Eugenia Maximova for input on the microscopy at the Max Planck Institute. A.S and S.P. were financed through the Max Planck Gesellschaft.

4.7 Supplementary information

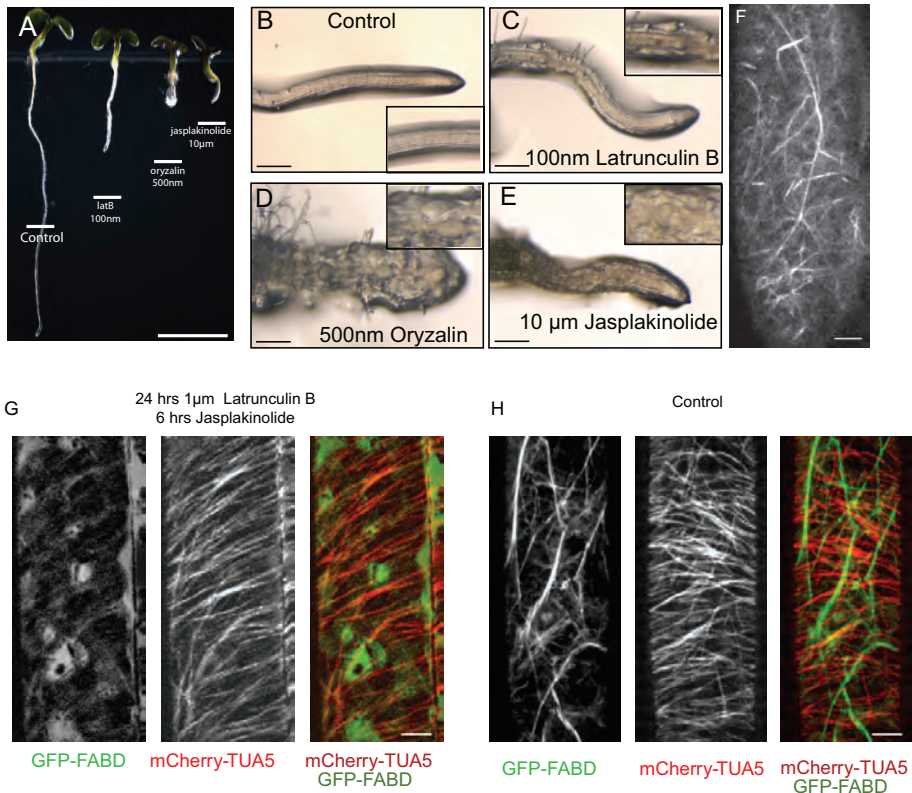


Figure S4.1: Effect of cytoskeleton inhibitors on seedling growth and morphology. (A) Five-day-old seedlings grown on media supplemented with different inhibitors (as indicated). Scale bar, 2 mm. (B to E) Roots of seedlings in (A). Inserts show enlargements of epidermal cells in the root elongation zone. Scale bar, 200 µm. (F) Recovery of AFs 48 h after jasplakinolide washout. (G and H) Average Z projection of 5 images of 0.1 µm slice thickness of five-day-old etiolated GFP-FABD- and mCherry-TUA5-expressing seedlings treated with 1 µM LatB (24 h), and subsequently with 5 µM jasplakinolide [six h; LatB treatment was maintained during the jasplakinolide treatment (G), or treated with control media (H)]. Scale bars, 5 µm.

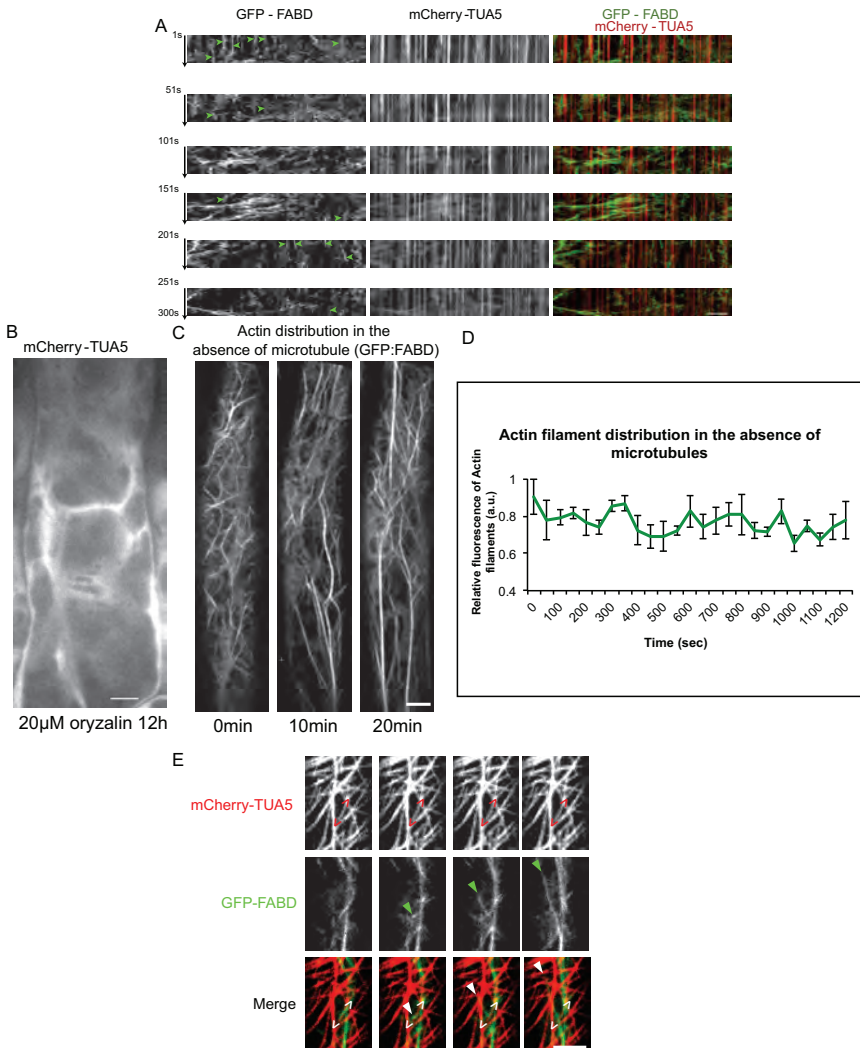


Figure S4.2: Light-induced changes to AF - MT co-alignment, and AF polymerization at sites of MTs. (A) Example of a complete series of kymographs represented in (Figure. 4.3A). (B) Treatment of mCherry-TUA5 with 20 μ M Oryzalin results in complete removal of MTs. (C and D) Actin distribution at the cortex remains unaffected in the absence of MTs ($n= 3$ cells), Error bars represent SE. (E) Polymerization of AF from sites co-incident with MT. Carets enclose MT co-aligning with AF blocked arrowheads indicate branching and polymerization of AF Scale bar, 5 μ m.

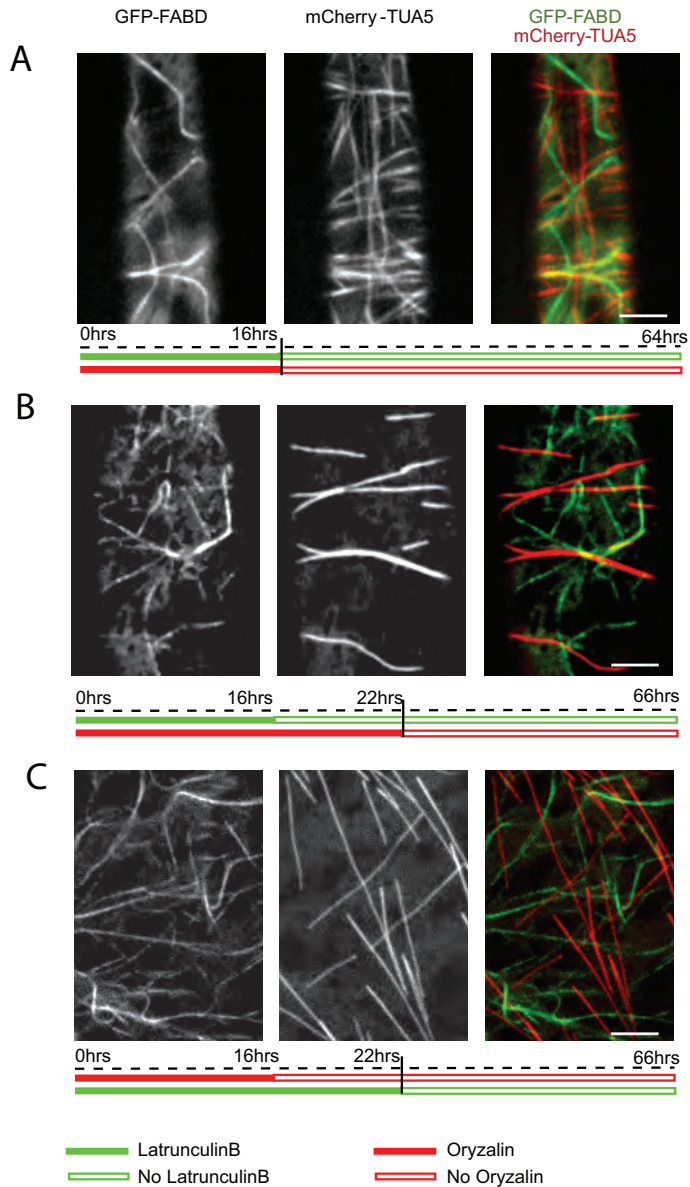


Figure S4.3: AF-MT recovery after drug-induced depolymerisation. (A) Recovery of AFs and MTs after 16 h of 1 μM latB and 20 μM oryzalin treatment. (B) Recovery of AFs and MTs following 16 h of 1 μM latB and 20 μM oryzalin treatment, with an additional six h of 20 μM oryzalin treatment. (C) Recovery of AFs and MTs following 16 h of 1 μM latB and 20 μM oryzalin treatment, with an additional six h of 1 μM latB treatment. Scale bars, 5 μm .

Mechanism of blue light induced microtubule reorientation

5

5.1 Abstract

In plant cells, the organization of cortical microtubules is closely related to the growth state of the cell. It had been observed that cortical microtubules in etiolated hypocotyl cells change their orientation in response to light however the mechanism of array reorientation and its function remained unresolved. In this study we found that the cortical microtubule reorientation in response to blue light was dependent on PHOTOTROPIN signaling. We found that the *spr3* and *ktn1-1* mutants show significantly reduced cortical microtubule reorientation speed in response to blue light. The *spr3* mutant shows defects in the orientation of microtubule nucleation from existing microtubules and in the *ktn1-1* mutant, is a null mutant for the microtubule severing protein KATANIN. We show PHOTOTROPIN signaling alters the ratio of branched and parallel nucleation. In addition, PHOTOTROPIN signaling increases the KATANIN severing rate. During the process of reorientation many of the newly formed microtubules originate from microtubule crossovers, which we show to be likely the result of microtubule severing events where the newly formed plus end is not in a shrinking but a growing state. We propose a two step process for microtubule array reorientation. First, the number of branching microtubules increases, increasing the chance of generating microtubules longitudinal to the elongation axis and perpendicular to the existing transverse microtubules. Then, the longitudinal microtubules make many crossovers and the increased severing rate combined fact that a proportion of the new plus ends are in a growing state gives a large amplification of longitudinally oriented microtubules, ultimately leading to reorientation. We also provide evidence blue light induced microtubule reorientation is required for photocurvature.

5.2 Introduction

Cytoskeletal arrays based on tubulin or tubulin-like proteins are ancient biological innovations found across all cellular life. These arrays support diverse and essential functions such as chromosome segregation, intracellular transport, cell motility and cell expansion, functions that depend critically on their organization. In the best studied microtubule arrays - those with astral architecture - a centralized organizer, such as spindle pole body in yeast or a centrosome in animals, acts to tether and position nucleation complexes, setting up the functional architecture of these arrays as radialized and polarized structures with central hubs. However, these astral arrays represent just a fraction of microtubule architectural diversity. Many differentiated animal cells and all higher plant cells create interphase microtubule arrays that are not organized by centrosomes and which have architectures distinct from astral arrays. Higher plants, for example, lack centrosomes altogether and create interphase arrays that lie in a plane adjacent to the plasma membrane, often with parallel ordering that is also oriented relative to cellular and tissue coordinates. While the mechanisms by which centrosomal arrays are created and organized are relatively well understood, comparatively little is known regarding the mechanisms used to organize and reorganize acentrosomal microtubule arrays in both plant and animal cells (Bartolini and Gundersen, 2006).

5.2.1 Microtubule organization and plant cell morphogenesis

The epidermal cells of the embryonic plant axis, or hypocotyl, serve as an excellent model for the organization and function of cortical microtubule arrays. When seeds germinate in the dark, these cells undergo a remarkable process of anisotropic expansion in which cell length increases by as much as ten times (Refregier, 2004), driving extension of the axis without cell division, a response that serves to push the first leaves out of the soil and into the light to support photosynthesis. In these rapidly elongating cells, cortical microtubule arrays show highly parallel ordering oriented transversely to the main axis of expansion (Figure 5.1). This transverse architecture is essential for directional cell expansion, as shown by both inhibitor and genetic studies, acting as an internal scaffold to organize the synthesis and structure of the external cell wall by positioning the delivery of cellulose biosynthetic complexes to the plasma membrane and guiding their trajectories as they extrude cellulose microfibrils (Green, 1962; Heath, 1974; Robinson and Preston, 1972; Giddings and Staehelin, 1988; Paredez et al., 2006). Thus cortical array organization is a primary determinant of the positions and ordering of cellulose. This material anisotropy in cell wall structure is proposed to be a principal cause for the anisotropy of cell wall growth (?). As cells grow anisotropically, changes in mechanical stress are hypothesized to influence cytoskeletal organization, which further influences cell wall growth anisotropy, creating a feedback loop that is exploited to generate tissue form.

5.2.2 Cortical array ordering

Live cell imaging studies have revealed cortical microtubule arrays as dynamic networks of interacting polymers. Microtubules are initiated by dispersed γ -tubulin ring complexes (γ -TURCs) recruited to the cell cortex, primarily along the sides of existing microtubules (Nakamura et al., 2010), where they nucleate new polymer growth either in parallel to the mother polymer (Chan et al., 2009; Nakamura et al., 2010) or at an angle of approximately 40° to the growing end (Murata et al., 2005; Chan et al., 2009; Nakamura et al., 2010), creating a branched geometry. The ratio of these two modes of initiation is under genetic control, as revealed by a significant preference for parallel over branching nucleation in *ton2*, a loss of function allele for the B \ddot{O} subunit of protein phosphatase 2A (Kirik et al., 2012). After initiation, daughter polymers are often detached from their nucleation sites by a KATANIN dependent mechanism (Nakamura et al., 2010), liberating the nucleation complex (Nakamura et al., 2010) and freeing the daughter to migrate along the cell cortex by a hybrid polymer treadmilling mechanism (Shaw et al., 2003). Interaction with the cell membrane confines these treadmilling polymers to a 2 dimensional plane, where plus end growth drives encounters with other microtubules. These encounters cause changes in polymerization behavior, including redirection of the angle of microtubule growth, severing or catastrophe; behaviors which are hypothesized to endow the dynamic polymer network with self organizing properties. This proposition is supported by analytic modeling (Hawkins et al., 2010; Tindemans et al., 2010) and computer simulation studies (Allard et al., 2010a; Eren et al., 2010; Hawkins et al., 2010; Tindemans, 2009), which provide a plausible explanation for the parallel ordering observed in cortical arrays.

5.2.3 Cortical array orientation

It has been proposed that localized regulation of microtubule stability could act to bias such a self ordering system to determine the orientation of the array relative to cellular coordinates (Shaw et al., 2003; Dixit and Cyr, 2004; Wasteney, 2002). Recent studies of CLASP mutants are consistent with this idea. Loss of CLASP function, a +TIP protein that also localizes along the lattice of cortical microtubules in *Arabidopsis* (Kirik et al., 2007), results in altered cortical array organization in young cells of the root and leaf epidermis (Ambrose et al., 2011) and defective orientation of cortical arrays in during specification of cell lineages in the root (Dhonukshe et al., 2012). GFP-CLASP has been observed to concentrate at the anticlinal walls and edges of these cells, where it is proposed to promote microtubule stabilization by suppressing polymerization catastrophe (Ambrose et al., 2011) thus to providing a positional bias for the orientation of the cortical array as a whole. This is an appealing model to explain cortical array orientation in these young cells, but more mature cells in the root and leaf show normal cortical array orientation in a CLASP null, indicating that cortical array organization is regulated by additional mechanisms that remain to be identified.

5.2.4 Reorientation of cortical arrays in response to light signals

Light is a powerful signal to plant growth, an observation first formalized in the literature by Charles Darwin. Blue light, for example, inhibits cell elongation of dark grown seedlings and stimulates phototropism towards the light source when presented at an angle to the axis. Phototropism is mediated in *Arabidopsis* by the LOV-domain photoreceptors PHOT1 and PHOT2, which alter the distribution of the growth promoting hormone auxin down and across the hypocotyl axis to promote differential growth and photocurvature (Christie et al., 2011). Inhibition of growth is signaled by both these receptors and the cryptochromes CRY1 and CRY2. PHOTOTROPIN mediated growth inhibition is rapid and transient, being mediated in part by the nearly immediate activation of anion channels (Folta and Spalding, 2001) and subsequent elevation of cytosolic calcium. By contrast, CRYPTOCHROME signaling facilitates a much slower and sustained inhibition, being evident only after an hour or more after stimulation.

Together with these changes in cell growth, cortical microtubules of elongating hypocotyl cells also reorient in response to light stimulation (refs), showing a dramatic 90° reorientation from a transverse to a longitudinal orientation that can be observed within minutes of exposure (Paredes et al., 2006). The photoreceptors responsible have not been identified, the mechanisms driving reorientation are not known, and the relationship between cortical array reorientation and cell growth response has not been settled. To address these questions, we took an approach combining genetic analysis, quantitative live cell imaging, computer simulation studies and physiological experiments. Our studies indicate that microtubule reorientation is controlled by PHOTOTROPIN signaling, and that it is facilitated by a two part mechanism promoted by regulation of microtubule branching geometry and dependent on production of new microtubules by KATANIN severing activity. Severing occurs primarily where microtubules cross over others, linking the orientation of new microtubules to the geometry of older microtubules, suggesting a templated orientational mechanism. We test the plausibility of this mechanism by computer simulation and link cortical array reorientation to the cellular growth underlying phototropism.

5.3 Results

5.3.1 Light induction of cortical microtubule reorientation in etiolated hypocotyl cells

Photoreceptor proteins as phytochromes, cryptochromes and phototropins were obvious candidates for regulating the observed microtubule reorientation. Phytochromes respond to red and far-red light whereas cryptochromes and phototropins respond to blue light. To narrow down the possibilities we stimulated *Arabidopsis* dark grown etiolated hypocotyl cells expressing the microtubule marker YFP-TUA5

with monochromatic red or blue light for 3h and assessed if microtubule reorientation had occurred on the microscope. The reorientation had only taken place in response to blue light exposure. Cryptochromes and phototropin both have two copies in the *Arabidopsis* genome (CRY1/CRY2 and PHOT1/PHOT2 respectively) (Briggs and Huala, 1999; Christie, 2007). We transformed cryptochrome and phototropin double mutants, kindly provided by the Briggs Lab, with YFP-TUA5 to assess the microtubule reorientation in these mutants.

To quantify microtubule orientation and order we developed an automated image analysis ImageJ plugin that identifies the orientation of high contrast linear objects in images (see Materials and Methods). The plugin labels the orientation per pixel of pixels that were above the threshold level (Movie S1). This information is then further processed in MATLAB to extract the microtubule orientation over time.

We argued that the automated analysis of microtubules we would help to find mutants defective in the light signaling pathways as well as mutants in the downstream targets of blue light signaling such as microtubule associated proteins. Studying microtubule reorientation may also help to uncover new microtubule regulating mechanisms that become more apparent during the change of one type of microtubule organization to another type than in maintaining a steady state organization.

5.3.2 Microtubule reorientation is linked to blue light photoreceptors

To investigate microtubule reorientation, we made movies of 1h with a 10s time interval to assess microtubule reorientation in the different genetic backgrounds (Figure 5.1 a) (Movie S2). The laser power we used was chosen to yield a reliable photo response and limited photobleaching to not affect the ability to detect microtubules. We analyzed the microtubule reorientation in wild type, *cry1 cry2* double mutant and *phot1 phot2* double mutant. The change of angular frequency distribution of microtubule orientation in individual but representative cells in wild type and *phot1 phot2* are shown in Figure 5.1 (b and c respectively). The angles are shown relative to the hypocotyl orientation in Figure 1 (a) where 90 degrees is the hypocotyl elongation axis. From the data presented in Figure 5.1 (b and c) we calculate the Longitudinal (L) and Transverse (T) order parameters (see Materials and Methods) shown in Figure 5.1 (d) for wild type and in Figure 5.1 (e) for *phot1 phot2*. To estimate the speed of reorientation we fit the L order parameter with a quadratic fit. From this fit we calculate the average increase in L until it reaches 0. Figure 5.1 (f) shows the average increase in longitudinal order of wild type compared to *cry1 cry2* and *phot1 phot2*. We found a small but significant reduction in the *cry1 cry2* mutant based on the Mann-Whitney U test and a larger reduction in the *phot1 phot2* mutant. We therefore focused on the influence of PHOT1 and PHOT2 on blue light induced microtubule reorientation.

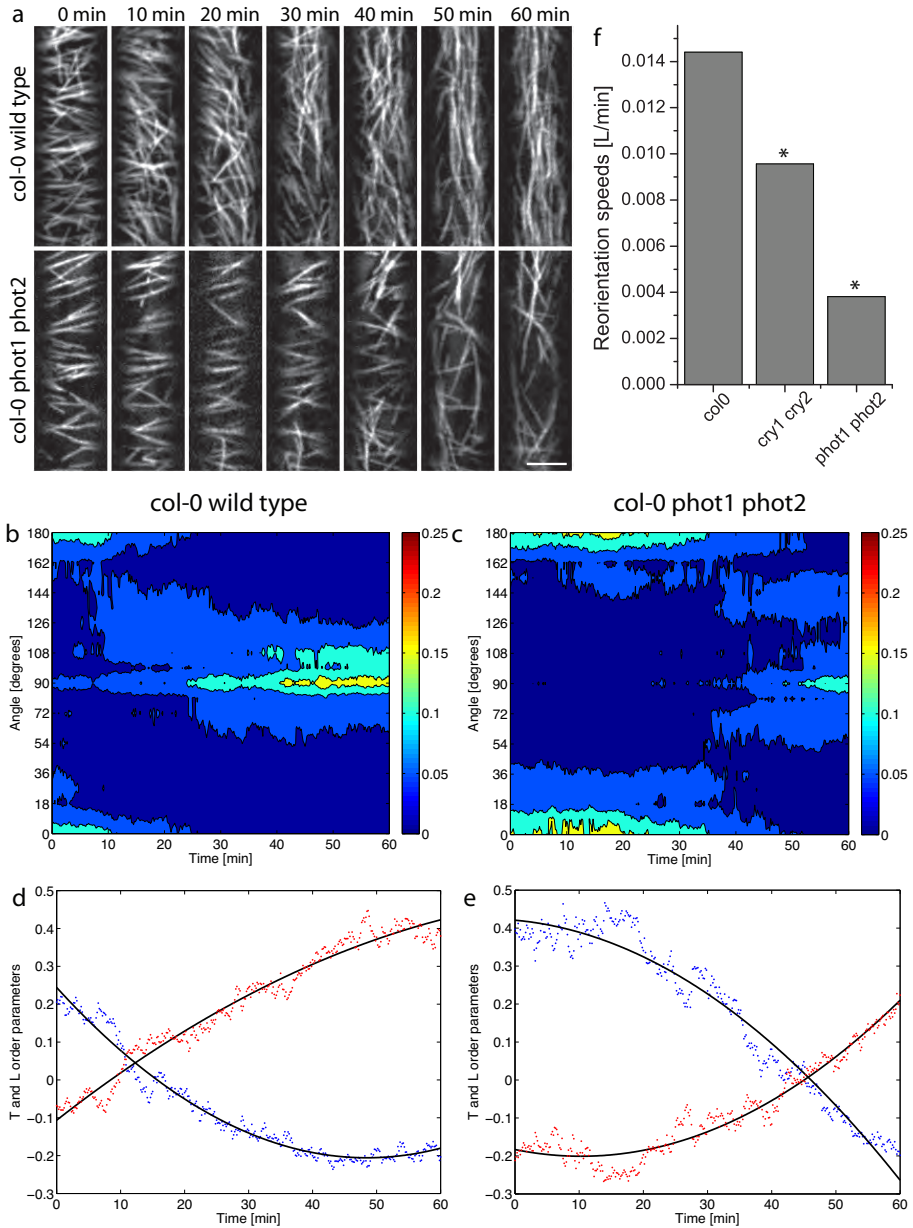


Figure 5.1: Microtubule reorientation in blue light receptor mutants. We image etiolated hypocotyl cells of *Arabidopsis* expressing YFP-TUA5 using blue excitation light which triggers microtubule reorientation. (a) Images of YFP-TUA5 in etiolated hypocotyl cells over time in *col-0* and *phot1 phot2* double mutant respectively. Scale bar 5 μm .

Figure 5.1: (b and c) Angular frequency distribution over time in a single representative cell of (b) col0 wild type and (c) col0 *phot1 phot2* double mutant. (d and e) Transverse (*T*) (blue dots) and longitudinal (*L*) (red dots) order parameters over time with a quadratic fit (black line) for a single representative cell of (b) col0 wild type and (c) col0 *phot1 phot2* double mutant. (f) Mean reorientation speed (*L*/min) comparing col0 wild type (18 cells) col0 *cry1 cry2* double mutant (13 cells) and col0 *phot1 phot2* double mutant (10 cells), asterisk indicates significant reduction compared to col0 wild type in Mann-Whitney U test.

5.3.3 Mutants *spr3* and *ktn1-1* have severe defects in microtubule reorientation

Microtubule nucleation is arguably the most potent mechanism to obtain microtubules with new orientations at the plant cell cortex (Chapter 2). To ask if microtubule nucleation is part of the microtubule reorientation mechanism we analyzed microtubule reorientation in *spr3* and *ktn1-1* mutants. The distribution of direction of microtubule nucleation is altered in the *spr3* mutant, a mutant allele of the γ -TuRC microtubule nucleation complex protein GCP2 (Nakamura and Hashimoto, 2009). The *ktn1-1* mutation has a premature stop codon in the gene for the microtubule severing protein KATANIN (Nakamura et al., 2010) KATANIN function was shown to be required for liberation of γ -TuRC complexes from newly created microtubules, so that they could only be recycled after complete microtubule depolymerization (Nakamura et al., 2010).

Figure 5.2 (a, b and c)(Movie S3) shows the cortical microtubule array over time in etiolated hypocotyl cells of (a) ws wild type, (b) ws *spr3* and (c) ws *ktn1-1*. Figure 5.2 (d) shows that both *spr3* and *ktn1-1* have a clear and significant reduction in cortical microtubule array reorientation speed. When we look at the angle frequency distributions histogram of wild type (Figure 5.2e), it appears that in wild type the transverse order goes down over time and the longitudinal order goes up, without significant in order in between transverse and longitudinal. The angle frequency distributions histogram of the *spr3* mutant (Figure 5.2 f) shows a transition from transverse to longitudinal microtubule order through ordered states in between longitudinal and transverse as is also illustrated in Figure 5.2 (b). Only 6 out of 11 cells in the *spr3* mutant background showed this type of behavior, the other 5 cells showed no indication of reorientation at all. The angle frequency distribution histogram of *ktn1-1* shows very little sign of reorientation, although there is a small tendency for the transverse order to decrease. None of the 14 cells we observed were able to reorient within 1h. The *T* and *L* order parameters further illustrate the difference between reorientation in wild type cells and *spr3* and *ktn1-1* mutants (Figure 5.2 h, i and j).

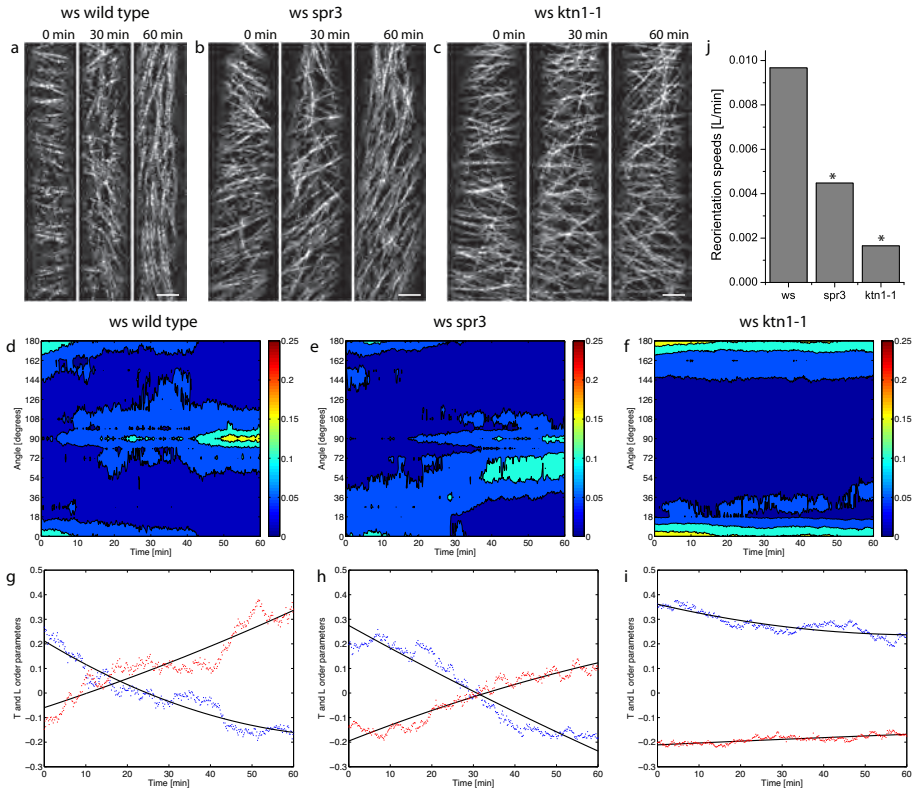


Figure 5.2: Microtubule reorientation in *spr3* and *ktn1-1*. We image etiolated hypocotyl cells of *Arabidopsis* expressing GFP-TUB6 using blue excitation light which triggers microtubule reorientation. (a, b and c) Images of GFP-TUB6 in etiolated hypocotyl cells over time in (a) ws wild type (b) ws *spr3* and (c) ws *ktn1-1*. Scale bar 5 μ m. (d, e and f) Angular frequency distribution over time in a single representative cell of (d) ws wild type (e) ws *spr3* and (f) ws *ktn1-1*. (g, h and i) Transverse (*T*) (blue dots) and longitudinal (*L*) (red dots) order parameters over time with a quadratic fit (black line) for a single representative cell of (g) ws wild type (h) ws *spr3* and (i) ws *ktn1-1*. (j) Mean reorientation speed (L/min) comparing ws wild type (13 cells) ws *spr3* (11 cells) and ws *ktn1-1* mutant (14 cells), asterisk indicates significant reduction compared to ws wild type in Mann-Whitney U test.

5.3.4 A large proportion of new microtubules originate from microtubule crossovers during blue light induced microtubule reorientation

Since we observed the decreased reorientation speed in the *spr3* and *ktn1-1* mutant, we argued that nucleation behavior is most likely important for blue light stimulated reorientation. Therefore we analyzed microtubule generation during light induced microtubule reorientation. We imaged the microtubule reorientation in *col0* wild type plants expressing the microtubule marker mCherry-TUA5 and the microtubule nucleation complex marker GCP2-3xGFP during 30 min with a 5s time interval. As a visual aid for detecting new microtubules we performed a walking image subtraction of three frames on the mCherry-TUA5 signal and selected the positive difference. This positive difference results in 'comets' reminiscent of fluorescent labeling of plus end binding proteins. We made these 'comets' green and added them to the grayscale mCherry-TUA5 images allowing us to assess the formation of new microtubules by scoring newly appearing green comet.

We encountered two distinct classes of new microtubule initiation, where one class was marked by the GCP2-3xGFP label and the other class not. Examples of each are shown in Figure 5.3 (a) (movie S4) and (b) (movie S5) respectively. Of the 212 new microtubules we detected in 7 movies, 79 were marked by a GCP2-3xGFP labeled complex and 133 were not.

We noticed a pattern in the new microtubules that were not marked by GCP2-3xGFP, namely that they almost exclusively originated from microtubule crossover sites. An example is shown in Figure 3 (d, e and f). The arrow with a dashed line indicates the location of the kymograph line (Figure 5.3 d) shown in Figure 5.3 (e) and shown with a heat lookup table in Figure 3 (f). The blue arrowhead indicates the position of microtubule initiation in (d, e and f). Because the fluorescence intensity increases after the crossover compared to before the crossover, we conclude that this was indeed an event where a new microtubule was created and not a rescue event within a microtubule bundle.

We noticed a pattern in the new microtubules that were not marked by GCP2-3xGFP, namely that they almost exclusively originated from microtubule crossover sites. An example is shown in Figure 5.3 (d, e and f). The arrow with a dashed line indicates the location of the kymograph line (Figure 5.3 d) shown in Figure 5.3 (e) and shown with a heat lookup table in Figure 5.3 (f). The blue arrowhead indicates the position of microtubule initiation in (d, e and f). Because the fluorescence intensity increases after the crossover compared to before the crossover, we conclude that this was indeed an event where a new microtubule was created and not a rescue event within a microtubule bundle.

We found that the proportion of microtubules originating from crossovers was significantly higher for the new microtubules that were not marked by GCP2-3xGFP compared to the ones that were ($p \ll 0.001$, binomial test). In fact, almost none of the new microtubules that were marked by GCP2-3xGFP originated from crossovers, whereas almost all of the new microtubules that were not marked by GCP2-3xGFP

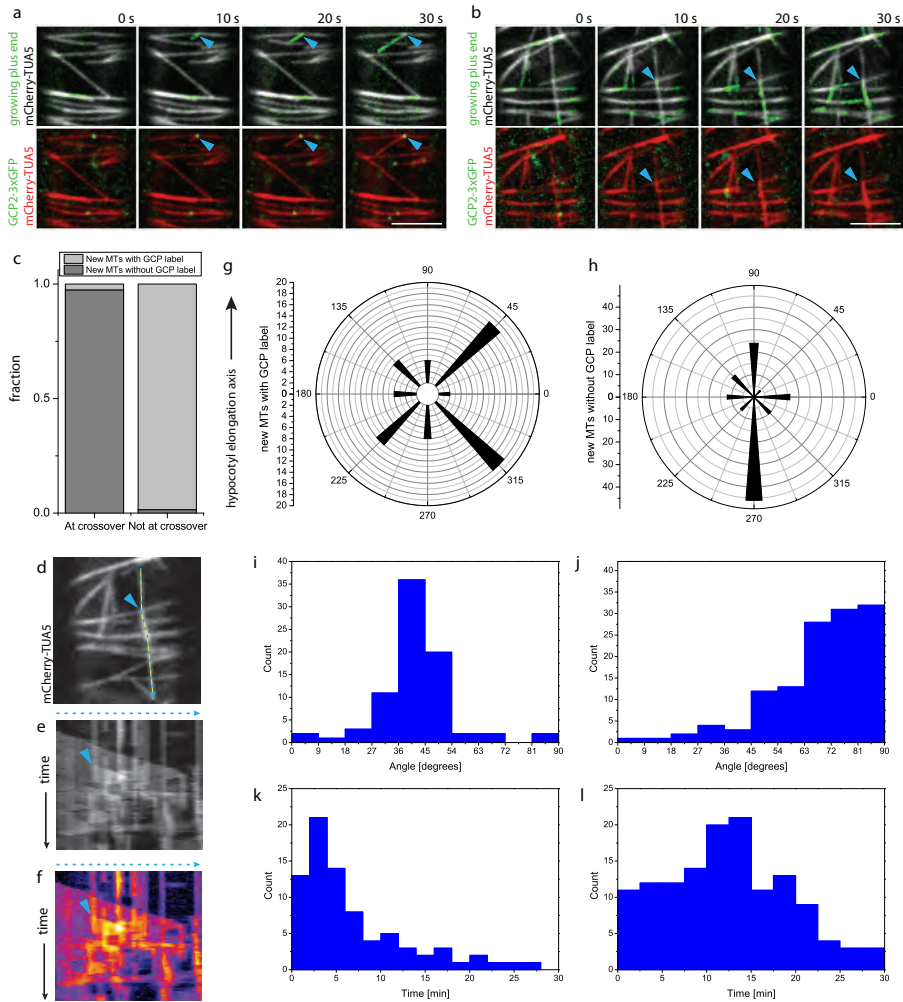


Figure 5.3: Generation of new microtubules during light induced microtubule reorientation (a) Example of a new microtubule being generated from a GCP-3xGFP labeled complex. The top panels show the mCherry-TUA5 in grayscale and the growing microtubule ends are shown in green and are generated from the positive difference using a walking image subtraction. Arrowhead shows the point of origin of the new microtubule. (b) Example of a new microtubule being generated at a microtubule crossover, without a GCP-3xGFP labeled complex. Arrowhead shows the point of origin of the new microtubule. (c) Fraction of new microtubules marked by a GCP-3xGFP labeled complex at microtubule crossovers and not at crossovers.

Figure 5.3: (d, e and f) Characterization of a new microtubule generated at a microtubule crossover. The arrow with a dashed line (d) indicates the location of the kymograph line shown in (e) and shown with a heat lookup table in (f). The blue arrowhead indicates the position of microtubule initiation in (d, e and f). (g and h) Polar histograms of orientation of new microtubules to the cell axis, where the elongation axis is at 90 degrees. Orientational distribution of new microtubules marked by a GCP-3xGFP labeled complex in (g) and not marked by a GCP-3xGFP labeled complex in (h). (i and j) Histogram of angle between mother microtubule and new microtubule in (i) and not marked by a GCP-3xGFP labeled complex in (j). (k and l) Histogram of time of microtubule initiation over time after the start of the blue light induction in (k) and not marked by a GCP-3xGFP labeled complex in (l). All data in this figure were collected from 7 cells of *col0* wild type plants expressing mCherry-TUA5 and GCP-3xGFP. Of the 212 new microtubules analyzed, 79 were marked by a GCP-3xGFP labeled complex and 133 were not. Scale bars, 5 μm

originated from microtubule crossovers (Figure 5.3 c).

The orientations of the newly created microtubules with respect to the cell axis are shown in Figure 5.3 (g and h). The new microtubules marked by GCP2-3xGFP show that most of those nucleations give rise to microtubules diagonal to the elongation axis (Figure 5.3 g), whereas the new microtubules that were not marked by GCP2-3xGFP are mostly longitudinal. Histograms of the angle of the new microtubules with respect to the microtubule they originate from are shown in Figure 5.3 (i and j). The new microtubules marked by GCP2-3xGFP mostly have an angle of 40 degrees with the microtubule they originate from (Figure 5.3 i) and most of the new microtubules that were not marked by GCP2-3xGFP are generated at high angles with the microtubules they originate from. We found in the blue light response that over time the number of new microtubules marked by GCP2-3xGFP is relatively high at first but quickly decreases (Figure 5.3 k). The number of new microtubules not marked by GCP2-3xGFP increases until 15 minutes after the start of blue light exposure and then decreases to a relatively low level at 30 minutes (Figure 3 l).

5.3.5 KATANIN localizes to microtubule initiations at crossovers

It has been shown previously that microtubules are severed preferentially at microtubule crossovers (Wightman and Turner, 2008), but where the microtubule severing protein KATANIN localizes to in plant cells has not been shown. In Figure 5.4 (a, b and c) we show that in *Arabidopsis* and we found that KTN localizes preferentially to microtubule crossovers. Figure 5.4 (a) (Movie S6) shows an example of a severing event at a microtubule crossover. GFP-KTN localizes to the crossover and the label

disappears shortly after the newly created plus end starts shrinking. In Figure 5.4 (b) (Movie S7) we show a microtubule initiation at a crossover. The GFP-KTN signal localizes to the crossover before we observe the growth starting from the crossover. In Figure 5.4 (c) (Movie S8) we show several new growing microtubules originate from a single crossover location within 80 s, where in each case GFP-KTN localizes to the crossover in the moments leading up to the initiation. Figure 5.4 (d) (Movie S9) we show again several microtubules initiate at a single crossover location and that the GCP2-3xGFP is absent from this crossover. In mCherry-TUA5 and GFP-TUA5 double labeled plants we never observed microtubule severing at a crossover that resulted in a depolymerizing new plus end without the GFP-KTN label being present at the microtubule crossover. The GFP-KTN signal was also present in all cases in which we observed a microtubule initiating at a crossover. In the *ktn1-1* mutant, we never observed microtubule severing resulting in a depolymerizing new plus end. We also never observed microtubule initiation at microtubule crossovers in the *ktn1-1* mutant. Taken together this information suggests that KATANIN severs microtubules at crossovers and that the newly created microtubule plus end can either obtain a shrinking or a growing state at the crossover.

5.3.6 The PHOT1/PHOT2 pathway increases the likelihood of branched nucleation

Because the *phot1 phot2* mutant had reduced reorientation speed, we analyzed microtubule initiation and we quantified the outcomes of microtubule crossovers in *phot1 phot2* and wild type in order to assess whether microtubule nucleation and microtubule severing is regulated by PHOT1/PHOT2. We assessed microtubule initiation in wild type and *phot1 phot2* etiolated hypocotyl cells during light induced microtubule reorientation. We made movies of 30 min with a 5s time interval, with the same approach as for the data presented in Figure 5.3. We made the distinction between two types of new microtubule initiation, those at microtubule crossovers and those that are not at microtubule crossovers.

When we compared the distribution of angles between the new microtubule and the mother microtubule (Figure 5.5 a, b and c) in wild type (Figure 5.5 a) and *phot1 phot2* (Figure 5.5 b) cells, we observed that the proportion of microtubules in the same orientation as the microtubules they originate from is higher in the *phot1 phot2* mutant (Figure 5 a). We found that the increase in this proportion was significant ($p \ll 0.001$, binomial test).

We found that the ratio between new microtubules initiating from microtubule crossovers and not initiating from crossovers between wild type and *phot1 phot2*, we found that the fraction of new microtubules created from crossovers was significantly lower in the *phot1 phot2* mutant ($p \ll 0.001$, binomial test) (Figure 5.5 g). In wild type the majority of new microtubules originate from microtubule crossovers during reorientation, whereas in *phot1 phot2* the majority of new microtubules does not originate from microtubule crossovers.

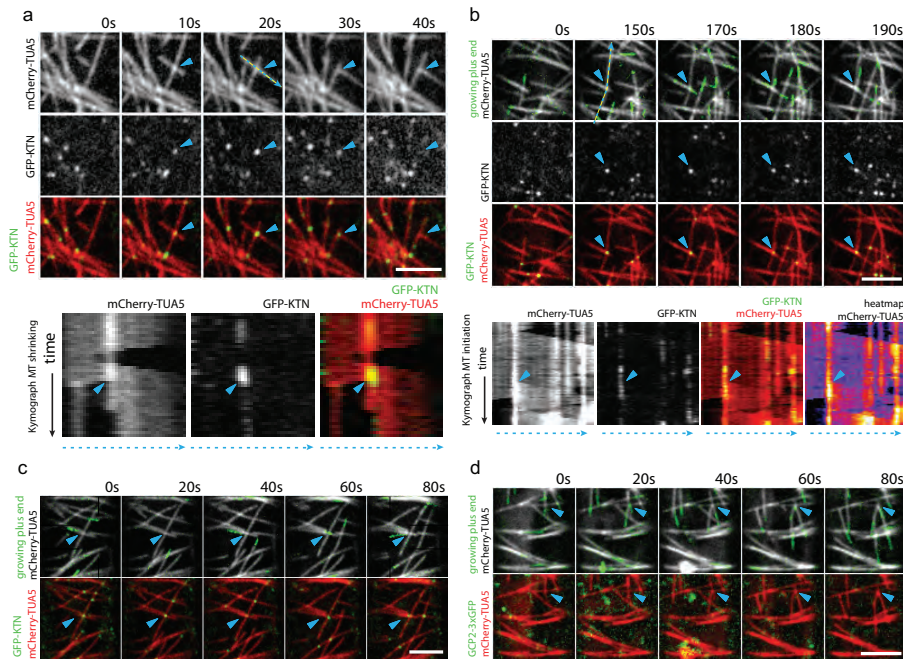


Figure 5.4: Characterization of microtubule initiation at crossovers. (a) Microtubule crossover where a microtubule severing event that results in a depolymerizing new microtubule plus end. The arrowheads indicate the position of the microtubule crossover. The GFP-KTN signal localizes to the crossover. The dashed blue line at 20s in the mCherry-TUA5 panel indicates the line used to make the kymographs in the panels below. The kymographs show that the GFP-KTN signal increases after the crossover occurs and disappears shortly after shrinkage of the newly formed plus end. (b) Microtubule crossover where a severing event results in a growing new plus end. The arrowheads indicate the position of the microtubule crossover. The dashed blue line at 20s in the mCherry-TUA5 panel indicates the line used to make the kymographs in the panels below. The kymographs for mCherry-TUA5 in grayscale and heatmap show that the new microtubule grows from the crossover and the GFP-KTN label in the kymographs colocalizes to the point where the new microtubule starts growing. (c) Image sequence where several new plus ends start growing from the same microtubule crossover point in colocalization with GFP-KTN signal. (d) Image sequence where several new plus ends start growing from the same microtubule crossover point. The GCP2-3xGFP label is absent from this microtubule crossover site. Scale bars, 5 μm .

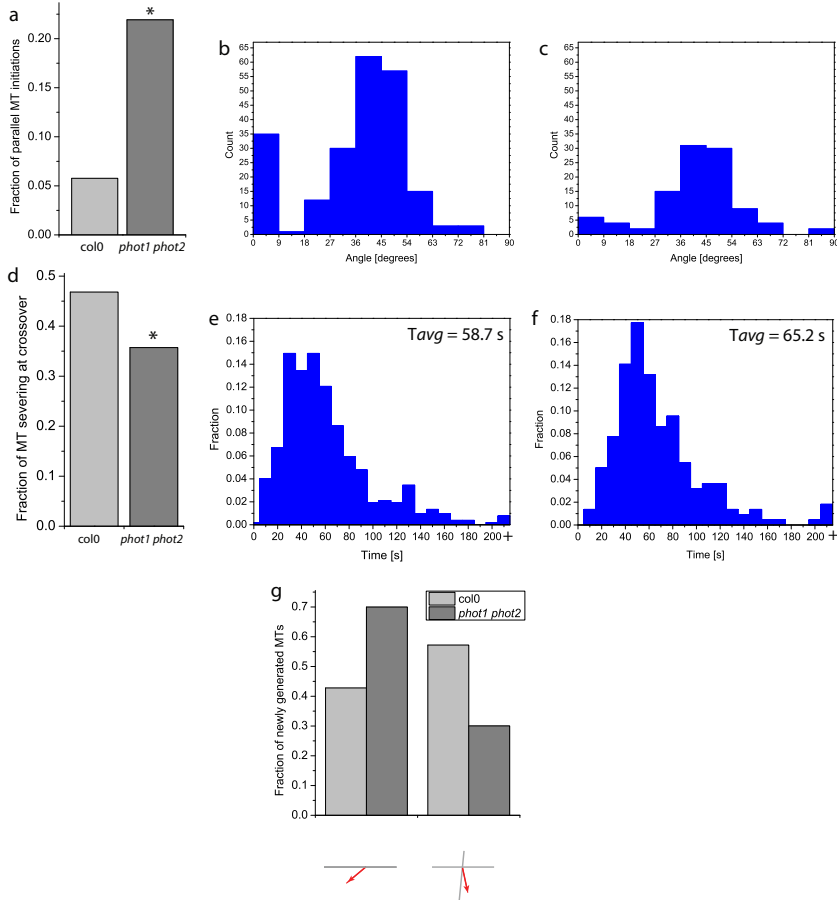


Figure 5.5: Differences between wild type and *phot1 phot2* mutant in microtubule nucleation and severing (a) Fraction of microtubules new microtubules - that do not originate from crossovers - that are initiated in the same orientation as the mother microtubule in *col0* wild type vs. branched initiation and *phot1 phot2*. (b and c) Histogram of angle between mother microtubule and new microtubule not originating from microtubule crossovers in (b) *col0* wild type and (c) the *col0 phot1 phot2* double mutant. (d) Fraction of microtubule crossovers resulting in severing, asterisks indicates significant reduction of microtubule severing in *phot1 phot2* compared to wild type.

Figure 5.5: (e and f) Normalized histograms of time after a microtubule crossover is created until severing takes place in (e) wild type (522 severing events, 5 cells) and (f) *phot1 phot2* double mutant (220 severing events, 5 cells). (g) Fraction of microtubules generated at microtubule crossovers and microtubules not generated at crossovers in *col0* wild type and *col0 phot1 phot2*. All data in (a, b, c and g) were collected from 5 cells of both *col0* wild type and the *col0 phot1 phot2* double mutant. In *col0* wild type we found in total 243 newly generated microtubules of which 129 formed at microtubule crossovers and 104 did not. In *col0 phot1 phot2* we found in total 313 newly generated microtubules of which 94 formed at microtubule crossovers and 219 did not. The data (d, e and f) was analyzed from 1115 crossovers, in 5 cells wild type *col0* and 616 crossovers, 5 cells in *col0 phot1 phot2*.

5.3.7 The PHOT1/PHOT2 pathway increases the severing chance at microtubule crossovers

We found that in wild type there were proportionally more microtubules formed at microtubule crossovers than in the *phot1 phot2* mutant, so now we wanted to establish what caused this difference. Since we assume that the new microtubules created at microtubules crossovers are the result of microtubule severing, creating a growing new plus end, we could imagine two possible mechanisms. The first possible mechanism is that the PHOT1/PHOT2 pathway increases the overall microtubule severing rate at microtubule crossovers. The second possible mechanism is that the PHOT1/PHOT2 pathway increases the probability of the newly created microtubule plus after severing at the crossover end is in a growing state.

To investigate these two hypotheses we analyzed microtubule crossovers in wild type and *phot1 phot2* in our 30-minute movies with 5s time intervals. For each crossover we marked if microtubule severing took place, what the time was between the creation of the crossover and the severing event and whether the newly created plus end was growing or shrinking. In wild type, out of 1115 crossovers, 522 resulted in microtubule severing (47%), whereas in *phot1 phot2* out of 616 crossovers, 220 resulted in microtubule severing (36%) (Figure 5.5 d). The lower microtubule severing rate in the *phot1 phot2* mutant was highly significant ($p < 0.001$, binomial test). Also, the time after the microtubule crossover had created severing was significantly longer in the *phot1 phot2* mutant than in wild type ($p = 0.0024$, Mann-Whitney U test) (Figure 5.5 e and f). When we compared the proportion of microtubule severing events that resulted in a new growing plus end, we did not observe a significant difference between wild type and *phot1 phot2* ($p = 0.201$, binomial test).

5.3.8 Phototropism requires cortical microtubule reorientation

The PHOT1/PHOT2 proteins have been shown to be involved in phototropism and growth inhibition and we wanted to find out if microtubule reorientation was required for any of these effects. We grew seedlings in the dark for wild type and the blue light photoreceptor double mutants *cry1 cry2* and *phot1 phot2* in *col0* and wild type and *ktn1-1* in *ws*. We compared their hypocotyl growth speed before and after we turned on the monochromatic blue light. Kymographs taken from the growing hypocotyls are shown in Figure 5.6 (a) and their average growth velocities before and after blue light exposure are shown in Figure 5.6 (b). Only in the *phot1 phot2* mutant did we not see a significant reduction in hypocotyl growth velocity after the blue light was turned on. The *ktn1-1* mutant that is deficient in microtubule reorientation shows an immediate reduction in growth velocity, with similar kinetics as wild type plants. The growth velocity in the blue light for the *ktn1-1* mutant was not significantly different from the growth velocity of wild type plants in blue light. These data indicate that microtubule reorientation is not required for the growth inhibition of the PHOTOTROPIN blue light response.

To find out if microtubule reorientation is required for phototropism we wanted to establish whether *ktn1-1* plants are defective in phototropism. To answer this question we used a photo curvature assay (Christie et al., 2011) (Figure 5.6 c). For comparison, wild type and *ktn1-1* seedlings were grown in the dark for 8h (Figure 5.6 d) or they were illuminated from the side by monochromatic blue light ($2 \mu\text{mol m}^{-2} \text{s}^{-1}$). We found that the *ktn1-1* (17.2 ± 7.2 , $n=14$) mutant showed a significantly lower hypocotyl bending than wild type (44.8 ± 16.4 , $n=14$) in response to the unidirectional blue light ($p \ll 0.0001$, Student's *t*-test). When we calculated the growth velocity of the hypocotyls in this assay, we found that the growth velocity of wild type and *ktn1-1* plants was not significantly different. In other words, the *ktn1-1* plants grow fast enough to perform phototropism, but yet they are defective in doing so. Therefore we propose that microtubule reorientation is required for phototropism.

5.4 Discussion

Our results show that microtubule reorientation in dark grown hypocotyl cells is a blue light response that is primarily mediated by the PHOT1/PHOT2 pathway. In the *phot1 phot2* mutant microtubule reorientation is slower but it can still take place. The *phot1 phot2* mutant used in our study, the *phot2* mutation is not a complete null. This could explain why we still observe microtubule reorientation in this mutant. In addition, it is also possible that the CRY1/CRY2 pathway has a role in microtubule reorientation, since we also observed a lower reorientation speed in the *cry1 cry2* double mutant. Furthermore, phototropins and cryptochromes are known to interact in blue light responses (Folta and Spalding, 2001).

We found two different mechanisms by which new microtubules were created during the blue light response in dark grown hypocotyl cells. The first type of new

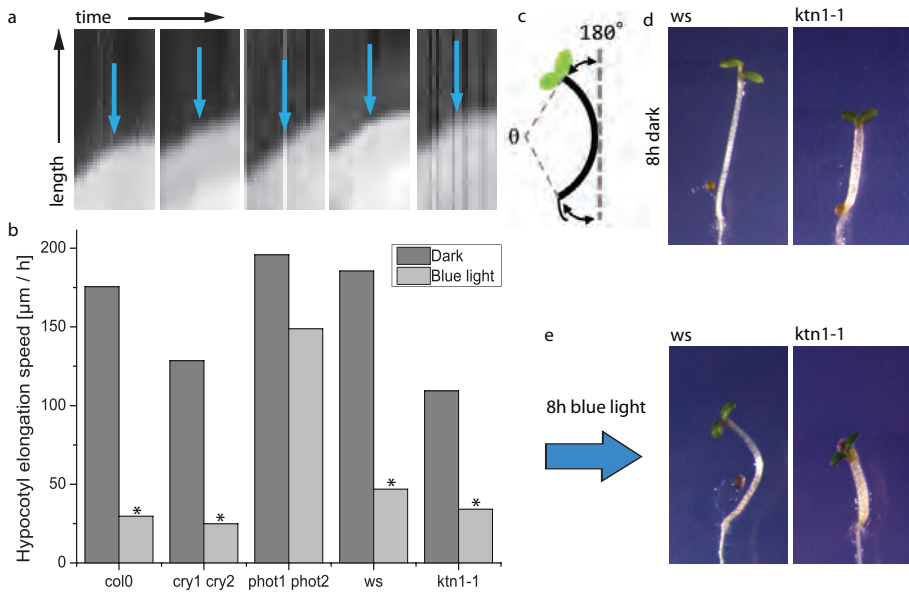


Figure 5.6: Microtubule reorientation and the phototropic response (a) Kymographs of etiolated hypocotyl elongation in different genotypes in red safelight for 1h. The blue arrows mark the moment the blue light is turned on for 1 h. (b) Mean growth speed of etiolated hypocotyls of *col0* wild type (22 plants), *col0 cry1 cry2* double (18 plants), *col0 phot1 phot2* (22 plants), *ws* wild type (16 plants) and *ws ktn1-1* (22 plants). The asterisks mark a significant reduction in Mann-Whitney U test of etiolated hypocotyl elongation speed after blue light induction. (c) Pictogram of the measurement of photocurvature of the hypocotyls. (d and e) Seedlings of wild type and *ktn1-1* germinated in a 16h light 8h dark cycle for three days and then grown in the dark for two days and (d) kept in the dark for 8h or (e) illuminated by blue light from the side.

microtubule initiation was nucleation from a γ -TuRC complex (Nakamura et al., 2010; Kirik et al., 2012). It was shown that for these nucleations there are two main classes, microtubules branching at 40° from the mother microtubule and growing in the same orientation as the mother microtubule (Chan et al., 2009; Nakamura et al., 2010; Kirik et al., 2012). We found that in the *phot1 phot2* double mutant there were significantly more microtubules nucleated parallel to the mother microtubule in proportion to branched nucleation than in wild type. This result indicates that the PHOT1/PHOT2 blue light response increases the degree of branching nucleation with respect to the parallel nucleations. The fraction of microtubule nucleations parallel the mother microtubule we found in wild type plants is lower than what was found in earlier studies (Chan et al., 2009; Nakamura et al., 2010; Kirik et al., 2012). This can perhaps partly be explained by the difference in laser power and exposure time used in the different experiments as the light response itself changes this ratio. It is not likely that the differences are caused by observer bias since part of the current data set was also analyzed by authors of one of the previous studies (Nakamura et al., 2010).

Wightman and Turner (2007) previously showed that microtubule severing preferentially occurs at microtubule crossovers. Here we show that indeed GFP-KTN signal accumulates at microtubule crossovers (Figure 5.4). We are not able to optically resolve the severing event itself, but we can observe the consequence of the severing event. It is relatively easy to observe severing events in which the newly created microtubule plus end starts depolymerizing (Figure 5.4 a) (Movie S6). We observed that during the blue light induced microtubule array reorientation a large number of new microtubules originated from microtubule crossover sites (Figure 5.3 and Figure 5.5). Our analysis showed that the microtubule nucleation complex marker GCP2-3xGFP was absent from the crossover site in most cases (> 97%) of microtubule initiation at microtubule crossovers, which makes microtubule nucleation an unlikely source for creating the microtubules initiating at crossovers. We argued that it could also be possible for the new plus end after severing to go into a growing state instead of a shrinking state. A severing event effectively creates two new microtubules and when the new microtubule plus end is growing, it would show what we observe; a new growing plus end originating from the point of severing, the microtubule crossover. Because the growing new plus end after severing generally grows in roughly the same direction as the new leading microtubule, a new growing plus end from a crossover visually stands out less than a new shrinking plus end. We show that GFP-KTN is present at the crossover when a microtubule starts shrinking from a crossover as well as when we see a new microtubule end originating from crossovers. We did not observe evidence for microtubule severing at crossovers in the *ktn1-1* mutant, nor did we observe new growing microtubules being generated at microtubule crossovers. We therefore propose that the newly formed growing plus ends at crossovers are the result of microtubule severing by KATANIN at the crossover site resulting in a new microtubule plus end in a growing state.

Mathematical modeling of microtubule severing has shown that if new plus ends created by severing start off in a shrinking state, the number of microtubules in the

system stays the same, and the average microtubule length is decreased (Tindemans and Mulder, 2010). This is an important consideration for the KATANIN mediated microtubule reorientation mechanism we have described here. This means that microtubule severing creating a shrinking plus end does not contribute to generating more microtubule length in the longitudinal orientation. So only the new microtubules created by severing that result in a new growing plus end can contribute to the increase in longitudinal order. The chemistry and proteins at microtubule plus ends are important for their stability (Howard and Hyman, 2003; Akhmanova and Steinmetz, 2008). We are investigating whether activity of plus end binding proteins is required for stabilization of the newly created microtubule plus ends by severing at microtubule crossovers. Figure S5.1 shows reorientation speeds in a number of plus end binding protein mutants in *Arabidopsis* expressing YFP-TUA5. The *clasp1* mutant plants show exceptionally low reorientation speeds. Interestingly, we had observed earlier (unpublished work) that the fluorescence intensity of labeled CLASP increased more at microtubule crossover sites than the microtubule fluorescence intensity at the microtubule crossover. Further examination is needed to show how these microtubule plus end binding proteins influence microtubule reorientation.

The chance of microtubule severing at microtubule crossovers was higher in wild type than in the *phot1 phot2* mutant. This shows that microtubule severing is upregulated by PHOTOTROPIN signaling. Therefore, we propose that the PHOTOTROPINS alter KATANIN activity in dark grown hypocotyl cells when exposed to blue light.

We propose mechanism with two components for the blue light induces microtubule reorientation Figure (5.7). The first step in reorientation is generating a number of longitudinal microtubules. A branched nucleation on a newly branched microtubule from a transverse microtubule will yield a more or less longitudinally oriented microtubule. The chance of such an event occurring is increased by the increase in the proportion of branched nucleation in the blue light response. These new longitudinal microtubules form a large number of microtubule crossovers with the existing transverse array and will therefore have a large chance to be severed by the upregulation of severing activity at microtubule crossovers. Each severing event has the potential to generate a new growing microtubule plus end that is also longitudinal. These new longitudinal microtubules have a higher chance of severing than the preexisting transverse microtubules. This new microtubule in turn also forms many crossovers and can also generate new longitudinal microtubules. Figure 5.3 (h) demonstrates that by far the largest proportion of new microtubules created at microtubule crossovers have a longitudinal orientation. In the PHOT1/PHOT2 response, the plant exploits the existing transverse microtubule array, which it seeds with a small number of longitudinal microtubules created by branched nucleation. A KATANIN based microtubule amplifier is then used to create a large number of longitudinal microtubules. This type of regulation of microtubule organization may also play a role in other acentrosomal microtubule arrays (Roll-Mecak and Vale, 2006).

In principal, this reorientation process could be reversible. In other words, why does the cortical microtubule organization not continually switch between transverse and longitudinal order? We observed that after reorientation the number of new

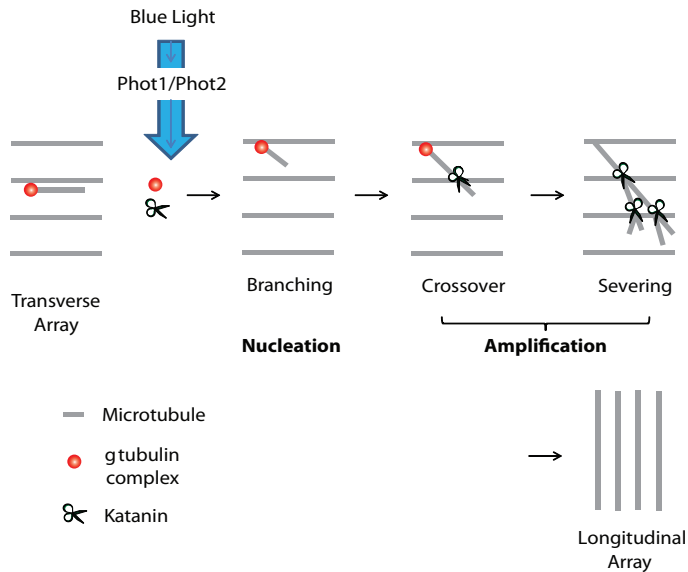


Figure 5.7: PHOTOTROPIN mediated reorientation of cortical microtubules.

microtubules created from severing as well as those from nucleation goes down. The decrease of new microtubules from microtubule severing is likely the result of the decrease in the number of microtubule crossovers. It is not clear whether the decrease in the number of microtubule nucleations over time is the result of active down regulation of the microtubule nucleating complexes or if it is the result of the increase of growing microtubule plus ends generated by the microtubule severing. We are currently setting up simulations, comparable to the simulations we used in Chapter 2, to address these questions.

The way in which a transverse cortical microtubule array is formed from a longitudinal arrangement does not seem to employ the same mechanism that we found in our research (Sambade et al., 2012). This process takes hours instead of minutes like we found, and the microtubule organization seems distinctly different. It is possible that regulation of KATANIN and microtubule nucleation mode also plays a role in this process.

PHOT1 and PHOT2 act as both kinases and transcription factors (Christie, 2007). Since the effect of these proteins on the ratio of 0 versus 40° branched nucleation and severing activity occur within a few minutes, it is unlikely that transcription plays a role in regulating microtubule nucleation direction and microtubule severing activity. Further study is required to establish whether the phototropins regulate these processes directly by their phosphorylation or if they act through intermediate molecules.

Phototropins are involved in growth inhibition and photo curvature (Christie and Briggs, 2001). Microtubule orientation is potentially important for each of these processes. We found that in *phot1 phot2* the growth was not significantly reduced after blue light exposure, which is in good agreement with earlier work (Folta and Spalding, 2001). In the *ktn1-1* mutant, where we did not observe microtubule reorientation within one hour, we found that growth inhibition by blue light was not impaired. This result suggests that microtubule reorientation is not required for growth inhibition, which is in agreement with a study that showed that growth inhibition preceded microtubule reorientation in the blue light response in pea shoots (Laskowski, 1990).

To assess whether microtubule reorientation plays a role in creating photo curvature, we compared photo curvature between wild type and the *ktn1-1* mutant. We found that the *ktn1-1* mutant was severely impaired in the ability to bend towards the direction of light. For growing towards the light, differential regulation of expansion between the side of the plant that perceives largest amount of light and the other side is required. A difference in auxin level, a plant growth hormone, is found between these two different sides, but how this regulates the difference in growth behavior between these sides is not known (Christie et al., 2011). In dark grown hypocotyl cells the expansion takes place perpendicular to the microtubule orientation. Our results indicate that perhaps light-induced bending the microtubule reorientation of the side that perceives the most light causes a change in direction of expansion, which is dependent on microtubule orientation. In other words, if the cells on the inside of the photo curvature grow thick and the cells on the other side grow long it creates an asymmetry in hypocotyl elongation. The advantage of this way of regulating growth asymmetry is that only the direction of expansion is regulated, allowing the rest of the cell's metabolism to remain the same in the cells of the hypocotyl. Further analysis of the relation between microtubule reorientation and its effect on growth during phototropism is needed to resolve the relation between microtubule orientation and photo curvature.

5.5 Materials and methods

5.5.1 Plant material

All experiments were performed in three-day-old dark grown etiolated hypocotyls of *Arabidopsis thaliana*. Three constructs were used for imaging of cortical microtubules, 35S-YFP-TUA5 (Shaw et al., 2003), 35S-GFP-TUB6 (Nakamura et al., 2004) and mCherry-TUA5 (Gutierrez et al., 2009). The *cry1 cry2* and *phot1 phot2* double mutants lines contain the YFP-TUA5 marker and are in the Columbia (col0) ecotype. The *ktn1-1* and *spr3* mutants contain the GFP-TUB6 marker and are in the Wassilewskija (ws) ecotype (Nakamura et al., 2004). Wild type *Arabidopsis* plants expressing YFP-TUA5 and mCherry-TUA5 were in the col-0 ecotype while the GFP-TUB6 was used in the ws ecotype.

The GFP-KTN construct was generated from katanin p60 subunit (At1g80350)

genomic region including a 1005-bp region 5'-upstream from initiation ATG and a 1039-bp region 3'-downstream from the stop codon and a smRS-GFP inserted at the Sma¹ and Nae¹ sites which had been introduced before initiation ATG codon of KAT by PCR. The insert was excised by NotI, and was inserted into the binary vector pBIN19. The resulting binary vector was used to transform *ktn1-2* mutant plants (CS816005) in which a single T-DNA was inserted after the 147th of the 5th exon from ABRC. The mCherry-TUA5 expressing plants were then crossed to the GFP-KTN / *ktn1-2* lines, and the F3 progeny plants expressing both reporters were analyzed.

5.5.2 Plant growth

Seeds were surface sterilized, stratified for 3 days at 4 °C, and sown on 1% agar containing Hoagland's No. 2 basal salts at pH 5.7. After 1 h of light exposure, the seedlings were grown in darkness for 60±72 h at 22 °C.

5.5.3 Specimen mounting

Seedlings were mounted under red safelight conditions to prevent de-etiolation. Seedlings were gently placed on a cover slip in sterile water and affixed with a 1 mm thick 1% agarose pad. The slide is left resting for at least 20 minutes before mounting it on the microscope to reduce specimen drift.

5.5.4 Microscopy

For microscopy we used a spinning disk confocal setup with a Yokogawa CSU-X1 spinning disk head on a Nikon Eclipse Ti body with perfect focus system (Chapter 2). To ensure that the imaging and light conditions were the same for every experiment we measured the laser power of the 491 nm laser (and 561nm for the mCherry excitation) at the optical fiber output that goes in the spinning disk head and set it to 8.2 mW. Image acquisition was done at 300 ms, every 10s over 60 minutes or at a 5s interval for 30 minutes. The mCherry-TUA5 GCP2-3xGFP plants were imaged with a 5s interval for 30 minutes using 8.2 mW laser output and 300 ms exposure time for both the 491 and 561 laser at the optical fiber.

5.5.5 Image analysis

To quantify microtubule orientation and order we developed an automated image analysis ImageJ plugin. In the plugin we define an elongated kernel for which we define a length and width. In our analysis we chose a width of 3 pixels and a length of 21 pixels. Images are padded with zeros depending on the length of the kernel. At each pixel of the image we rotate the kernel and sum up the intensity in the kernel. Intensities are calculated using bilinear interpolation. For each pixel, the angle that resulted in the highest integrated kernel intensity was marked as the angle at the pixel. The user can define the number of angles. We used 20 angles for all our orientation

analysis. The plugin labels the orientation per pixel of pixels that were above the threshold level (supplemental movie S1). This information is then further processed in MATLAB to extract the microtubule orientation over time. We aim to make the plugin freely available.

5.5.6 Microtubule reorientation analysis

From the image analysis we have the orientation of all pixels above the threshold value over twenty bins. To be able to pinpoint the moment in time where the longitudinal microtubule order becomes dominant over the transverse order we defined two filter functions: T for transverse order and L for longitudinal order. For T , the fraction of angles between 67.5° and 112.5° is multiplied by 1, the rest by $-1/3$. For L the fraction of angles between 0° and 22.5° plus the ones between 157.5° and 180° are multiplied by 1, also the rest by $-1/3$. When the angular distribution is random, T and L have a value of 0. Positive T or L values show overrepresentation in the corresponding orientation, negative values underrepresentation. We fitted the data of T and L over time with a cubic polynomial fit. We wanted to focus on the build up of the longitudinal order so we used the average increase in longitudinal order over time as the measure for the speed of reorientation. We calculated the average increase of L over time from the start of acquisition until L reached 0, as this part has an approximately linear increase. When longitudinal order is obtained, the increase in L levels off, therefore we excluded this part from the calculation of L . In cases L did not reach zero, we divided the total increase in L by the total observation time. All steps mentioned in this 'data analysis' section were incorporated into a MATLAB script. Hereby we were able to work through large data sets quickly and limit observer bias.

5.5.7 Microtubule initiation analysis

As a visual aid for detecting new microtubules we performed a walking image subtraction of three frames on the mCherry-TUA5 signal and selected the positive difference. This approach results in 'comets' reminiscent of fluorescent labeling of plus end binding proteins. We made these 'comets' green and added them to the grayscale microtubule images. We found that a difference of 3 frames was optimal for the visibility of the growing microtubule ends. Because we wanted the growing end to precede the already existing part of the microtubule we deleted the last three frames of the original file. This approach works correctly for the growing ends but this means that the shrinking are not shown correctly. Therefore we also used the original image of which the first three frames were deleted as the correct representation.

For all new microtubules we scored the position, time, if it originated from a preexisting microtubule, the angle of the preexisting microtubule, the angle of the new microtubule, if the new microtubule originated from a microtubule crossover and if GCP was present (in the double labeled line).

For the crossover analysis we marked the position and moment of crossover creation, moment of crossover disappearance. When a crossover disappeared we asked

if severing of the preexisting microtubule had taken place and if that microtubule started off in a growing or shrinking state. We asked the same question for severing of the new microtubule at the crossover.

5.5.8 Hypocotyl elongation and photocurvature

Plates with seedlings were imaged in red safelight (Paterson) with a 5 minute time interval. After 1h we turned on a blue light with a diode array (EagleLight). We made kymographs along the elongation axis of the hypocotyls to measure the growth velocities before and after blue light induction. For photo curvature we used the assay described in (Christie et al., 2011).

5.6 Acknowledgements

We thank Winslow Briggs and Takashi Hashimoto for sharing materials and we thank Angus Murphy for helpful discussions.

5.7 Supplementary information

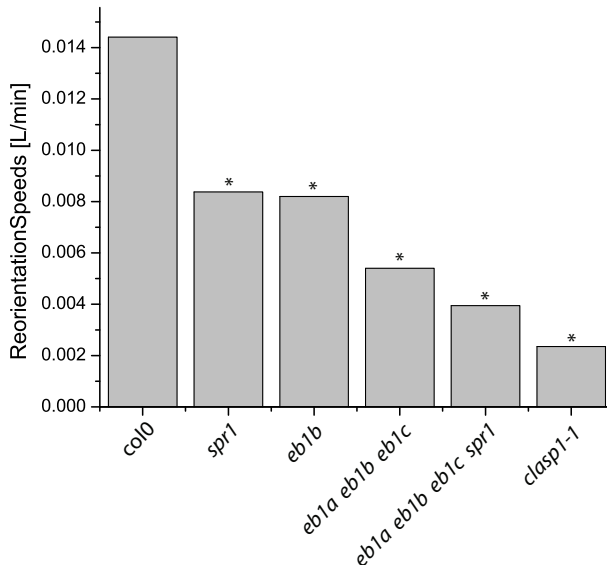


Figure S5.1 Microtubule reorientation speeds in wild type and plus end binding proteins. Asterisks indicate significant reduction from wild type (Mann-Whitney U test).

6

General discussion

As they are not able to move, higher plants have evolved flexible mechanisms of development and growth that allow them to optimize crucial functions such as photosynthesis, nutrient uptake, water balance and reproduction in response to spatial and temporal environment heterogeneity. Morphogenetic flexibility is due both to the modular design of plant development and the ability to regulate the geometry and magnitude of individual cell expansion, a process that drives the growth and shape of the organs they make up.

It is crucial for plants to be able to adjust their growth to their environment constantly. We know that the microtubule cytoskeleton and cell wall deposition are important, but we do not understand by what mechanism they regulate plant cell growth. Cortical microtubules organize cellulose deposition by guiding delivery and movement of the cellulose synthase complexes (Paredez et al., 2006). However, this is not sufficient to explain how plants can readjust their cellular growth behavior in response to environmental cues. In this final chapter we will discuss possible additional roles for the cortical microtubule array in regulating anisotropic cell expansion.

6.1 Cell expansion and turgor pressure

Turgor pressure is the driving force for cell expansion (Ray et al., 1972). As turgor pressure is the same in all directions (isotropic), the acquisition of differentiated cell shape requires generating material anisotropies in the cell wall. In addition, the cell must tune the physical properties of the cell wall very precisely because the cell wall must yield to the turgor pressure, but only partially. If the cell wall is too stiff, the cell cannot grow and if the cell wall is not stiff enough the growth and pressure cannot be contained within the cell wall and the cell will rupture. The mechanisms for regulating cell wall mechanical anisotropy and yield tuning are fundamental to plant growth and shape, but are not well understood. When cell grow, they take up

water causing the turgor pressure to drop, therefore the turgor pressure needs to be tuned during cell elongation.

6.2 The plant cell wall as a gel

The plant cell wall can in physical terms be regarded as a gel (Jarvis, 1984). Plant cell walls consist of cellulose microfibrils and matrix materials such as pectin and hemicellulose. In this matrix, the cellulose microfibrils are thought to be the load-bearing component (Somerville, 2006). Cellulose microfibrils are long cable like structures synthesized at the plasma membrane by cellulose synthase complexes. The cellulose microfibrils are coupled by cross-linked hydrogen bonds in the cell wall matrix materials (Cosgrove, 2005).

Pectins consist of a backbone of β -galacturonic acid. The carboxyl groups on the β -galacturonic acid are found with different degrees of esterification depending on the cell type and developmental stage. Pectins arrive in the cell wall in the esterified form and can be gradually be de-esterified by enzymes in the cell wall. The negative charge of the carboxyl group can be coupled to the carboxyl groups of other pectin chains by covalent anions as calcium and form a gel or network. The more carboxyl groups are esterified, the sparser potential cross-links, which influences the gel properties of the pectins in the cell wall matrix. The plant cell can regulate the degree of cross-linking by adjusting pH, calcium and sodium levels in the cell wall (reviewed by Jarvis, 1984).

Cell wall loosening cannot be solely attributed to the regulation of cross-linking of pectin gels and McQueen-Mason et al. (1992) identified a new class of cell wall proteins. These proteins could be extracted from the cell wall and when this fraction was reapplied to cell walls it induced cell wall loosening (McQueen-Mason and Cosgrove, 1994). It was also shown that the cell wall loosening activity was pH dependent (McQueen-Mason and Cosgrove, 1994). Although extensively they have been extensively tested for it, expansins do not appear to have enzymatic activities (Cosgrove, 2005). It has been proposed that expansins loosen cell wall by binding to cellulose microfibrils where they explore them by one-dimensional diffusion and disrupt hydrogen bonds between the cellulose microfibrils and the cell wall matrix polymers (Cosgrove, 2005). The turgor pressure on the cell wall provides the force needed for sliding cellulose microfibrils relative to each other, allowing the cell wall surface area to increase and the cell to expand (Cosgrove, 2005).

6.3 Cortical microtubules are required for anisotropy of growth

Microtubules are protein polymers that assemble linearly as cylinders and are associated to the plasma membrane of plant cells (Hardham and Gunning, 1978; Shaw et al., 2003). In growing plant cells, the cortical microtubules self organize transverse

to the elongation axis through microtubule - microtubule interactions (Allard et al., 2010a; Eren et al., 2010; Hawkins et al., 2010; Tindemans et al., 2010).

When microtubule organization is compromised by the use of microtubule specific drugs or mutations, the cells lose their ability to expand anisotropically and bulge (Buschmann and Lloyd, 2008). Two important functions for cortical microtubules in regulating cellulose synthase complex behavior at the plasma membrane are known. Firstly, microtubules guide cellulose synthase complexes as they deposit cellulose, thus modulating the direction of cellulose deposition (Paredes et al., 2006). Secondly, microtubules position cellulose synthase complex insertion into the plasma membrane (Gutierrez et al., 2009). Cellulose orientation is thought to be a significant determinant of the anisotropic yielding properties of the cell wall (Baskin, 2001). While these insights into cortical microtubule array function have been important advances, significant questions remain about the function of cellulose synthase complex positioning in modulating patterns of wall growth. Another open question is whether cellulose orientation alone is sufficient to explain regulation of cell growth anisotropy by the cortical cytoskeleton (Paredes et al., 2006; Gutierrez et al., 2009).

6.4 Regulation of cell wall properties by cortical microtubules

Anisotropic plant cell growth has been associated with the organization of cellulose microfibrils and the microtubule cytoskeleton (Somerville, 2006). As the cell wall itself is not part of the living cell, adaptations to the environment are most likely regulated from inside the cell. In tip growing cells of fission yeast, fungi and plant root hairs, microtubules have been shown to be important for determining the direction of growth (Mata and Nurse, 1997; Riquelme, 1998; Ketelaar et al., 2003). Also, during cytokinesis in plant cells, the microtubules in the phragmoplast control the formation of the new cell wall separating the daughter cells (Kakimoto and Shibaoka, 1987). It is therefore interesting to investigate whether the cortical microtubule array plays a role in direction of cell growth of cylindrical cells of the root and shoot beyond guiding the insertion and movement of cellulose synthase complexes.

6.5 A model for microtubule localized regulation of cell wall extendibility

Cortical microtubules may regulate plant cell growth and morphogenesis by spatially organizing activities at the plasma membrane in addition to cellulose synthase complex insertion and guiding of cellulose microfibril deposition. Because the ordering and orientation of the microtubules at the plasma membrane is critical for the regulation of the direction of growth, it is likely that microtubule localization is important for the localization of proteins that are directly involved in cell growth. In

other words, cortical microtubules may act as a scaffold for recruiting factors that influence cell wall extendibility and thereby setting up an anisotropic pattern of cell wall extendibility.

Expansins are cell wall proteins that mediate cell wall extendibility in a pH dependent manner by disrupting hydrogen bonds in the cell wall matrix (McQueen-Mason and Cosgrove, 1994), and also pectin networks can be loosened by reduction of the pH (Jarvis, 1984). In addition, it has been shown that acidification of the cell wall is an essential step in root hair formation (Bibikova et al., 1998). We propose a model for plant cell growth where the cortical microtubule array creates anisotropy in the mechanical properties of the cell wall beyond cellulose microfibril orientation. In this model, the cortical microtubules create localized pH-mediated cell wall loosening, by which the microtubule orientation biases the direction of cell expansion. In growing cells, the microtubules are transverse to the growth axis and if the cell wall loosening is dependent on the microtubule orientation, wall extension is perpendicular to the microtubule orientation. This model leads to two alternative, but not mutually exclusive predictions: (1) Expansin exocytosis is targeted to cortical microtubules, similar to what was found for cellulose synthase complexes (Gutierrez et al., 2009) (Chapter 3). (2) Microtubules localize proteins that are involved in acidification of the cell wall and create localized bands of low extracellular pH.

For the microtubule targeted expansin exocytosis hypothesis to work, the lifetime of expansins needs to be short on the timescale of cell wall extension in order for the active expansins to have a non uniform distribution in the cell wall. The fact that expansins can easily be extracted and have cell wall loosening activity when added to cell walls and their relatively high degree of glycosylation suggest the protein is relatively stable.

The second hypothesis offers easier adjustment of extendibility than the first. The cell wall components, such as cellulose, cell wall matrix material and expansins are in place in the cell wall, so for changing the direction of cell expansion, the microtubule orientation can be adjusted at the plasma membrane as occurs for instance in the phototropin response (Chapter 5). Another link between cell growth and acidification that the plant growth hormone auxin, that is essential for hypocotyl elongation, promotes acidification of the cell wall by regulating the activity of H⁺-ATPases (reviewed by Hager, 2003). The cortical microtubules could either asymmetrically localize factors that increase or decrease cell wall acidification in this model.

6.6 A possible role of MAP65 family proteins in anisotropic cell expansion

The microtubule associated protein MAP65 is the plant member of the eukaryotic PRC/ASE1/MAP65 protein family. MAP65 localized to microtubule bundles but are not required for microtubule bundle formation in planta (Lucas and Shaw, 2012; Lucas et al., 2011). The MAP65 proteins in plant cells do not appear to have any

microtubule bundling activity at the cell cortex (Lucas et al., 2011), and microtubule bundling does not alter microtubule dynamics (Lucas et al., 2011). Reducing expression of the MAP65-1 and MAP65-2 by T-DNA insertion and/ or RNAi caused repression of apical elongation in etiolated hypocotyl cells, while the number of cells in the hypocotyl did not change. The authors therefore hypothesize that MAP65 proteins positively regulate cell elongation by recruiting growth-promoting factors to the sites of microtubule bundles (Lucas et al., 2011). Cortical microtubule ordering generally precedes bundle formation (Chapter 2), so localizing these growth activities specifically to bundles and not to single microtubules has the advantage that the influence of single microtubules in discordant orientations has little effect on the anisotropy of cell growth.

6.7 Cellulose deposition to counterbalance cell wall extension

Cellulose microfibrils have a high tensile strength, which means they are not likely to break under stress. In growing cells the cellulose microfibrils are oriented transversely to the elongation axis, and this material anisotropy in cell wall material has long been proposed to be the main facilitator of uniaxial cell growth (reviewed by Baskin, 2001). However, cell wall acidification, which is essential for cell growth, affects the degree of cross-linking of the cell wall matrix, allowing cell wall creep under turgor pressure (Jarvis, 1984; Cosgrove, 2005). A model in which the cellulose microfibrils determine the direction of expansion does not allow for changes in the axis of growth during cell development. For instance a growing cell has transverse cellulose microfibrils so therefore it cannot grow in width. Microtubule reorientation and subsequent new orientation of new cellulose microfibril deposition can therefore only restrict growth in other directions. However, we know that for instance etiolated hypocotyls grow thicker after de-etiolation.

If we assume that indeed the microtubules localize regions of cell wall loosening, the cell wall area around the microtubules will extend more, locally diluting cell wall materials. This dilution needs to be counterbalanced in order to not create weak spots in the cell wall that could result in catastrophic failure. This offers an alternative explanation for why the cellulose synthase complexes are inserted preferentially at sites in the plasma membrane with cortical microtubules (Gutierrez et al., 2009) (Chapter 3), and why a large proportion of cellulose synthase complexes move along cellulose microfibrils (Paredes et al., 2006). This mechanism of regulation of cell elongation may offer an explanation for the fact that in electron micrographs cellulose microfibrils are packed extremely ordered and evenly spaced while the cortical microtubules are spaced much further apart and are less ordered.

Bibliography

- M. Abramowitz and I. A. Stegun. *Handbook of mathematical functions with formulas, graphs, and mathematical tables*. U.S. Govt. Print. Off., Washington,, 9th print edition, 1970.
- A. Akhmanova and M. O. Steinmetz. Tracking the ends: a dynamic protein network controls the fate of microtubule tips. *Nature reviews. Molecular cell biology*, 9(4):309–322, 2008.
- J. E. Allard, J. C. Ambrose, G. O. Wasteneys, and E. N. Cytrynbaum. A mechanochemical model explains interactions between cortical microtubules in plants. *Biophysical Journal*, 99(4): 1082–1090, 2010a.
- J. E. Allard, G. O. Wasteneys, and E. N. Cytrynbaum. Mechanisms of self-organization of cortical microtubules in plants revealed by computational simulations. *Molecular Biology of the Cell*, 21(2):278–286, 2010b.
- C. Ambrose, J. F. Allard, E. N. Cytrynbaum, and G. O. Wasteneys. A CLASP-modulated cell edge barrier mechanism drives cell-wide cortical microtubule organization in Arabidopsis. *Nature communications*, 2:430, 2011.
- J. C. Ambrose and G. O. Wasteneys. CLASP modulates microtubule-cortex interaction during self-organization of acentrosomal microtubules. *Molecular Biology of the Cell*, 19(11): 4730–4737, 2008.
- F. Bartolini and G. G. Gundersen. Generation of noncentrosomal microtubule arrays. *Journal of Cell Science*, 119(Pt 20):4155–4163, 2006.
- D. A. Barton and R. L. Overall. Cryofixation rapidly preserves cytoskeletal arrays of leaf epidermal cells revealing microtubule co-alignments between neighbouring cells and adjacent actin and microtubule bundles in the cortex. *Journal of microscopy*, 237(1):79–88, 2010.
- D. a. Barton, M. Vantard, and R. L. Overall. Analysis of cortical arrays from *Tradescantia virginiana* at high resolution reveals discrete microtubule subpopulations and demonstrates that confocal images of arrays can be misleading. *The Plant Cell*, 20(4):982–994, 2008.
- T. I. Baskin. On the alignment of cellulose microfibrils by cortical microtubules: A review and a model. *Protoplasma*, 215(1-4):150–171, 2001.
- T. I. Baskin, J. E. Wilson, A. Cork, and R. E. Williamson. Morphology and microtubule organization in Arabidopsis roots exposed to oryzalin or taxol. *Plant and Cell Physiology*, 35(6): 935–942, 1994.
- D. C. Bassham, A. A. Sanderfoot, V. Kovaleva, H. Zheng, and N. V. Raikhel. AtVPS45 complex formation at the trans-Golgi network. *Molecular Biology of the Cell*, 11(7):2251–2265, 2000.

- R. Basu and F. Chang. Shaping the actin cytoskeleton using microtubule tips. *Current Opinion in Cell Biology*, (19):88–94, 2007.
- T. N. Bibikova, T. Jacob, I. Dahse, and S. Gilroy. Localized changes in apoplastic and cytoplasmic pH are associated with root hair development in *Arabidopsis thaliana*. *Development*, 125(15):2925–2934, 1998.
- K. Birnbaum, D. E. Shasha, J. Y. Wang, J. W. Jung, G. M. Lambert, D. W. Galbraith, and P. N. Benfey. A gene expression map of the *Arabidopsis* root. *Science*, 302(5652):1956–1960, 2003.
- E. B. Blancaflor. *Journal of Plant Growth Regulation*, Volume 19, Number 4 - SpringerLink. *Journal of Plant Growth Regulation*, 2000.
- S. Bolte, C. Talbot, Y. Boutte, O. Catrice, N. D. Read, and B. Satiat-Jeunemaitre. FM-dyes as experimental probes for dissecting vesicle trafficking in living plant cells. *Journal of microscopy*, 214(Pt 2):159–173, 2004.
- W. R. Briggs and E. Huala. Blue-light photoreceptors in higher plants. *Annual review of cell and developmental biology*, 15:33–62, 1999.
- R. M. Brown Jr and I. M. Saxena. Cellulose biosynthesis: A model for understanding the assembly of biopolymers. *Plant Physiology and Biochemistry*, 38(1-2):57–67, 2000.
- M. R. Bubb, A. M. Senderowicz, E. A. Sausville, K. L. Duncan, and E. D. Korn. Jasplakinolide, a cytotoxic natural product, induces actin polymerization and competitively inhibits the binding of phalloidin to F-actin. *Journal of Biological . . .*, 1994.
- D. H. Burk and Z.-H. Ye. Alteration of Oriented Deposition of Cellulose Microfibrils by Mutation of a Katanin-Like Microtubule-Severing Protein. *The Plant Cell Online*, 2002.
- H. Buschmann and C. W. Lloyd. *Arabidopsis* mutants and the network of microtubule-associated functions. *Molecular plant*, 1(6):888–898, 2008.
- N. C. Carpita and D. M. Gibeaut. Structural models of primary cell walls in flowering plants: consistency of molecular structure with the physical properties of the walls during growth. *The Plant journal*, 3(1):1–30, 1993.
- J. Chan, G. M. Calder, J. H. Doonan, and C. W. Lloyd. EB1 reveals mobile microtubule nucleation sites in *Arabidopsis*. *Nature Cell Biology*, 5(11):967–971, 2003.
- J. Chan, G. Calder, S. Fox, and C. Lloyd. Cortical microtubule arrays undergo rotary movements in *Arabidopsis* hypocotyl epidermal cells. *Nature Cell Biology*, 9(2):171–175, 2007.
- J. Chan, A. Sambade, G. Calder, and C. Lloyd. *Arabidopsis* cortical microtubules are initiated along, as well as branching from, existing microtubules. *The Plant Cell*, 21(8):2298–2306, 2009.
- J. Chan, E. Crowell, M. Eder, G. Calder, S. Bunnewell, K. Findlay, S. Vernhettes, H. Höfte, and C. Lloyd. The rotation of cellulose synthase trajectories is microtubule dependent and influences the texture of epidermal cell walls in *Arabidopsis* hypocotyls. *Journal of Cell Science*, 123(Pt 20):3490–3495, 2010.

- J. Chan, M. Eder, E. F. Crowell, J. Hampson, G. Calder, and C. Lloyd. Microtubules and CESA tracks at the inner epidermal wall align independently of those on the outer wall of light-grown *Arabidopsis* hypocotyls. *Journal of Cell Science*, 124(Pt 7):1088–1094, 2011.
- I. Chaves, R. Pokorný, M. Byrdin, N. Hoang, T. Ritz, K. Brettel, L.-O. Essen, G. T. J. van der Horst, A. Batschauer, and M. Ahmad. The cryptochromes: blue light photoreceptors in plants and animals. *Annual review of plant biology*, 62:335–364, 2011.
- J. M. Christie. Phototropin blue-light receptors. *Annual review of plant biology*, 58:21–45, 2007.
- J. M. Christie and W. R. Briggs. Blue light sensing in higher plants. *Journal of Biological Chemistry*, 276(15):11457–11460, 2001.
- J. M. Christie, H. Yang, G. L. Richter, S. Sullivan, C. E. Thomson, J. Lin, B. Titapiwatanakun, M. Ennis, E. Kaiserli, O. R. Lee, J. Adamec, W. A. Peer, and A. S. Murphy. phot1 inhibition of ABCB19 primes lateral auxin fluxes in the shoot apex required for phototropism. *PLoS Biology*, 9(6):e1001076, 2011.
- D. Collings. Crossed-wires: interactions and cross-talk between the microtubule and microfilament networks in plants. *Plant Microtubules*, pages 47–79, 2008.
- D. A. Collings and G. O. Wasteneys. Actin microfilament and microtubule distribution patterns in the expanding root of *Arabidopsis thaliana*. *Canadian journal of botany*, 83(6):579–590, 2005.
- D. J. Cosgrove. Growth of the plant cell wall. *Nature reviews. Molecular cell biology*, 6(11):850–861, 2005.
- E. F. Crowell, H. Timpano, T. Desprez, T. Franssen-Verheijen, A.-M. Emons, H. Höfte, and S. Vernhettes. Differential regulation of cellulose orientation at the inner and outer face of epidermal cells in the *Arabidopsis* hypocotyl. *The Plant Cell Online*, 23(7):2592–2605, 2011.
- S. Debolt, R. Gutierrez, D. W. Ehrhardt, C. V. Melo, L. Ross, S. R. Cutler, C. Somerville, and D. Bonetta. Morlin, an inhibitor of cortical microtubule dynamics and cellulose synthase movement. *Proceedings of the National Academy of Sciences of the United States of America*, 104(14):5854–5859, 2007a.
- S. Debolt, R. Gutierrez, D. W. Ehrhardt, and C. Somerville. Nonmotile cellulose synthase subunits repeatedly accumulate within localized regions at the plasma membrane in *Arabidopsis* hypocotyl cells following 2,6-dichlorobenzonitrile treatment. *Plant physiology*, 145(2):334–338, 2007b.
- E. E. Deinum, S. H. Tindemans, and B. M. Mulder. Taking directions: the role of microtubule-bound nucleation in the self-organization of the plant cortical array. *Physical biology*, 8(5):056002, 2011.
- D. P. Delmer. CELLULOSE BIOSYNTHESIS: Exciting Times for A Difficult Field of Study. *Annual Review of Plant Physiology and Plant Molecular Biology*, 50:245–276, 1999.
- T. Desprez, M. Juraniec, E. F. Crowell, H. Jouy, Z. Pochylova, F. Parcy, H. Höfte, M. Gonneau, and S. Vernhettes. Organization of cellulose synthase complexes involved in primary cell wall synthesis in *Arabidopsis thaliana*. *Proceedings of the National Academy of Sciences of the United States of America*, 104(39):15572–15577, 2007.

- P. Dhonukshe, F. Baluska, M. Schlicht, A. Hlavacka, J. Samaj, J. Friml, and T. W. J. Gadella. Endocytosis of cell surface material mediates cell plate formation during plant cytokinesis. *Developmental cell*, 10(1):137–150, 2006.
- P. Dhonukshe, D. A. Weits, A. Cruz-Ramirez, E. E. Deinum, S. H. Tindemans, K. Kakar, K. Prasad, A. P. Mähönen, C. Ambrose, M. Sasabe, G. Wachsmann, M. Luijten, T. Bennett, Y. Machida, R. Heidstra, G. Wasteneys, B. M. Mulder, and B. Scheres. A PLETHORA-auxin transcription module controls cell division plane rotation through MAP65 and CLASP. *Cell*, 149(2):383–396, 2012.
- F. Diotallevi and B. Mulder. The cellulose synthase complex: a polymerization driven supramolecular motor. *Biophysical Journal*, 92(8):2666–2673, 2007.
- R. Dixit and R. Cyr. Encounters between dynamic cortical microtubules promote ordering of the cortical array through angle-dependent modifications of microtubule behavior. *The Plant Cell*, 16(12):3274–3284, 2004.
- K. W. Earley, J. R. Haag, O. Pontes, K. Opper, T. Juehne, K. Song, and C. S. Pikaard. Gateway-compatible vectors for plant functional genomics and proteomics. *The Plant journal*, 45(4): 616–629, 2006.
- D. W. Ehrhardt. Straighten up and fly right: microtubule dynamics and organization of non-centrosomal arrays in higher plants. *Current Opinion in Cell Biology*, 20(1):107–116, 2008.
- D. W. Ehrhardt and S. L. Shaw. Microtubule dynamics and organization in the plant cortical array. *Annual review of plant biology*, 57:859–875, 2006.
- A. Emons. Winding threads around plant cells: a geometrical model for microfibril deposition. *Plant Cell and Environment*, 17(1):3–14, 2006.
- A. Emons, J. Derksen, and M. Sassen. Do microtubules orient plant cell wall microfibrils? *Physiologia plantarum*, 84(3):486–493, 2006.
- A. M. Emons and B. M. Mulder. The making of the architecture of the plant cell wall: how cells exploit geometry. *Proceedings of the National Academy of Sciences of the United States of America*, 95(12):7215–7219, 1998.
- A. M. C. Emons. Plasma-membrane rosettes in root hairs of *Equisetum hyemale*. *Planta*, 163(3):350–359, 1985.
- A. M. C. Emons. The cytoskeleton and secretory vesicles in root hairs of *Equisetum* and *Limnobium* and cytoplasmic streaming in root hairs of *Equisetum*. *Annals of Botany*, 60(6): 625–632, 1987.
- A. M. C. Emons. Methods for visualizing cell wall texture. *Acta botanica neerlandica*, 37(1): 31–38, 1988.
- A. M. C. Emons. Helicoidal microfibril deposition in a tip-growing cell and microtubule alignment during tip morphogenesis: a dry-cleaving and freeze-substitution study. *Canadian journal of botany*, 67(8):2401–2408, 1989.

- A. M. C. Emons. The role of particle rosettes and terminal globules in cellulose synthesis. *Book*, pages 71–98, 1991.
- A. M. C. Emons and J. A. Traas. Coated pits and coated vesicles on the plasma membrane of plant cells. *European journal of cell biology. Supplement*, 41(1):57–64, 1986.
- A. M. C. Emons and A. Wolters-Arts. Cortical microtubules and microfibril deposition in the cell wall of root hairs of *Equisetum hyemale*. *Protoplasma*, 117(1):68–81, 1983.
- A. M. C. Emons, J. W. Vos, and H. Kieft. A freeze fracture analysis of the surface of embryonic and non-embryogenic suspension cells of *Daucus carota*. *Plant Science*, 87(1):85–97, 1992.
- A. M. C. Emons, H. Höfte, and B. M. Mulder. Microtubules and cellulose microfibrils: how intimate is their relationship? *Trends in plant science*, 12(7):279–281, 2007.
- E. C. Eren, R. Dixit, and N. Gautam. A three-dimensional computer simulation model reveals the mechanisms for self-organization of plant cortical microtubules into oblique arrays. *Molecular Biology of the Cell*, 21(15):2674–2684, 2010.
- K. M. Folta and E. P. Spalding. Unexpected roles for cryptochrome 2 and phototropin revealed by high-resolution analysis of blue light-mediated hypocotyl growth inhibition - Folta - 2001 - The Plant Journal - Wiley Online Library. *The Plant journal*, 26(5):471–478, 2001.
- D. M. Friedrichsen, C. A. Joazeiro, J. Li, T. Hunter, and J. Chory. Brassinosteroid-insensitive-1 is a ubiquitously expressed leucine-rich repeat receptor serine/threonine kinase. *Plant physiology*, 123(4):1247–1256, 2000.
- Y. Fu, Y. Gu, Z. Zheng, G. Wasteneys, and Z. Yang. Arabidopsis interdigitating cell growth requires two antagonistic pathways with opposing action on cell morphogenesis. *Cell*, 120(5):687–700, 2005.
- M. Fujita, R. Himmelspach, C. H. Hocart, R. E. Williamson, S. D. Mansfield, and G. O. Wasteneys. Cortical microtubules optimize cell-wall crystallinity to drive unidirectional growth in Arabidopsis. *The Plant journal*, 66(6):915–928, 2011.
- D. K. Fygenson, E. Braun, and A. Libchaber. Phase diagram of microtubules. *Physical Review E*, 50(2):1579, 1994.
- T. H. Giddings and L. A. Staehelin. Spatial relationship between microtubules and plasma-membrane rosettes during the deposition of primary wall microfibrils in *Closterium* sp. *Planta*, 173(1):22–30, 1988.
- B. L. Goode, D. G. Drubin, and G. Barnes. Functional cooperation between the microtubule and actin cytoskeletons. *Current Opinion in Cell Biology*, 12(1):63–71, 2000.
- P. B. Green. Mechanism for Plant Cellular Morphogenesis. *Science (New York, NY)*, 138(3548):1404–1405, 1962.
- E. L. Grishchuk, I. S. Spiridonov, V. A. Volkov, A. Efremov, S. Westermann, D. Drubin, G. Barnes, F. I. Ataulkhanov, and J. R. McIntosh. Different assemblies of the DAM1 complex follow shortening microtubules by distinct mechanisms. *Proceedings of the National Academy of Sciences of the United States of America*, 105(19):6918–6923, 2008.

- R. Gutierrez, J. J. Lindeboom, A. R. Paredez, A. M. C. Emons, and D. W. Ehrhardt. Arabidopsis cortical microtubules position cellulose synthase delivery to the plasma membrane and interact with cellulose synthase trafficking compartments. *Nature Cell Biology*, 11(7):797–806, 2009.
- A. Hager. Role of the plasma membrane H⁺-ATPase in auxin-induced elongation growth: historical and new aspects. *Journal of plant research*, 116(6):483–505, 2003.
- C. H. Haigler and R. M. Brown. Transport of rosettes from the golgi apparatus to the plasma membrane in isolated mesophyll cells of *Zinnia elegans* during differentiation to tracheary elements in suspension culture. *Protoplasma*, 134(2):111–120, 1986.
- S. Handa, R. A. Bressan, A. K. Handa, N. C. Carpita, and P. M. Hasegawa. Solutes contributing to osmotic adjustment in cultured plant cells adapted to water stress. *Plant physiology*, 73(3):834–843, 1983.
- A. R. Hardham and B. E. Gunning. Structure of cortical microtubule arrays in plant cells. *The Journal of Cell Biology*, 77(1):14–34, 1978.
- R. J. Hawkins, S. H. Tindemans, and B. M. Mulder. Model for the orientational ordering of the plant microtubule cortical array. *Physical review. E, Statistical, nonlinear, and soft matter physics*, 82(1 Pt 1):011911, 2010.
- I. B. Heath. A unified hypothesis for the role of membrane bound enzyme complexes and microtubules in plant cell wall synthesis. *Journal of theoretical biology*, 1974.
- P. K. Hepler and E. H. Newcomb. MICROTUBULES AND FIBRILS IN THE CYTOPLASM OF COLEUS CELLS UNDERGOING SECONDARY WALL DEPOSITION. *The Journal of Cell Biology*, 20:529–532, 1964.
- W. Herth. Calcofluor white and Congo red inhibit chitin microfibril assembly of *Poterioochromonas*: evidence for a gap between polymerization and microfibril formation. *The Journal of Cell Biology*, 87(2):442–450, 1980.
- W. Herth. Arrays of plasma-membrane “rosettes” involved in cellulose microfibril formation of *Spirogyra*. *Planta*, 159(4):347–356, 1983.
- R. Himmelspach, R. E. Williamson, and G. O. Wasteneys. Cellulose microfibril alignment recovers from DCB-induced disruption despite microtubule disorganization. *The Plant journal*, 36(4):565–575, 2003.
- A. Hirase, T. Hamada, T. J. Itoh, T. Shimmen, and S. Sonobe. n-Butanol induces depolymerization of microtubules in vivo and in vitro. *Plant and Cell Physiology*, 47(7):1004–1009, 2006.
- J. Howard and A. A. Hyman. Dynamics and mechanics of the microtubule plus end. *Nature*, 422(6933):753–758, 2003.
- P. J. Hussey, M. Yuan, G. Calder, S. Khan, and C. W. Lloyd. Microinjection of pollen-specific actin-depolymerizing factor, ZmADF1, reorientates F-actin strands in *Tradescantia* stamen hair cells. *The Plant journal*, 14(3):353–357, 1998.

- N. M. Iraki, R. A. Bressan, P. M. Hasegawa, and N. C. Carpita. Alteration of the physical and chemical structure of the primary cell wall of growth-limited plant cells adapted to osmotic stress. *Plant physiology*, 91(1):39–47, 1989.
- M. C. Jarvis. Structure and properties of pectin gels in plant cell walls. *Plant Cell and Environment*, 7(3):153–164, 1984.
- D. Job, O. Valiron, and B. Oakley. Microtubule nucleation. *Current Opinion in Cell Biology*, 15(1):111–117, 2003.
- T. Kakimoto and H. Shibaoka. Actin filaments and microtubules in the preprophase band and phragmoplast of tobacco cells. *Protoplasma*, 140(2):151–156, 1987.
- C. J. Kennedy, G. J. Cameron, A. Šturcová, D. C. Apperley, C. Altaner, T. J. Wess, and M. C. Jarvis. Microfibril diameter in celery collenchyma cellulose: X-ray scattering and NMR evidence. *Cellulose*, 14(3):235–246, 2007.
- T. Ketelaar, N. C. A. de Ruijter, and A. M. C. Emons. Unstable F-actin specifies the area and microtubule direction of cell expansion in Arabidopsis root hairs. *The Plant Cell*, 15(1):285–292, 2003.
- T. Ketelaar, E. G. Allwood, R. Anthony, B. Voigt, D. Menzel, and P. J. Hussey. The actin-interacting protein AIP1 is essential for actin organization and plant development. *Current Biology*, 14(2):145–149, 2004.
- T. Ketelaar, M. E. GALWAY, B. M. Mulder, and A. M. C. Emons. Rates of exocytosis and endocytosis in Arabidopsis root hairs and pollen tubes. *Journal of microscopy*, 231(2):265–273, 2008.
- B. M. Kiedaisch, R. L. Blanton, and C. H. Haigler. Characterization of a novel cellulose synthesis inhibitor. *Planta*, 217(6):922–930, 2003.
- S. Kimura, W. Laosinchai, T. Itoh, X. Cui, C. Linder, and R. Brown. Immunogold labeling of rosette terminal cellulose-synthesizing complexes in the vascular plant vigna angularis. *The Plant Cell*, 11(11):2075–2086, 1999.
- A. Kirik, D. W. Ehrhardt, and V. Kirik. TONNEAU2/FASS regulates the geometry of microtubule nucleation and cortical array organization in interphase Arabidopsis cells. *The Plant Cell*, 24(3):1158–1170, 2012.
- V. Kirik, U. Herrmann, C. Parupalli, J. C. Sedbrook, D. W. Ehrhardt, and M. Hülskamp. CLASP localizes in two discrete patterns on cortical microtubules and is required for cell morphogenesis and cell division in Arabidopsis. *Journal of Cell Science*, 120(Pt 24):4416–4425, 2007.
- H. Kobayashi, H. Fukuda, and H. Shibaoka. Interrelation between the spatial disposition of actin filaments and microtubules during the differentiation of tracheary elements in cultured Zinnia cells. *Protoplasma*, 143(1):29–37, 1988.
- F. Kumagai, A. Yoneda, T. Tomida, T. Sano, T. Nagata, and S. Hasezawa. Fate of nascent microtubules organized at the M/G1 interface, as visualized by synchronized tobacco BY-2 cells stably expressing GFP-tubulin: time-sequence observations of the reorganization of cortical microtubules in living plant cells. *Plant and Cell Physiology*, 42(7):723–732, 2001.

- M. C. Lagomarsino, C. Tănase, J. W. Vos, A. M. C. Emons, B. M. Mulder, and M. Dogterom. Microtubule organization in three-dimensional confined geometries: evaluating the role of elasticity through a combined in vitro and modeling approach. *Biophysical Journal*, 92(3): 1046–1057, 2007.
- M. Laskowski. Microtubule orientation in pea stems: a change in orientation follows the initiation of growth rate decline. *Planta*, 181:44–52, 1990.
- M. C. Ledbetter and K. R. Porter. A "microtubule" in plant cell fine structure. *The Journal of Cell Biology*, 19(1):239–250, 1963.
- Y. Li, Y. Shen, C. Cai, C. Zhong, L. Zhu, M. Yuan, and H. Ren. The type II Arabidopsis formin14 interacts with microtubules and microfilaments to regulate cell division. *The Plant Cell Online*, 22(8):2710–2726, 2010.
- C. Lloyd and J. Chan. Microtubules and the shape of plants to come. *Nature reviews. Molecular cell biology*, 5(1):13–22, 2004.
- J. R. Lucas and S. L. Shaw. MAP65-1 and MAP65-2 promote cell proliferation and axial growth in Arabidopsis roots. *The Plant journal*, 71(3):454–463, 2012.
- J. R. Lucas, S. Courtney, M. Hassfurder, S. Dhingra, A. Bryant, and S. L. Shaw. Microtubule-Associated Proteins MAP65-1 and MAP65-2 Positively Regulate Axial Cell Growth in Etiolated Arabidopsis Hypocotyls. *The Plant Cell Online*, 23(5):1889–1903, 2011.
- C. A. Mandato and W. M. Bement. Actomyosin transports microtubules and microtubules control actomyosin recruitment during *Xenopus* oocyte wound healing. *Current Biology*, 13(13):1096–1105, 2003.
- J. Marc, C. Granger, J. Brincat, D. Fisher, T. Kao, A. McCubbin, and R. Cyr. A GFP-MAP4 reporter gene for visualizing cortical microtubule rearrangements in living epidermal cells. *The Plant Cell*, 10(11):1927–1940, 1998.
- S. G. Martin and F. Chang. New end take off: regulating cell polarity during the fission yeast cell cycle. - Abstract - UK PubMed Central. *Cell cycle (Georgetown)*, 2005.
- J. Mata and P. Nurse. *tea1* and the microtubular cytoskeleton are important for generating global spatial order within the fission yeast cell. *Cell*, 89(6):939–949, 1997.
- M. C. McCann, M. Bush, D. Milioni, P. Sado, N. J. Stacey, G. Catchpole, M. Defernez, N. C. Carpita, H. Hofte, P. Ulvskov, R. H. Wilson, and K. Roberts. Approaches to understanding the functional architecture of the plant cell wall. *Phytochemistry*, 57(6):811–821, 2001.
- H. E. McFarlane, R. E. Young, G. O. Wasteneys, and A. L. Samuels. Cortical microtubules mark the mucilage secretion domain of the plasma membrane in Arabidopsis seed coat cells. *Planta*, 227(6):1363–1375, 2008.
- S. McQueen-Mason and D. J. Cosgrove. Disruption of hydrogen bonding between plant cell wall polymers by proteins that induce wall extension. *Proceedings of the National Academy of Sciences of the United States of America*, 91(14):6574–6578, 1994.

- S. McQueen-Mason, D. M. Durachko, and D. J. Cosgrove. Two endogenous proteins that induce cell wall extension in plants. *The Plant Cell*, 4:1425–1433, 1992.
- E. Meijering, M. Jacob, J. C. F. Sarria, P. Steiner, H. Hirling, and M. Unser. Design and validation of a tool for neurite tracing and analysis in fluorescence microscopy images. *Cytometry. Part A: the journal of the International Society for Analytical Cytology*, 58(2):167–176, 2004.
- D. D. Miller, N. C. A. de Ruijter, and A. M. C. Emons. From signal to form: aspects of the cytoskeleton-plasma membrane—cell wall continuum in root hair tips. *Journal of experimental botany*, 48(11):1881–1896, 1997.
- D. D. Miller, H. B. L.-t. Klooster, and A. M. C. Emons. Lipochito-Oligosaccharide Nodulation Factors Stimulate Cytoplasmic Polarity with Longitudinal Endoplasmic Reticulum and Vesicles at the Tip in Vetch Root Hairs. *Molecular Plant-Microbe Interactions*, 13(12):1385–1390, 2000.
- L. C. Morejohn, T. E. Bureau, J. Mol Bajer, A. S. Bajer, and D. E. Fosket. Oryzalin, a dinitroaniline herbicide, binds to plant tubulin and inhibits microtubule polymerization in vitro. *Planta*, 172(2):252–264, 1987.
- D. J. Morre and W. J. VanDerWoude. Origin and growth of cell surface components. - Abstract - UK PubMed Central. *The symposium/The Society for . . .*, 1974.
- S. C. Mueller and R. M. Brown Jr. Evidence for an intramembrane component associated with a cellulose microfibril-synthesizing complex in higher plants. *The Journal of Cell Biology*, 84(2):315–326, 1980.
- B. M. Mulder and A. Emons. A dynamical model for plant cell wall architecture formation. *Journal of mathematical biology*, 42(3):261–289, 2001.
- T. Murata, S. Sonobe, T. I. Baskin, S. Hyodo, S. Hasezawa, T. Nagata, T. Horio, and M. Hasebe. Microtubule-dependent microtubule nucleation based on recruitment of gamma-tubulin in higher plants. *Nature Cell Biology*, 7(10):961–968, 2005.
- M. Nakamura, K. Naoi, T. Syouji, and T. Hashimoto. Observation of the plant interphase microtubule dynamics in vivo. *Plant and Cell Physiology*, 45:S113–S113, 2004.
- M. Nakamura, D. W. Ehrhardt, and T. Hashimoto. Microtubule and katanin-dependent dynamics of microtubule nucleation complexes in the acentrosomal Arabidopsis cortical array. *Nature Cell Biology*, 12(11):1064–1070, 2010.
- A. Nebenführ, L. A. Gallagher, T. G. Dunahay, J. A. Frohlick, A. M. Mazurkiewicz, J. B. Meehl, and L. A. Staehelin. Stop-and-go movements of plant Golgi stacks are mediated by the acto-myosin system. *Plant physiology*, 121(4):1127–1142, 1999.
- A. Nebenführ, C. Ritzenthaler, and D. G. Robinson. Brefeldin A: deciphering an enigmatic inhibitor of secretion. *Plant physiology*, 130(3):1102–1108, 2002.
- Y. Oda, T. Mimura, and S. Hasezawa. Regulation of secondary cell wall development by cortical microtubules during tracheary element differentiation in Arabidopsis cell suspensions. *Plant physiology*, 137(3):1027–1036, 2005.

- A. Paradez, A. Wright, and D. W. Ehrhardt. Microtubule cortical array organization and plant cell morphogenesis. *Current Opinion in Plant Biology*, 9(6):571–578, 2006.
- A. R. Paredez, C. R. Somerville, and D. W. Ehrhardt. Visualization of cellulose synthase demonstrates functional association with microtubules. *Science*, 312(5779):1491–1495, 2006.
- M. Pastuglia, J. Azimzadeh, M. Goussot, C. Camilleri, K. Belcram, J. L. Evrard, A. C. Schmit, P. Guerche, and D. Bouchez. gamma-tubulin is essential for microtubule organization and development in Arabidopsis. *The Plant Cell*, 18(6):1412–1425, 2006.
- J. R. Pear, Y. Kawagoe, W. E. Schreckengost, D. P. Delmer, and D. M. Stalker. Higher plants contain homologs of the bacterial celA genes encoding the catalytic subunit of cellulose synthase. *Proceedings of the National Academy of Sciences of the United States of America*, 93(22):12637–12642, 1996.
- S. Persson, H. Wei, J. Milne, G. P. Page, and C. R. Somerville. Identification of genes required for cellulose synthesis by regression analysis of public microarray data sets. *Proceedings of the National Academy of Sciences of the United States of America*, 102(24):8633–8638, 2005.
- S. Persson, A. Paredez, A. Carroll, H. Palsdottir, M. Doblin, P. Poindexter, N. Khitrov, M. Auer, and C. R. Somerville. Genetic evidence for three unique components in primary cell-wall cellulose synthase complexes in Arabidopsis. *Proceedings of the National Academy of Sciences of the United States of America*, 104(39):15566–15571, 2007.
- C. S. Peskin, G. M. Odell, and G. F. Oster. Cellular motions and thermal fluctuations: the Brownian ratchet. *Biophysical Journal*, 65(1):316–324, 1993.
- J. Petrášek and K. Schwarzerová. Actin and microtubule cytoskeleton interactions. *Current Opinion in Plant Biology*, 12(6):728–734, 2009.
- J. M. Picton and M. W. Steer. Determination of secretory vesicle production rates by dictyosomes in pollen tubes of Tradescantia using cytochalasin D. *Journal of Cell Science*, 49: 261–272, 1981.
- J. M. Picton and M. W. Steer. The effect of cycloheximide on dictyosome activity in Tradescantia pollen tubes determined using cytochalasin D. *European Journal of Cell Biology*, 29(2):133–138, 1983.
- N. S. Poulter, S. Vatovec, and V. E. Franklin-Tong. Microtubules are a target for self-incompatibility signaling in Papaver pollen. *Plant physiology*, 146(3):1358–1367, 2008.
- M. L. Preuss, D. R. Kovar, Y. R. J. Lee, C. J. Staiger, D. P. Delmer, and B. Liu. A plant-specific kinesin binds to actin microfilaments and interacts with cortical microtubules in cotton fibers. *Plant physiology*, 136(4):3945–3955, 2004a.
- M. L. Preuss, J. Serna, T. G. Falbel, S. Y. Bednarek, and E. Nielsen. The Arabidopsis Rab GTPase RabA4b localizes to the tips of growing root hair cells. *The Plant Cell*, 16(6):1589–1603, 2004b.
- W. S. Rasband. ImageJ: Image processing and analysis in Java. *Astrophysics Source Code Library*, -1:06013, 2012.

- P. M. Ray, P. B. Green, and R. CLELAND. Role of turgor in plant cell growth. 1972.
- I. Reichardt, Y. D. Stierhof, U. Mayer, S. Richter, and H. Schwarz. ScienceDirect.com - Current Biology - Plant Cytokinesis Requires De Novo Secretory Trafficking but Not Endocytosis. *Current Biology*, 17:2046–2053, 2007.
- T. A. Richmond and C. R. Somerville. The Cellulose Synthase Superfamily. *Plant physiology*, 2000.
- M. Riquelme. What Determines Growth Direction in Fungal Hyphae? *Fungal Genetics and Biology*, 24(1-2):101–109, 1998.
- S. Robert, A. Bichet, O. Grandjean, D. Kierzkowski, B. Satiat-Jeuñemaître, S. Pelletier, M.-T. Hauser, H. Höfte, and S. Vernhettes. An Arabidopsis Endo-1,4-β-d-Glucanase Involved in Cellulose Synthesis Undergoes Regulated Intracellular Cycling. *The Plant Cell*, 2005.
- E. Roberts, R. W. Seagull, C. H. Haigler, and R. M. Brown. Alteration of Cellulose Microfibril Formation in Eukaryotic Cells: Calcofluor White Interferes with Microfibril Assembly and Orientation in *Oocystis apiculata*. *Protoplasma*, 1982.
- D. G. Robinson and R. D. Preston. Plasmalemma structure in relation to microfibril biosynthesis in *Oocystis*. *Planta*, 104(3):234–246, 1972.
- A. Roll-Mecak and R. D. Vale. Making more microtubules by severing: a common theme of noncentrosomal microtubule arrays? *The Journal of Cell Biology*, 175(6):849–851, 2006.
- R. Saedler, N. Mathur, B. P. Srinivas, B. Kernebeck, M. Hülskamp, and J. Mathur. Actin Control Over Microtubules Suggested by DISTORTED2 Encoding the Arabidopsis ARPC2 Subunit Homolog. *Plant and Cell . . .*, 2004.
- D. Sage, F. R. Neumann, F. Hediger, S. M. Gasser, and M. Unser. Automatic tracking of individual fluorescence particles: application to the study of chromosome dynamics. *Ieee Transactions on Image Processing*, 14(9):1372–1383, 2005.
- W. C. Salmon, M. C. Adams, and C. M. Waterman-Storer. Dual-wavelength fluorescent speckle microscopy reveals coupling of microtubule and actin movements in migrating cells. *The Journal of Cell Biology*, 158(1):31–37, 2002.
- A. Sambade, A. Pratap, H. Buschmann, R. J. Morris, and C. Lloyd. The influence of light on microtubule dynamics and alignment in the Arabidopsis hypocotyl. *The Plant Cell Online*, 24(1):192–201, 2012.
- N. C. Shaner, R. E. Campbell, P. A. Steinbach, B. N. G. Giepmans, A. E. Palmer, and R. Y. Tsien. Improved monomeric red, orange and yellow fluorescent proteins derived from *Discosoma* sp. red fluorescent protein. *Nature biotechnology*, 22(12):1567–1572, 2004.
- S. L. Shaw, R. Kamyar, and D. W. Ehrhardt. Sustained microtubule treadmilling in Arabidopsis cortical arrays. *Science*, 300(5626):1715–1718, 2003.
- M. B. Sheahan, C. J. Staiger, R. J. Rose, and D. W. McCurdy. A green fluorescent protein fusion to actin-binding domain 2 of Arabidopsis fimbrin highlights new features of a dynamic actin cytoskeleton in live plant cells. *Plant physiology*, 136(4):3968–3978, 2004.

- C. Somerville. Cellulose synthesis in higher plants. *Annual review of cell and developmental biology*, 22:53–78, 2006.
- C. Somerville, S. Bauer, G. Brininstool, M. Facette, T. Hamann, J. Milne, E. Osborne, A. Paredez, S. Persson, T. Raab, S. Vorwerk, and H. Youngs. Toward a systems approach to understanding plant cell walls. *Science*, 306(5705):2206–2211, 2004.
- A. L. Staehelin and H. T. Giddings. Membrane mediated control of microfibrillar order, in Developmental order, its origin and regulation. pages 133–147. Alan R. Liss., New York, 1982.
- C. J. Staiger, M. B. Sheahan, P. Khurana, X. Wang, D. W. McCurdy, and L. Blanchoin. Actin filament dynamics are dominated by rapid growth and severing activity in the Arabidopsis cortical array. *The Journal of Cell Biology*, 184(2):269–280, 2009.
- S. D. Strachan and F. D. Hess. The biochemical mechanism of action of the dinitroaniline herbicide oryzalin. *Pesticide Biochemistry and Physiology*, 20(2):141–150, 1983.
- N. Suetsugu, N. Yamada, T. Kagawa, H. Yonekura, T. Q. P. Uyeda, A. Kadota, and M. Wada. Two kinesin-like proteins mediate actin-based chloroplast movement in Arabidopsis thaliana. *Proceedings of the National Academy of Sciences of the United States of America*, 107(19):8860–8865, 2010.
- K. Sugimoto, R. Himmelpach, R. E. Williamson, and G. O. Wasteneys. Mutation or Drug-Dependent Microtubule Disruption Causes Radial Swelling without Altering Parallel Cellulose Microfibril Deposition in Arabidopsis Root Cells. *The Plant Cell*, 2003.
- D. B. Szymanski and D. J. Cosgrove. Dynamic coordination of cytoskeletal and cell wall systems during plant cell morphogenesis. *Curr Biol*, 19(17):R800–11, 2009.
- K. Takesue and H. Shibaoka. The cyclic reorientation of cortical microtubules in epidermal cells of azuki bean epicotyls: the role of actin filaments in the progression of the cycle. *Planta*, 205(4):539–546, 1998.
- N. G. Taylor, R. M. Howells, A. K. Huttly, K. Vickers, and S. R. Turner. Interactions among three distinct CesA proteins essential for cellulose synthesis. *Proceedings of the National Academy of Sciences of the United States of America*, 100(3):1450–1455, 2003.
- P. Thevenaz, U. E. Ruttimann, and M. Unser. A pyramid approach to subpixel registration based on intensity. *Ieee Transactions on Image Processing*, 7(1):27–41, 1998.
- A. C. J. Timmers, P. Vallotton, C. Heym, and D. Menzel. Microtubule dynamics in root hairs of *Medicago truncatula*. *European Journal of Cell Biology*, 86(2):69–83, 2007.
- S. H. Tindemans. *Biomolecular design elements : cortical microtubules and DNA-coated colloids*. PhD thesis, Wageningen University, 2009.
- S. H. Tindemans and B. M. Mulder. Microtubule length distributions in the presence of protein-induced severing. *Physical review. E, Statistical, nonlinear, and soft matter physics*, 81(3 Pt 1):031910, 2010.
- S. H. Tindemans, R. J. Hawkins, and B. M. Mulder. Survival of the aligned: ordering of the plant cortical microtubule array. *Physical Review Letters*, 104(5):058103, 2010.

- J. A. Traas, J. H. Doonan, D. J. Rawlins, P. J. Shaw, J. Watts, and C. W. Lloyd. An actin network is present in the cytoplasm throughout the cell cycle of carrot cells and associates with the dividing nucleus. *The Journal of Cell Biology*, 105(1):387–395, 1987.
- K. Ueda and T. Matsuyama. Rearrangement of cortical microtubules from transverse to oblique or longitudinal in living cells of transgenic *Arabidopsis thaliana*. *Protoplasma*, 213(1-2): 28–38, 2000.
- T. Uemura, T. Ueda, R. L. Ohniwa, A. Nakano, K. Takeyasu, and M. H. Sato. Systematic analysis of SNARE molecules in *Arabidopsis*: dissection of the post-Golgi network in plant cells. *Cell structure and function*, 29(2):49–65, 2004.
- J. W. Vos, M. Dogterom, and A. M. C. Emons. Microtubules become more dynamic but not shorter during preprophase band formation: a possible "search-and-capture" mechanism for microtubule translocation. *Cell motility and the cytoskeleton*, 57(4):246–258, 2004.
- G. O. Wasteneys. Microtubule organization in the green kingdom: chaos or self-order? *Journal of Cell Science*, 115(7):1345–1354, 2002.
- G. O. Wasteneys and J. C. Ambrose. Spatial organization of plant cortical microtubules: close encounters of the 2D kind. *Trends in cell biology*, 19(2):62–71, 2009.
- G. O. Wasteneys and R. E. Williamson. Reassembly of Microtubules in *Nitella Tasmanica* - Quantitative-Analysis of Assembly and Orientation. *European Journal of Cell Biology*, 50(1): 76–83, 1989a.
- G. O. Wasteneys and R. E. Williamson. Reassembly of microtubules in *Nitella tasmanica*: assembly of cortical microtubules in branching clusters and its relevance to steady-state microtubule assembly. *Journal of Cell Science*, 93(4):705–714, 1989b.
- C. Weerdenburg and R. W. Seagull. The effects of taxol and colchicine on microtubule and microfibril arrays in elongating plant cells in culture. *Can J Bot*, 66(66):1707–1716, 1988.
- Y. Wen, C. H. Eng, J. Schmoranzer, N. Cabrera-Poch, E. J. S. Morris, M. Chen, B. J. Wallar, A. S. Alberts, and G. G. Gundersen. EB1 and APC bind to mDia to stabilize microtubules downstream of Rho and promote cell migration. *Nature Cell Biology*, 6(9):820–830, 2004.
- S. Westermann, H.-W. Wang, A. Avila-Sakar, D. G. Drubin, E. Nogales, and G. Barnes. The Dam1 kinetochore ring complex moves processively on depolymerizing microtubule ends. *Nature*, 440(7083):565–569, 2006.
- a. T. Whittington, O. Vugrek, K. J. Wei, N. G. Hasenbein, K. Sugimoto, M. C. Rashbrooke, and G. O. Wasteneys. MOR1 is essential for organizing cortical microtubules in plants. *Nature*, 411(6837):610–613, 2001.
- R. Wightman and S. R. Turner. The roles of the cytoskeleton during cellulose deposition at the secondary cell wall. *The Plant journal*, 54(5):794–805, 2008.
- X. Wu, X. Xiang, and J. A. Hammer. Motor proteins at the microtubule plus-end. *Trends in cell biology*, 16(3):135–143, 2006.

- T. Xu, Z. Qu, X. Yang, X. Qin, J. Xiong, Y. Wang, D. Ren, and G. Liu. A cotton kinesin GhKCH2 interacts with both microtubules and microfilaments. *The Biochemical journal*, 421(2): 171–180, 2009.
- C. Y. L. Yuen, R. S. Pearlman, L. Silo-Suh, P. Hilson, K. L. Carroll, and P. H. Masson. WVD2 and WDL1 modulate helical organ growth and anisotropic cell expansion in Arabidopsis. *Plant physiology*, 131(2):493–506, 2003.
- H. Zheng, S. Y. Bednarek, A. A. Sanderfoot, J. Alonso, J. R. Ecker, and N. V. Raikhel. NPSN11 is a cell plate-associated SNARE protein that interacts with the syntaxin KNOLLE. *Plant physiology*, 129(2):530–539, 2002.

Summary

In this thesis we study the roles of microtubules at the plasma membrane and the cellulose microfibrils in the cell wall and how they are organized. This topic is introduced in chapter 1. In chapter 2 we study the formation of the transverse cortical microtubule array that is characteristic for elongating plant cells. We found that the cortical microtubule array starts ordered, and that the first direction of microtubule order is not transverse to the axis of cell elongation but have a diagonal bias. Quantification of the orientation of microtubule nucleations revealed a significant diagonal bias, which we confirmed by simulations to be sufficient to explain the initial diagonal order. We found that during disassembly the microtubules also showed a diagonal bias and a significant amount of early microtubule nucleations were not generated from γ -TuRC microtubule nucleating complexes. This led to the idea that a proportion of the initial nucleations stem from small microtubule fragments of preexisting microtubules that remained at the cell cortex during cytokinesis or drug induced microtubule disassembly. We showed with simulations that this type of nucleation has the capacity to increase the speed with which the cortical microtubule array is reformed.

In chapter 3 we investigate the trafficking of cellulose synthase complexes from assembly in the Golgi system to their insertion into the plasma membrane. We find that the actin cytoskeleton is important for the global distribution of Golgi bodies, which in turn is important for the global distribution of cellulose synthase complexes in the plasma membrane. Cellulose synthase complexes were inserted into the membrane preferentially at locations where cortical microtubules were present. We showed that osmotic stress and a number of cellulose synthesis inhibitors blocked cellulose synthase insertion into the plasma membrane. The cellulose synthase complex containing compartments were seemingly still being delivered to the cortical microtubules where they accumulated. These compartments tracked depolymerizing microtubule ends. When the osmotic stress was relieved, cellulose synthase complex insertion was resumed from these compartments.

Rapid movement of proteins, organelles and metabolites in the cytoplasm of plant cells depends on the actin cytoskeleton, whereas microtubules are important in regulating the location of proteins and cellular processes. In chapter 4 we found physical interactions between cortical microtubules and actin. We also found that the formation of the actin cytoskeleton after washing out the actin depolymerizing drug latrunculin B was dependent on the presence of microtubules. In the presence of cortical microtubules, new actin filaments initiated on and in the direction of

cortical microtubules.

In chapter 5 we investigate the mechanism reorientation of the cortical microtubule array from transverse to longitudinal in response to light signaling. We found that cortical microtubule array reorientation in dark grown hypocotyl cells was regulated by phototropin a blue light photoreceptor. We found that microtubule reorientation was delayed in *phot1 phot2* mutants. We also found that *ktn1-1*, a null mutant of KATANIN P60, and *spr3*, a GCP2 allele with impaired function, severely retarded microtubule array reorientation in response to light. *spry* has altered angles of microtubule nucleation relative to the mother polymer, and *ktn1-1* abolishes liberation of microtubules from their nucleation complexes to yield treadmilling polymers and microtubule severing at microtubule crossovers. We found that in response to blue light, the proportion of microtubule nucleations branching at 40 degrees from the mother microtubule to nucleation at 0 degrees from the mother microtubule was higher in wild type plant than in the *phot1 phot2* mutant. We also found that the chance of microtubule severing at microtubule crossovers was significantly higher in wild type than in the *phot1 phot2* mutant. We propose that upregulation of the branching nucleations is needed to create a number of longitudinally oriented microtubules. These microtubules make a large number of crossovers with the existing transverse array and have an increased chance of being severed. Severing events that result in a stable new tip contribute to the increase in longitudinal microtubule order and ultimately lead to complete reorientation from transverse to longitudinal.

The spatial organization of cortical microtubules and cellulose microfibrils are essential for plant morphogenesis, but the mechanism by which is unclear. Chapter 6 discusses the process of cell elongation and offers possible additional roles for cortical microtubules beyond guiding cellulose microfibril deposition in this process.

Samenvatting

Het onderzoek dat in dit proefschrift beschreven staat gaat over de relatie tussen de microtubuli aan de binnenkant van de plasmamembraan en de cellulose microfibrillen in de celwand aan de buitenkant van die membraan. Dit onderwerp wordt geïntroduceerd in hoofdstuk 1. In hoofdstuk 2 bestuderen we hoe de corticale microtubuli zich dwars op de groeirichting van de cel organiseren. We hebben vast kunnen stellen dat de eerste microtubuli die terugkomen in de celcortex na celdeling of experimentele afbraak niet voornamelijk dwars, maar voornamelijk diagonaal, op de groeirichting van de cel terugkomen. Door de richting van de nucleaties van nieuwe microtubuli te kwantificeren hebben we gevonden dat de nieuwe microtubuli bij voorkeur diagonaal op de cel-as nucleëren. Met computersimulaties hebben we laten zien dat wanneer we experimenteel een bepaalde mate van voorkeur voor diagonale microtubuli nucleaties gebruiken, de simulaties de gemeten ontwikkeling van de organisatie van de corticale microtubuli dwars op de groeirichting bijna exact reproduceren. Verder vonden we dat tijdens het verdwijnen van de corticale microtubuli de microtubuli ook tijdelijk een diagonale organisatie hadden en dat een deel van de eerste nieuwe microtubuli niet colocaliseerden met γ -tubuline nucleatie-complexen. Dit heeft geleid tot het idee dat een deel van de eerste nieuwe microtubuli ontstaan uit kleine fragmenten van microtubuli die niet volledig zijn verdwenen tijdens de afbraak van de corticale microtubuli. De computersimulaties hebben verder laten zien dat de opbouw van de dichtheid van de corticale microtubuli sneller verloopt wanneer deze fragmenten aanwezig zijn.

In hoofdstuk 3 onderzoeken we hoe de cellulose synthase-complexen vanuit het Golgi-systeem naar in het plasmamembraan worden gebracht. We hebben gevonden dat het actine-cytoskelet belangrijk is voor de globale distributie van Golgi lichaampjes, die op hun beurt weer bepalend zijn voor de globale distributie van cellulose synthasecomplexen in het plasmamembraan. We hebben vastgesteld dat cellulose synthasecomplexen bij voorkeur in het plasmamembraan gebracht worden op plaatsen waar corticale microtubuli aanwezig zijn. Daarnaast hebben we ontdekt dat onder osmotische stress en na het toedienen van enkele cellulose productieremmers, minder cellulose synthasecomplexen in de plasmamembraan gebracht worden. Compartimenten die cellulose synthasecomplexen bevatten verzamelen onder deze omstandigheden op microtubuli en volgen depolymeriserende microtubule einden. Wanneer deze stress wordt weggenomen wordt het inbrengen van cellulose synthasecomplexen vanuit de op de microtubuli verzamelde compartimenten hervat.

De snelle beweging van eiwitten, organellen en metabolieten in het cytoplasma van plantencellen, cytoplasmastroming, is afhankelijk van het actine cytoskelet, terwijl het microtubuli cytoskelet belangrijk blijkt te zijn voor het reguleren van de plaatsing van eiwitten zoals bijvoorbeeld hierboven beschreven. In hoofdstuk 4 beschrijven we de fysieke interacties die we hebben gevonden tussen actine filamenten en microtubuli. Daarnaast hebben we aangetoond dat het opbouwen van het actine cytoskelet afhankelijk is van de aanwezigheid van microtubuli. In de aanwezigheid van microtubuli ontstaan de eerste nieuwe actine filamenten op microtubuli en nemen daarnaast ook dezelfde oriëntatie aan.

In hoofdstuk 5 onderzoeken we het mechanisme van heroriëntatie van de corticale microtubuli van een organisatie dwars op de groeirichting naar parallel aan de groeirichting tijdens de lichtrespons. In *Arabidopsis* hypocotylcellen, die in het donker waren gegroeid, bleek de heroriëntatie voornamelijk afhankelijk van photophine, een blauw-licht fotoreceptor. De heroriëntatie was significant vertraagd in *phot1 phot2* planten, waarin beide phototropinen zeer sterk zijn gereduceerd zijn. Daarnaast vonden we dat *ktn1-1* een nulmutant voor een KATANIN P60 onderdeel en *spr3*, een allel voor GCP2 met verzwakte functionaliteit zeer sterk vertraagd waren in de snelheid waarmee deze planten tot heroriëntatie van corticale microtubuli in staat bleken in reactie op blauw licht. *spr3* planten hebben een veranderde richting van microtubuli-nucleatie ten opzichte van de microtubuli van waaraf ze nucleëren. In *ktn1-1* is het vrijmaken van de microtubuli vanaf het γ -tubuline nucleatiecomplex uitgeschakeld, waardoor de microtubuli niet in staat zijn vanaf de - kant te depolymeriseren. Daarnaast is het breken van microtubuli op plaatsen waar corticale microtubuli elkaar overkruisen in *ktn1-1* volledig afwezig. In reactie op blauw licht is de proportie van microtubuli-nucleaties die onder een hoek van 40 graden ten opzichte van een bestaande microtubuli plaatsvinden in vergelijking tot de proportie van nucleaties in dezelfde oriëntatie als de bestaande microtubuli hoger in wildtype planten dan in *phot1 phot2* mutanten. Verder is de kans dat microtubuli breken op de plaats waar ze elkaar overkruisen significant hoger in wildtype dan in *phot1 phot2*. We veronderstellen dat de eerste stap van heroriëntatie het verhogen van de microtubuli-nucleaties onder een hoek van 40 graden met een bestaande microtubuli is. Dit is nodig om de mogelijkheid te creëren dat er microtubuli ontstaan die parallel aan de groeirichting van de cel liggen. Deze microtubuli maken een groot aantal overkruisingen met bestaande microtubuli. Door de verhoogde kans op het breken van microtubuli op deze overkruisingen wordt het aantal microtubuli parallel aan de groeirichting van de cel verhoogd. Doordat een deel van de microtubuli die ontstaan zijn door het breken van microtubuli stabiel is, verandert de oriëntatie van dwars op de groeirichting naar parallel aan de groeirichting.

De ruimtelijke organisatie van corticale microtubuli en cellulose microfibrillen zijn essentieel voor plantmorfogenese, maar welk mechanisme hier aan ten grondslag ligt is nog onduidelijk. Hoofdstuk 6 behandelt het proces van celgroei en biedt ideeën mogelijk aanvullende rollen voor corticale microtubuli naast het leiden van cellulose synthasecomplexen en dus de oriëntatie van depositie van cellulosemicrofibrillen.

Acknowledgements

Many people have contributed to the work presented in this thesis. I received a lot of scientific input from my colleagues to keep the projects moving forward, and many people helped to keep me motivated.

First of all I would like to thank my advisor Anne Mie Emons, for her support. Anne Mie, you have been a great mentor from the first moment I attended a course you were teaching. You have a great combination of a very critical mind, the ability to bring people together and lot of drive and enthusiasm. You gave me a lot of trust and freedom and I think we worked very well together.

During my master's thesis project with Jan Vos I really felt like I was becoming a proper scientist. Jan, I learned a lot from you about how to do careful experimentation, microscopy and about scientific writing. Tijs, also a big thanks to you for sharing your amazing troubleshooting skills and your role as co-advisor. Our daily discussions on scientific and not so scientific topics made my time in Wageningen a lot of fun.

Of all the people I worked with, my co-adviser Bela Mulder has had the most profound impact on my scientific career. As a master's student I worked for one year in his group at the FOM institute AMOLF in Amsterdam learning how to do modeling and programming. Thank you for challenging me to leave the relative comfort of experimental biology to come and explore treacherous world of physics and math. Besides being an excellent teacher you were always very entertaining company in Wageningen, at AMOLF and on our numerous trips abroad. Simon, thank you for teaching me the basics of programming and all kinds of other computer related skills. Also a big thanks to Simon and Kostya for patiently and explaining the language of physics, I really enjoyed working with you guys. Eva, thank you for running a staggering amount of valuable simulations, your insightful interpretations of those simulations were very valuable.

Just after I started my PhD, Anne Mie sent me to the Ehrhardt lab at the Carnegie Institution for Science (Stanford, USA) for half a year, to learn new microscopy techniques. This period at Carnegie was very productive for starting new and exciting projects, including those in chapter 3 and 5. Ryan and Viktor, thank you guys for teaching me pretty much everything I know about molecular biology. Thanks again to Ryan and Viktor, and thanks to Masayoshi for being such eager, sharp and generous collaborators. Of course, a special thanks to David Ehrhardt. Thank you for your hospitality, the never-ending stream of brilliant ideas, practical solutions and always making me go the extra mile. I also really appreciate the fact that you were always

available for advice after I had left the lab.

I would also like to thank Arun and Staffan from the Max Planck Institute in Golm (Germany) for the spontaneous collaboration that resulted in the content of chapter 4 and another forthcoming paper. You guys always bring a lot of drive and momentum which is really contagious and productive.

During the time as a PhD student I worked together with many different people at Cell Biology in Wageningen. I really enjoyed, the coffee and lunch breaks together. I would like to thank Marcel Janson for many helpful discussions and for carefully picking the microscopes that were crucial to almost all my experiments. We also had a lot of fun during the many movie nights and other social events, thanks to all of you. I would like to thank Zdenek Lansky in particular, the large overlap in our interests made for many excellent conversations ranging from fancy scientific experiments all the way to the Holy Stone of Clonrickert. During my PhD I supervised three master's students, Kris, Anneke and Rik. Thank you for the excellent work and being great company.

Last but not least I want to thank my family and friends. All of you have always been very supportive of anything I do which has kept me happy and motivated throughout my PhD. A special thanks to my housemates from my studenthouse 'VGH' in Wageningen for all the good times we had together. I want to thank Sabine, JanPeter, Don and Hans in particular for keeping me happy and motivated. JanPeter and Don, thanks as well for your role as 'paranimphen', we have been friends since we were about four years old so I am very glad you guys are helping me through the PhD ceremony as well.

Jelmer Lindeboom

Curriculum Vitae

Jelmer Lindeboom was born in Ureterp, The Netherlands, on 2 January 1982. He attended the 'Liudger' high school in Drachten. After that he obtained a bachelor's degree in Food Science at the Van Hall Institute in Leeuwarden between 1999 and 2003. During this period he performed an internship at Sheffield Hallam University (UK) and his bachelor's thesis at FrieslandCampina Corporate Research. Between 2003 and 2007 he studied biology at Wageningen University. For his Master's thesis at Plant Cell Biology he was rewarded with the thesis prize for best thesis in life sciences at Wageningen University. Jelmer did his internship in the group of prof. dr. Bela Mulder at the FOM institute AMOLF on modeling microtubule ordering in plant cells.

In 2007, Jelmer started as a PhD student with prof. dr. Anne Mie Emons at the laboratory of Plant Cell Biology on the organization of cortical microtubules and cellulose microfibrils in plant cells. In his first year he spent six months as a guest in the group of dr. David Ehrhardt at the Carnegie Institution for Science, Department of Plant Biology, Stanford (USA). In 2010 Jelmer was selected to attend the Physiology Course at the Marine Biology Laboratory in Woods Hole (USA).

In 2012 Jelmer started his work as a post-doctoral fellow in the group of dr. David Ehrhardt at the Carnegie Institution for Science, Department of Plant Biology, Stanford (USA).

List of publications

The work presented in this thesis is partly based on the following references.

Lindeboom, J., Mulder, B.M., Vos, J.W., Ketelaar, T., and Emons, A.M.C. (2008). *Cellulose microfibril deposition: coordinated activity at the plant plasma membrane*. J Microsc 231: 192-200.

Lindeboom, J.J., Lioutas, A., Deinum, E.E., Tindemans, S.H., Ehrhardt, D.W.E., Emons, A.M.C., Vos, J.W. and Mulder, B.M. *Cortical microtubule arrays are initiated from a non-random pre-pattern driven by atypical microtubule initiation*. Submitted.

Gutierrez, R., Lindeboom, J.J., Paredez, A.R., Emons, A.M.C., and Ehrhardt, D.W. (2009). *Arabidopsis cortical microtubules position cellulose synthase delivery to the plasma membrane and interact with cellulose synthase trafficking compartments*. Nat Cell Biol 11: 797-806.

Sampathkumar, A., Lindeboom, J.J., Debolt, S., Gutierrez, R., Ehrhardt, D.W., Ketelaar, T., and Persson, S. (2011). *Live cell imaging reveals structural associations between the actin and microtubule cytoskeleton in Arabidopsis*. The Plant Cell 23: 2302-2313.

Lindeboom, J.J., Nakamura, M, Hibbel, A., Shundyak, K., Gutierrez, R., Ketelaar, T., Emons, A.M.C., Mulder, B.M., Kirik, V. and Ehrhardt, D.W. *PHOTOTROPIN signaling stimulates reorientation of acentrosomal cortical arrays mediated by branching nucleation and microtubule amplification by KATANIN*. In preparation.

Education Statement of the Graduate School
Experimental Plant Sciences



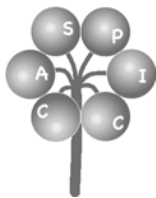
Issued to: Jelmer Lindeboom
Date: 14 November 2012
Group: Cell Biology, Wageningen University & Research Centre

1) Start-up phase <ul style="list-style-type: none"> ▶ First presentation of your project The Formation and Organisation of Cellulose Patterns in Plant Cell Walls ▶ Writing or rewriting a project proposal Cellulose Patterns in Plant Cell Walls: Their Formation and Organisation ▶ Writing a review or book chapter Lindeboom, J., Mulder, B. M., Vos, J. W., Ketelaar, T., & Emons, A. M. C. (2008). Cellulose microfibril deposition: coordinated activity at the plant plasma membrane <i>Journal of microscopy</i>, 231(2), 192-200. doi:10.1111/j.1365-2818.2008.02035.x ▶ MSc courses ▶ Laboratory use of isotopes 	<p align="right"><u>date</u></p> <p align="right">Feb 03, 2007</p> <p align="right">Mar 2007</p> <p align="right">Apr 2007</p>
<i>Subtotal Start-up Phase</i> 7,5 credits*	
2) Scientific Exposure <ul style="list-style-type: none"> ▶ EPS PhD student days EPS PhD student day, Utrecht University ▶ EPS theme symposia EPS theme symposium Theme 1, Wageningen University EPS theme symposium Theme 1, Wageningen University ▶ NWO Lunteren days and other National Platforms EPS meeting Lunteren Cellular and Molecular Biophysics meeting Veldhoven EPS meeting Lunteren Dutch Cellular and Molecular Biophysics meeting, Veldhoven EPS meeting Lunteren Dutch Cellular and Molecular Biophysics meeting, Veldhoven Dutch Cellular and Molecular Biophysics meeting, Veldhoven Dutch Cellular and Molecular Biophysics meeting, Veldhoven ▶ Seminars (series), workshops and symposia Seminar series 'Plant Cell Biology' + Flying Seminars + Individual Seminars (20 x) ▶ Seminar plus Flying Seminars (Zhenbiao Yang, Hiroo Fukuda) ▶ International symposia and congresses COST meeting Cell Wall Max Planck Institute Golm, Germany Systems Biology for Plant Design, Wageningen SEB cell Symposium, Durham, UK Gordon Conference Plant and Microbial Cytoskeleton, Andover, NH, USA EMBO Conference Series: 'Microtubules - Structure, Regulation and Functions', EMBL Heidelberg, Germany Botanical microscopy, Wageningen EMBO Conference Series: 'Microtubules - Structure, Regulation and Functions', EMBL Heidelberg, Germany Gordon Conference Plant and Microbial Cytoskeleton, Andover, NH, USA ▶ Presentations COST meeting Cell Wall Max Planck Institute Golm (oral) Dutch meeting on Molecular and Cellular Biophysics, Veldhoven (poster) Systems Biology for Plant Design, Wageningen (oral) SEB cell Symposium, Durham, UK, (oral) Dutch meeting on Molecular and Cellular Biophysics, Veldhoven (oral) EPS Theme 1, Wageningen (oral) EMBO Conference: 'Microtubules - Structure, Regulation and Functions', EMBL Heidelberg, Germany (poster) Botanical microscopy, Wageningen (oral) EMBO Conference: 'Microtubules - Structure, Regulation and Functions', EMBL Heidelberg, Germany (poster) Gordon Conference Plant and Microbial Cytoskeleton, Andover, NH, USA (poster) ▶ IAB interview ▶ Excursions 	<p align="right"><u>date</u></p> <p align="right">Jun 01, 2010</p> <p align="right">Oct 11, 2007 Jan 28, 2010</p> <p align="right">Apr 02-03, 2007 Oct 01-02, 2007 Apr 07-08, 2008 Sep 29-30, 2008 Apr 06-07, 2009 Sep 28-29, 2009 Oct 04-05, 2010</p> <p align="right">2007-2011</p> <p align="right">2007-2008</p> <p align="right">Sep 26-28, 2007 Jul 08-11, 2009 Aug 24-26, 2009 Aug 08-13, 2010 Jun 02-05, 2010 Apr 16-21, 2011 May 23-26, 2012 Aug 12-17, 2012</p> <p align="right">Sep 26-28, 2007 Sep 29-30, 2008 Jul 08-11, 2009 Aug 24-26, 2009 Sep 28-29, 2009 Jan 28, 2010 Jun 02-05, 2010 Apr 16-21, 2011 May 23-26, 2012 Aug 12-17, 2012 Dec 2009</p>
<i>Subtotal Scientific Exposure</i> 27,6 credits*	
3) In-Depth Studies <ul style="list-style-type: none"> ▶ EPS courses or other PhD courses PhD Course 'Mathematics in Biology' PhD Course 'Gateway to Gateway Technology' ▶ Journal club Literature discussion at Plant Cell Biology ▶ Individual research training 	<p align="right"><u>date</u></p> <p align="right">Jul 01-15, 2008 Nov 17-21, 2008</p> <p align="right">2007-2011</p>
<i>Subtotal In-Depth Studies</i> 10,2 credits*	
4) Personal development <ul style="list-style-type: none"> ▶ Skill training courses MBL Physiology Course: Modern Cell Biology using Microscopic, Biochemical and Computational Approaches ▶ Organisation of PhD students day, course or conference Systems Biology for Plant Design, Wageningen Botanical microscopy, Wageningen ▶ Membership of Board, Committee or PhD council 	<p align="right"><u>date</u></p> <p align="right">Jun 12-Aug 01, 2010</p> <p align="right">Jul 08-11, 2009 Apr 16-21, 2011</p>
<i>Subtotal Personal Development</i> 24,4 credits*	
TOTAL NUMBER OF CREDIT POINTS* 69.7	

Herewith the Graduate School declares that the PhD candidate has complied with the educational requirements set by the Educational Committee of EPS which comprises of a minimum total of 30 ECTS credits

* A credit represents a normative study load of 28 hours of study.

The work described in this thesis was performed at the Laboratory of Cell Biology, Wageningen University, The Netherlands.



The work in this thesis was supported by the EU NEST program under project number 028974 (CASPIC).



Netherlands Organisation for Scientific Research

Funding was obtained from the Division for Earth and Life Sciences (ALW) with financial aid from the Netherlands Organization for Scientific Research (NWO).

Financial support for the printing of this thesis was kindly provided by the Laboratory of Cell Biology and Wageningen University.